N O T I C E

THIS DOCUMENT HAS BEEN REPRODUCED FROM MICROFICHE. ALTHOUGH IT IS RECOGNIZED THAT CERTAIN PORTIONS ARE ILLEGIBLE, IT IS BEING RELEASED IN THE INTEREST OF MAKING AVAILABLE AS MUCH INFORMATION AS POSSIBLE

NASA CR-165283

(NASA-CR-165283) PROCESSING OF SILICON SOLAR CELLS BY ION IMPLANTATION AND LASER ANNEALING Final Report (Spire Corp., Bedford, Mass.) 78 p HC A05/MF A01 CSCL 10A G3/44

N82-11546

Unclas 08236

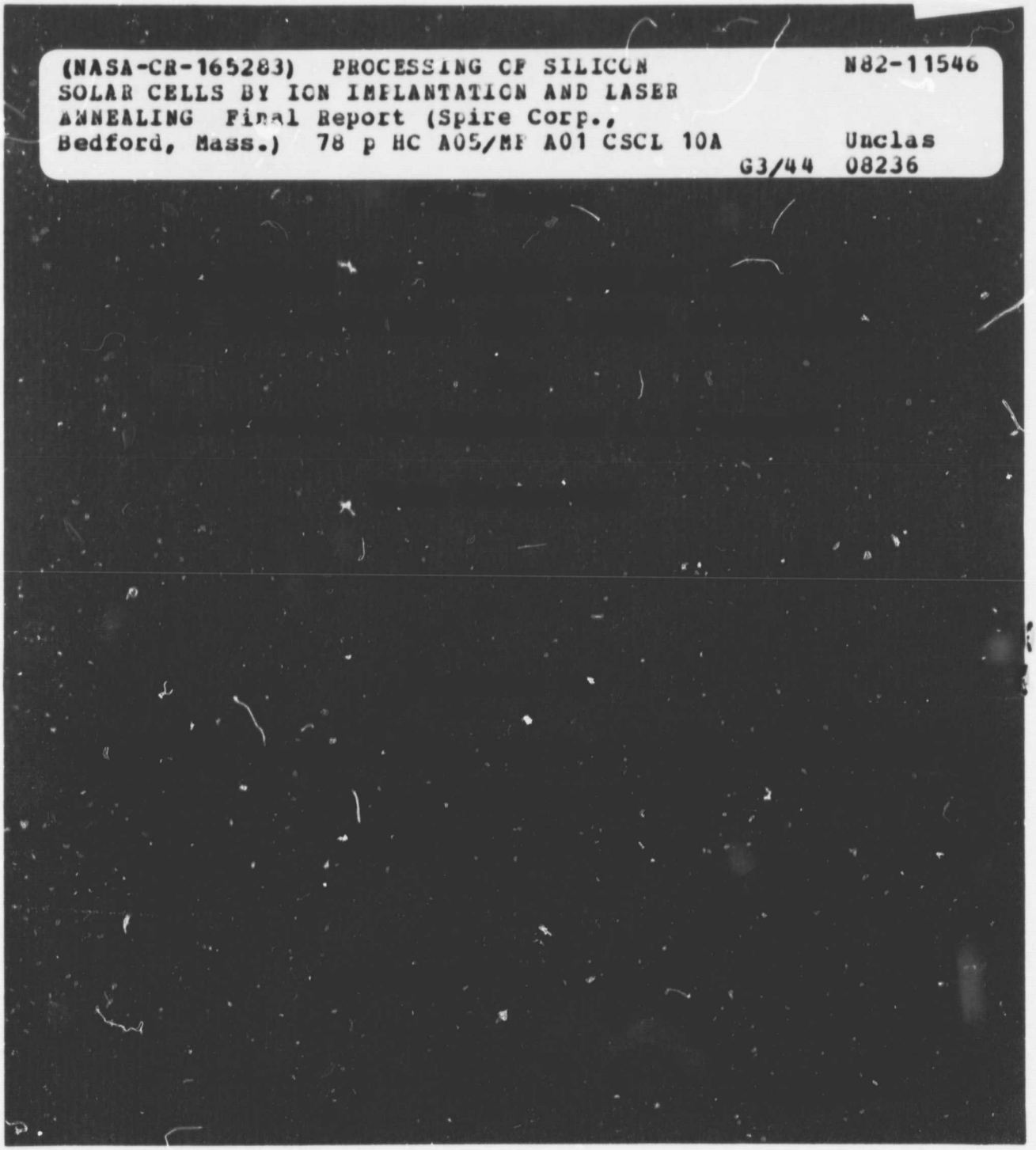

spire
PATRIOTS PARK
BEDFORD, MA 01730

1 Report No	2 Government Accession No	3 Recipient's Catalog No
NASA CR-165283		

4 Title and Subtitle	5 Report Date
PROCESSING OF SILICON SOLAR CELLS BY ION IMPLANTATION AND LASER ANNEALING	February 1981
	6 Performing Organization Code
7 Author(s) J. A. Minucci and K. W. Matthei (Draft) A. C. Greenwald (Revised)	8 Performing Organization Report No PR-19066
	10 Work Unit No
9 Performing Organization Name and Address Spire Corporation Patriots Park Bedford, MA 01730	11 Contract or Grant No NAS3-21276
	13 Type of Report and Period Covered Contractor Report
12 Sponsoring Agency Name and Address National Aeronautics and Space Administration Washington, DC 20546	14 Sponsoring Agency Code

15 Supplementary Notes

Project Manager: I. Weinberg, NASA-Lewis Research Center, Cleveland, OH 44135

16 Abstract

This report describes the results of a 14-month program to improve the radiation tolerance of silicon cells for spacecraft use. The major emphasis of the program was to reduce the process-induced carbon and oxygen impurities in the junction and base regions of the solar cell, and to measure the effect of reduced impurity levels on the radiation tolerance of cells.

Substrates of 0.1, 1.0 and 10.0 ohm-cm float-zone material were used as starting material in the process sequence. High-dose, low-energy ion implantation was used to form the junction in n+p structures. Implant annealing was performed by conventional furnace techniques and by pulsed laser and pulsed electron beam annealing.

Cells were tested for radiation tolerance at Spire and NASA-LeRC. After irradiation by 1 MeV electrons to a fluence of 10^{16} cm^{-2}, the cells tested at Spire showed no significant process induced variations in radiation tolerance. However, for cells tested at Lewis to a fluence of 10^{15} cm^{-2}, ion-implanted cells annealed in vacuum by pulsed electron beam consistently showed the best radiation tolerance for all cell resistivities.

17 Key Words (Suggested by Author(s))	18 Distribution Statement
silicon solar cells, ion-implanted junctions, radiation damage to solar cells, process introduced C and O in silicon, ion implantation, pulsed laser annealing, pulsed electron beam annealing	Unclassified - unlimited

19 Security Classif (of this report)	20 Security Classif (of this page)	21 No of Pages	22 Price*
Unclassified	Unclassified	88	

* For sale by the National Technical Information Service, Springfield, Virginia 22161

FOREWORD

Contributions to this program were made by many individuals at Spire Corporation. The Program Manager was J. A. Minnucci and the Principal Investigator was K. W. Matthei. The project team was staffed as follows:

W. A. Butts - Ion Implantation Facility
W. S. Kreisman - Analytical Studies
A. C. Greenwald - Pulsed Electron Beam Application

The contributions of personnel at NASA Lewis Research Center, particularly I. Weinberg, the Technical Manager, and H. Brandhorst are gratefully acknowledged.

TABLE OF CONTENTS

LIST OF FIGURES

LIST OF FIGURES (Continued)

LIST OF FIGURES (Concluded)

LIST OF TABLES

SUMMARY

This is the final report under Contract NAS 3-21276, "Processing of Silicon Solar Cells by Ion Implantation and Laser Annealing", performed for NASA Lewis Research Center as a part of NASA-LeRC's efforts to improve the end-of-life power levels of silicon cells for spacecraft use. The objective of the program was to process cells by ion implantation and pulse annealing without introducing either carbon or oxygen. The contract goal was to maintain both carbon and oxygen impurities at levels below the $5x10^{15}$ cm^{-3} typical of the best available float-zone silicon that could be manufactured in 1979.

The contract consisted of two major tasks: process development and cell performance measurements following 1 MeV electron irradiations. Process development included assessment of state-of-the-art ion-implant vacuum systems and modifications to meet the contract requirements. Reduction of adsorbed hydrocarbons which can be implanted by the knock-on process was of major importance to the program. Solar cells were processed using 0.1, 1.0 and 10.0 ohm-cm float-zone silicon, irradiated up to a $1x10^{16}$ e^{-} cm^{-2} fluence, and then characterized by AM0 and diffusion length measurements.

The results of the measurements and data analysis at Spire showed that no difference in radiation hardness could be correlated with a specific processing method. The measurements and data analysis at NASA-LeRC showed slightly better radiation tolerance (10 percent effect) for cells processed by ion implantation and pulsed electron beam annealing compared to laser annealing.

SECTION 1
INTRODUCTION

This contract was initiated to improve the radiation hardness of silicon solar cells for spacecraft application and was part of the effort by NASA-Lewis Research Center to understand and control defects produced by the radiation environment.

Recent work by J. W. Corbett[1] has shown that some of the major electron irradiation induced defects, which reduce solar cell efficiency, contain oxygen and/or carbon complexes (K-centers). Typical solar cell degradation can be minimized by either reducing carbon and oxygen levels or by introducing additional dopants such as lithium. Lithium acts to reduce the formation of defect complexes by migrating into vacancies and acting as a sink for interstitials. The approach utilized in this contract was to minimize carbon and oxygen impurities by selecting state-of-the-art float-zone silicon and by using state-of-the-art processes.

The objective of the work was to compare cells processed by ion implantation and pulse annealing with cells processed by conventional diffusion. It is the first time that cells manufactured by different methods have been compared using the same starting material and contacting process. The study included junctions processed with:

1. Diffusion
2. Implantation/furnace annealing
3. Implantation/laser annealing
4. Implantation/electron beam annealing

A very simple cell structure was employed to facilitate analysis of the pre- and postirradiation performance. The cells were processed without back surface fields or antireflection coatings, so that p+p degradation would not complicate the analysis of n+p junction performance measurements.

SECTION 2
TECHNICAL DISCUSSION

The major technical efforts under this contract emphasized procurement of a suitable silicon material, development of processing technology that could be utilized to manufacture cells without adding nonintentional dopants and testing of cell performance following electron irradiation. Each of these efforts is described in detail within the follcwing sections.

2.1 SILICON MATERIALS

Float-zone silicon specifications were initially defined to include carbon and oxygen contents less than 5×10^{15} cm^{-3}. However, discussions with each of the major silicon manufacturers resulted in realization that these specifications for carbon and oxygen could not be met without significant development in a laboratory environment. Of the two impurity specifications, carbon is the more difficult to meet, particularly for vacuum float-zone material.

2.1.1 Procurement

Preliminary discussions were arranged with Shin-Etsu Malaysia, Monsanto Electronic Materials Division, Hughes Industrial Products Division and Wacker Siltronic Corporation. None of these suppliers would accept a purchase order with this contract's specifications.

Hughes agreed to process high-resistivity, detector-grade silicon by implanting the rod, then float-zoning. This technique was developed under a materials development contract with Wright-Patterson AFB for radiation hardened solar cells. Hughes was, however, unwilling to accept a purchase order with carbon and oxygen specifications, and would quote on a best effort basis only. The Hughes production methods are not yet routine.

Monsanto's Electronic Materials division agreed that these specifications were attainable if a dedicated float-zone furnace were prepared and trial runs performed, but such a level of effort was beyond the scope of this contract.

Wacker Siltronic uses the Siemens, vacuum-float-zone method to produce dislocation-free material. Because of the oil-based diffusion pumps carbon concentrations have been higher than the level required for this program. Previous

samples have been measured by Spire to contain approximately 2.6×10^{16} cm^{-3} of carbon and 2×10^{16} cm^{-3} of oxygen. Wacker Siltronic has since installed oil-free vacuum pumps to minimize process-induced carbon impurities to a level close to the specifications for this contract. The measured carbon and oxygen impurity levels determined by Spire and others are summarized below:

Wacker FZ Crystal Resistivity (ohm-cm)	Measurement Technique	Measured Impurity Conc. (atoms/cm^3) Carbon	Oxygen	Measured by
1.0	Neutron Activation	—	1×10^{14}	[illegible]. 2
1.0	Neutron Activation	—	3×10^{15}	Ref. 2
1-10	IR	5×10^{15}	$1\text{-}5 \times 10^{15}$	Ref. 3
All	IR	5×10^{16}	1×10^{16}	Ref. 4
0.1	IR	2.6×10^{16}	2×10^{16}	Spire

Silicon rods were ordered from Wacker according to the specifications outlined in Table 2-1. Rods from Wacker were then sliced and polished. The starting wafers for cell processing had polished fronts and etched backs.

TABLE 2-1. SILICON MATERIAL SPECIFICATIONS FOR LOW-CARBON SOLAR CELL FABRICATION

Item	Specification
Material:	p-Boron doped
Orientation:	(100) $\pm$0.5 degrees
Diameter:	50 mm $\pm$0.5 mm Centerless ground and etched
Thickness:	300 micrometers $\pm$12 micrometers
Resistivity:	0.1, 1.0 and 10.0-ohm-cm $\pm$25%
Resistivity Tolerances	
Wafer to wafer:	$\pm$15%
Radial gradient:	$\pm$8%
Striations:	None
Dislocation Density:	None
Growth Technique:	Float-zone
Carbon Content[+]:	5×10^{15} cm^{-3}
Oxygen Content[+]:	5×10^{15} cm^{-3}

[+] Not all material met specifications; see Section 2.1.2.

2.1.2 Silicon Ingot Characterization

The carbon and oxygen concentrations of the 1.0 and 10 ohm-cm silicon ingots used as starting material for this contract were determined by infrared absorption measurements of specially prepared test crystals. The test crystals were polished slices of the ingot, 10 mm thick for oxygen content measurements, and 2 mm thick for carbon concentration determination. Both sides of each of the four test slices had to be optically polished and parallel to within 5 minutes of arc.

For an accurate determination of carbon and oxygen concentrations in float zone refined silicon, the sample must be measured with a double beam infrared grating spectrophotometer. A reference specimen prepared to the same tolerances as the test specimen is placed in the reference beam of the spectrophotometer. The reference specimen must have undetectable amounts of carbon and oxygen (usually achieved by multiple passes through a float-zone refining furnace). Since Spire did not have the necessary reference specimens, Wacker Siltronic Corporation agreed to perform the infrared absorption measurements. The oxygen concentration in both the 1.0 ohm-cm and 10 ohm-cm ingots was less than the detection limit of 5×10^{15} atoms cm^{-3}. The carbon concentration in the 1.0 ohm-cm ingot was 1.3×10^{16} atoms cm^{-3} and in the 10 ohm-cm ingot, 1.0×10^{16} atoms cm^{-3}.

The 0.1 ohm-cm silicon impurity characterization was performed by Dr. H. Gatos at MIT. Dr. Gatos measured the carbon and oxygen concentrations with a Nicolet Fourier transform infrared spectrophotometer. This instrument has a greater sensitivity and resolution than a standard infrared grating spectrophotometer and can more accurately measure the decreased infrared transmission of highly doped silicon. The results for 0.1 ohm-cm silicon were 2.6×10^{16} atoms cm^{-3} for oxygen, and 2.0×10^{16} atoms cm^{-3} for carbon.

2.2 CELL PROCESSING

The process parameters necessary to fabricate both ion-implanted and diffused-junction solar cells by means of state-of-the-art processes and starting material were determined. The objective was to provide the necessary samples for a comparison of the relative radiation tolerance of silicon solar cells fabricated by two processing

techniques: ion implantation and diffusion. Major emphasis was placed on minimizing the amount of carbon and oxygen introduced into the silicon during both process options. To simplify the comparisons, these cells did not have back surface fields or antireflection coatings. Fabricated cells have efficiencies of at least 8 percent AM0 and fill factors of at least 70 percent when processed according to the sequence shown in Table 2-2.

TABLE 2-2. PROCESS SEQUENCE OUTLINE FOR 2x2 cm SOLAR CELLS

Step	Description
Clean -	Sulfuric/peroxide
Clean -	Buffered HF
Clean -	Fronts only, UV/ozone etch
Inspection -	Wetting test (ASTM F21-65)
Ion implant -	2.5×10^{15} $^{31}P^{+}$ cm^{-2} 10 keV
Clean -	Both sides, UV/ozone etch
Anneal -	Furnace, laser or pulsed e-beam
Clean -	Sulfuric/peroxide
Clean -	Buffered HF
Postpulse anneal -	550°C - 2 hours
Clean -	Buffered HF
Evaporate Al -	Backs only
Alloy Al in furnace -	650°C - 15 min
Clean -	Fronts only, UV/ozone etch
Evaporate -	TiPdAg - both sides
Sinter contacts -	400°C - 5 min
Electroplate -	6 microns Ag
Sinter contacts -	400°C - 5 min
Saw -	2x2 cm

The geometry of the front surface junction-layer contacts was optimized for a sheet resistance of 100 ohms per square. The contact design of 2 x 2 cm has approximately one-half the shadowing and series resistance losses of previously available contact designs. Conventional photolithographic methods were used to define the junction-layer contacts, as shown in Figure 2-1. TiPdAg metallization was used for front contacts, and AlTiPdAg metallization was employed for ohmic back contacts. No p+ layer was included in the cell process, so that back surface field effects would not interfere with radiation damage analyses.

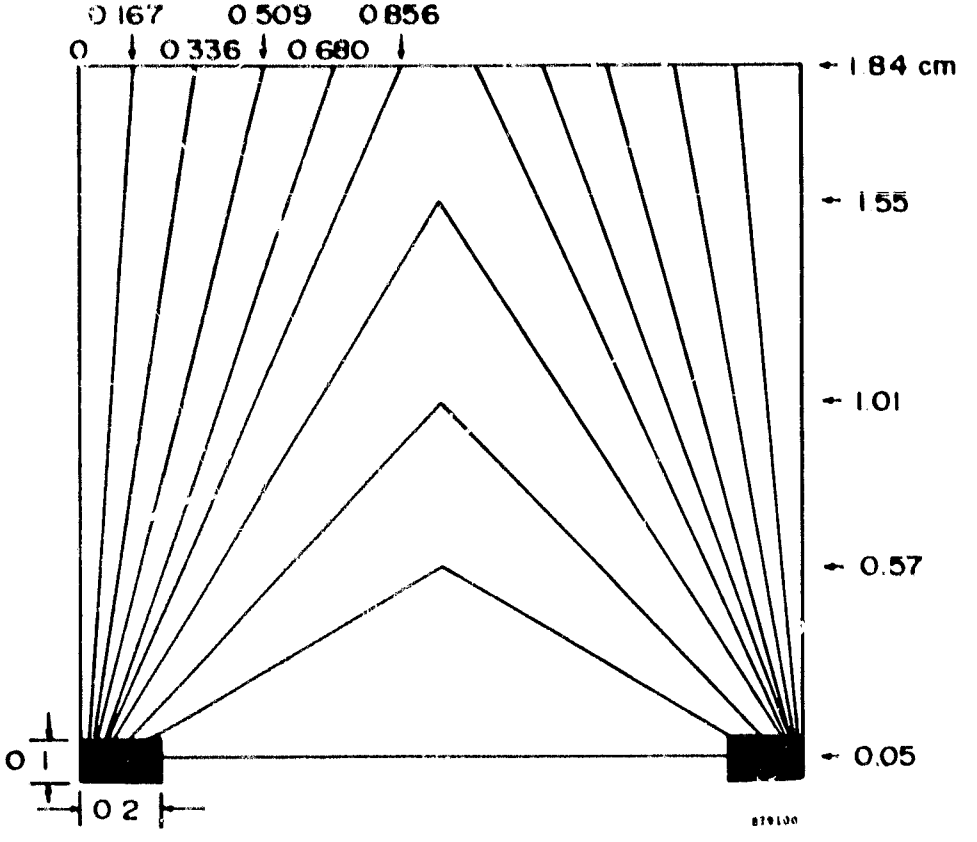

FIGURE 2-1. FRONT CONTACT GRID DESIGN FOR 2x2 cm SOLAR CELLS

2.2.1 Wafer Cleaning Procedures

To avoid the contamination of the junction region by surface contaminants, it was imperative that the silicon surfaces be absolutely clean prior to cell processing. The most important cleaning step took place just prior to ion implantation, when any surface contaminants can be "knocked on" into the silicon by the 10 keV phosphorus ions. Also during high-temperature processing, such as furnace annealing, surface contaminants can diffuse into the bulk if they are not first removed by adequate cleaning. Likewise, the adhesion of evaporated metallization on silicon is affected by surface contaminants.

The wafers were initially cleaned in a hot sulfuric acid/hydrogen peroxide solution followed by a buffered HF dip and DI rinse. Immediately preceding ion implantation, anneal or metal evaporation, the wafers were cleaned by intense shortwave UV radiation in air to remove any remaining monolayers of organic contaminants. The UV cleaning procedures we utilized were similar to those used at Sandia Laboratories, developed by Mattox et al.[5,6,7] An Ultraviolet Products Inc. Model R-52 Mineralight lamp was purchased for this application.

Clean surfaces were tested for hydrophobic contaminants using a water droplet wetting test according to ASTM specification F 21-65. This test will detect less than one monolayer of organic contaminant on a polished surface. Exactly what fraction of a monolayer remains on the surface is difficult to determine, but exposure to UV radiation for less than 1 minute will consistently clean surfaces to less than 0.1 monolayer of contamination.[8]

2.2.2 Ion Implantation

Solar cells processed under this contract were ion-implanted at Spire Corporation using the Extrion Model 200-1000 WF system. As delivered, this facility was equipped with oil-diffusion vacuum pumps and minimal trapping. Initial calculations indicated that high-dose ion implantation could contaminate wafers with carbon. To avoid this carbon contamination, the oil-diffusion vacuum pump on the wafer process chamber was replaced with an oil-free cryopump, and oil traps were added to the roughing pumps. Experiments were then performed to measure the level of contamination.

The source of the carbon contamination is the partial pressure of oil molecules in the vacuum system, which are generally present from the tetramethyltetraphenyl trisiloxane (DC 704) silicone diffusion pumping fluid. During the time required for a high-dose (greater than 10^{15} ions cm^{-2}) ion-implant, films several hundred angstroms thick can be deposited on the wafer surface. Carbon atoms can then be introduced into the lattice by a "knock-on" process. "Knock-ons" occur when an incident ion, phosphorus in our case, collides with a carbon atom on the surface of the wafer and transfers enough of its energy to the carbon atom to implant the atom to a significant depth in the silicon lattice. The calculation[9] indicated that the carbon contamination by knock-on implantation, due to the presence of diffusion pump oil in the end chamber, could be as high as 10^{18} carbon atoms cm^{-3}, two orders of magnitude greater than the bulk impurity concentration of 5×10^{15} carbon atoms cm^{-3}.

This calculated result implied that the high-vacuum pump in the implanter end station had to be changed. Before doing so, two other sources of contamination were considered: (1) diffusion of hydrocarbon vapors from other parts of the vacuum system in the implanter, and (2) surface films on the wafer. The amount of oil vapor from the mass analyzer segment of the ion implanter that enters the end station is limited by an aperture. The contribution from this additional source of oil vapor to knock-on implantation of carbon was calculated to be less than 5×10^{14} carbon atoms cm^{-3}. This contamination level, 10 percent that of the bulk concentration, was assumed to be acceptable.

The second source of contamination, a native oxide surface film, was reduced by cleaning the wafers just prior to insertion in the implanter. The SiO_2 density is 9×10^{22} atoms cm^{-3} [10]; therefore, 20A of native oxide, typical for silicon[11], will have a total of 1.4×10^{16} atoms cm^{-2}. Since the probability of a knock-on collision between a high-energy ion and any one atom in the target is very small, this 20A film would not contribute any significant oxygen or carbon to the bulk concentration for the 2.5×10^{15} $^{31}P^{+}$ cm^{-2} implant dose used. Also, the sputtering action of the implanter ion beam, assuming a sputtering coefficient near one, would reduce the surface concentration of oxygen and further reduce contamination in the solar cell.

To test the results of the theoretical study and obtain accurate information about knock-on carbon implantation, experiments were performed to measure the carbon content of implanted junctions and correlate the results with measurements of hydrocarbons in the end station. A residual gas analyzer (mass spectrometer) was used to detect the presence of hydrocarbons in the implanter end station, and secondary ion mass spectroscopy (SIMS) was investigated to determine if the carbon sensitivity of this technique is adequate to measure the low-level, knock-on concentration in silicon.

The schematic of the ion implanter's modified wafer process chamber vacuum system is shown in Figure 2-2. Modifications included the substitution of a cryopump for an oil diffusion pump and the addition of copper mesh oil traps on all of the roughing pumps. The source and analyzer regions of the implanter still have oil diffusion pumps, but the DC 704 diffusion pump fluid has been replaced with a lower vapor pressure silicone pump fluid, DC 705. The wafer process chamber and analyzer regions are joined by an aperture (0.7 cm^2) that has a sufficiently low conductance to limit the flow of hydrocarbon molecules into the wafer process chamber.

A Spectrum Systems Model M1000 residual gas analyzer has been used to compare the cleanness of the vacuum in the process chamber before and after the addition of a cryopump and foreline trap. Figure 2-3 shows the major gas species present in the diffusion pumped end station. The higher m/e spectrum was particularly rich. (Some gases, such as chlorine, are residues of compounds used in the ion implanter source and are normally not found in the end station. Their presence, unlike hydrocarbons from pump oil, diminished with time as the system outgassed.) A mass spectrum after modifications were made to the end station is shown in Figure 2-4. The partial pressure of major gas species, as shown, is a factor of 10 to 100 less. Hydrocarbon contamination has apparently been reduced below 0.5×10^{-8} torr.

Before cells were processed, clean wafers (free of hydrophobic contaminants) were cycled through the wafer process chamber, remaining in the chamber long enough to simulate actual implant time. These wafers were tested for hydrophobic contaminants after their removal from the process chamber. The wetting test, performed according to ASTM specification F21-65, did not detect any hydrophobic contaminants on the wafer surface. The same test was also performed to determine if any hydrophobic contaminants were on the wafer following a 10 keV phosphorus implant, 2.5×10^{15} ions cm^{-2}, and none were detected.

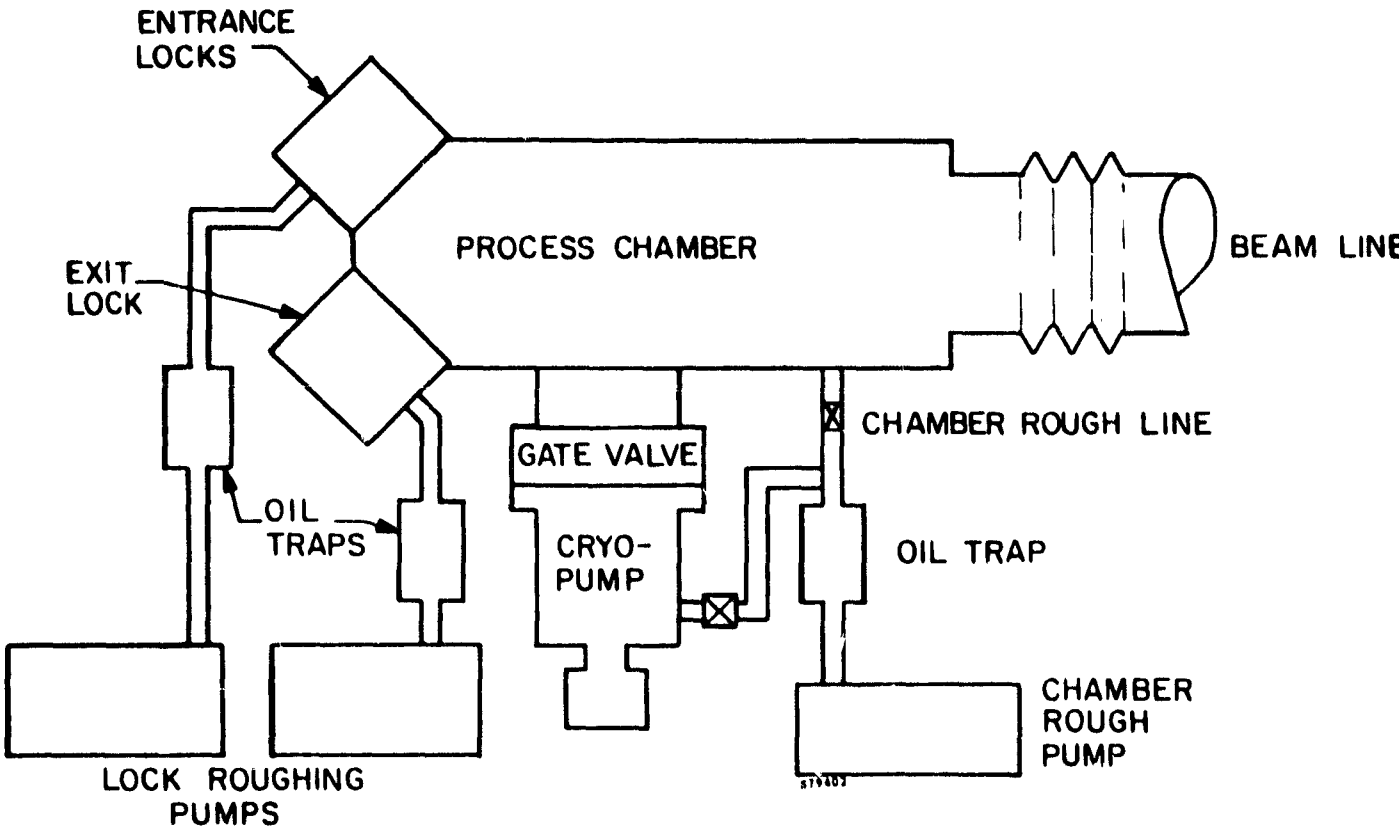

FIGURE 2-2. SCHEMATIC DIAGRAM OF THE ION IMPLANTER END STATION VACUUM SYSTEM

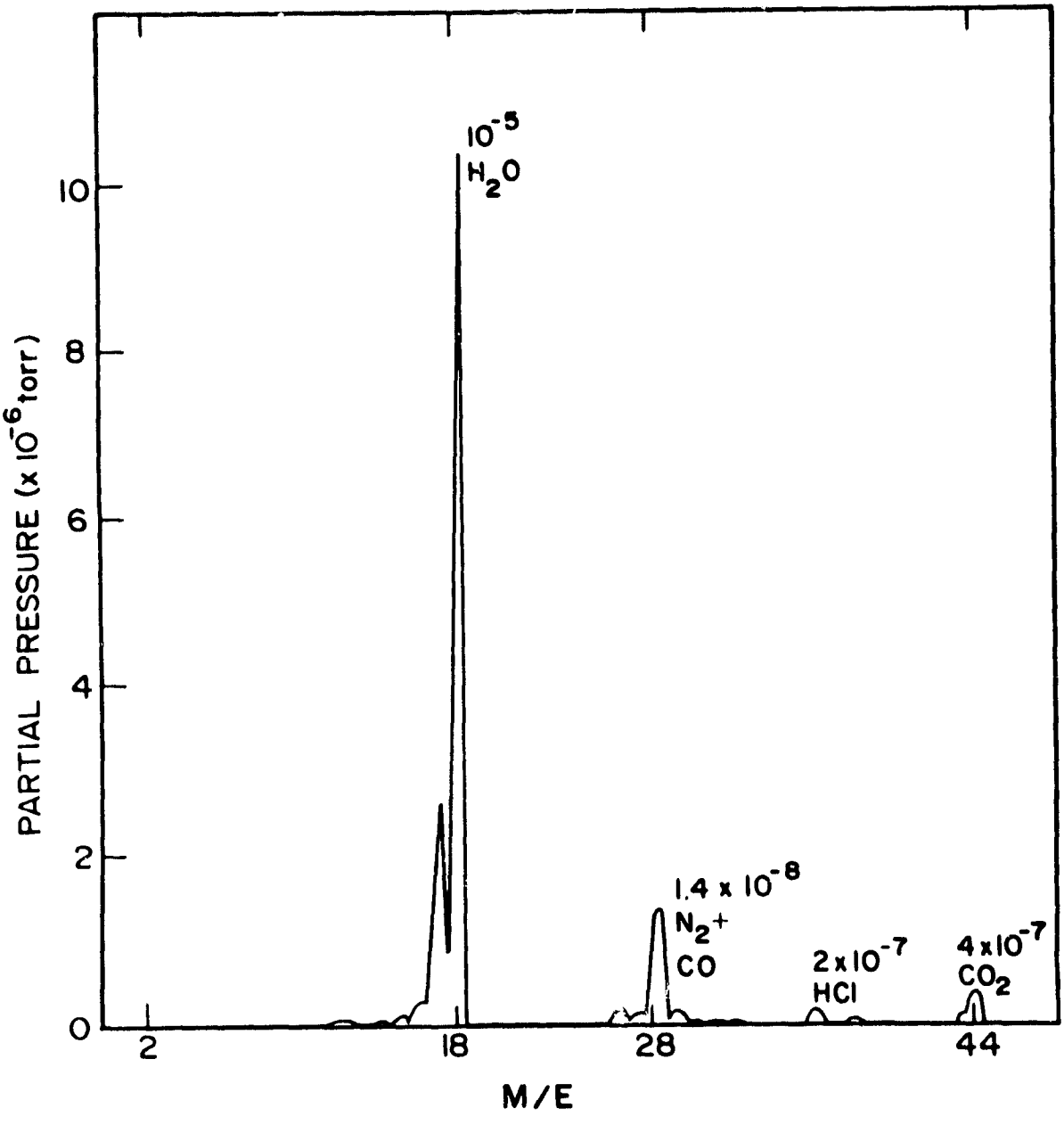

FIGURE 2-3. RESIDUAL GAS ANALYZER SCAN OF THE ION IMPLANTER END STATION WITH AN UNTRAPPED DC 704 OIL DIFFUSION PUMP

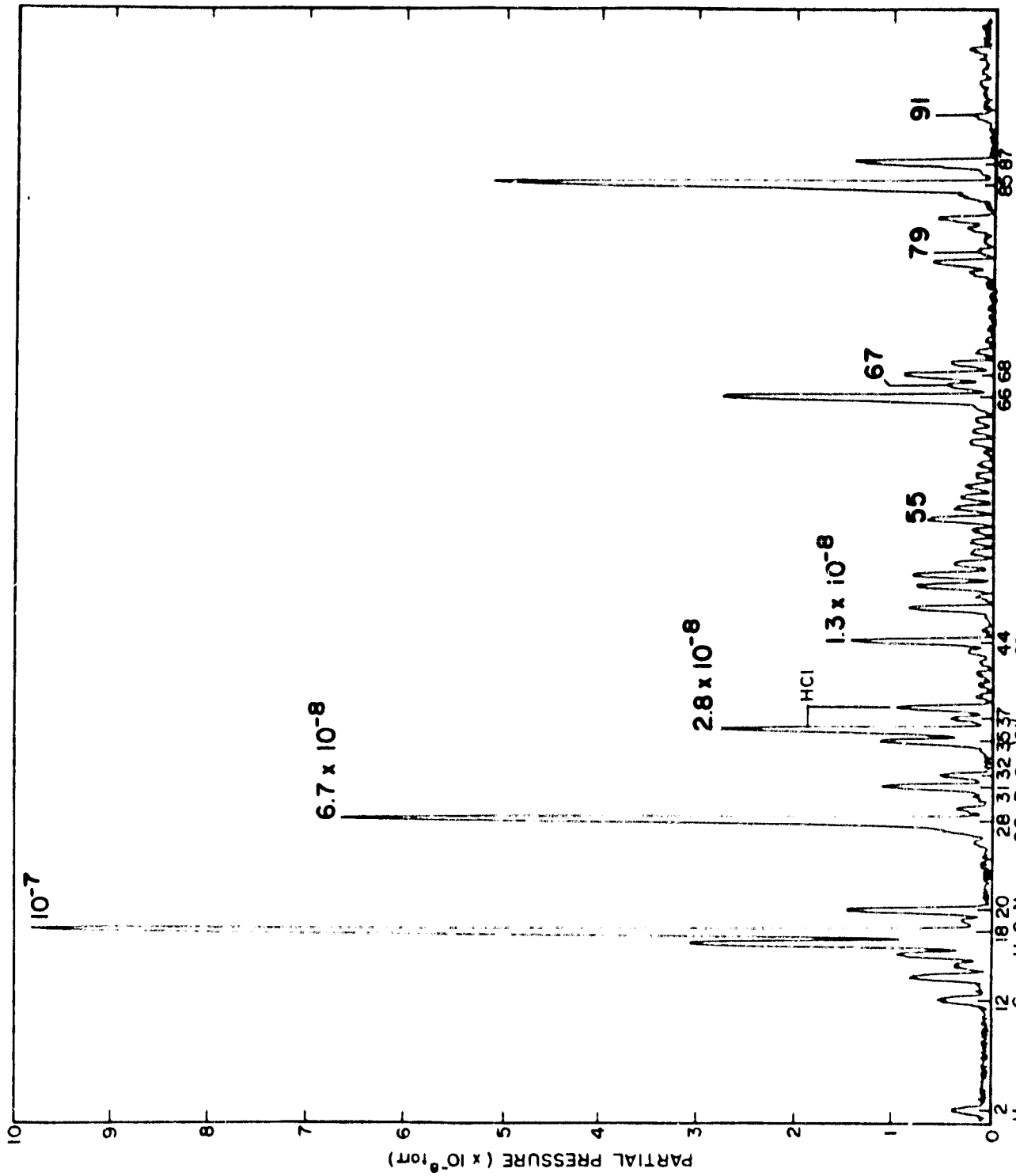

FIGURE 2-4. A RESIDUAL GAS ANALYZER SCAN OF THE ION IMPLANTER END STATION WITH A CRYOPUMP VACUUM SYSTEM

2.2.3 Pulse Annealing

A high-vacuum wafer process chamber was designed at Spire for laser annealing. The construction of this chamber was postponed until experiments proved that a vacuum was necessary to prevent oxygen and carbon contamination of the implanted layer by the laser annealing process. At this time laser annealing is performed routinely in air without increasing oxide growth beyond that which is nascent.

We have annealed ion implant damage in silicon (in air) with two types of Nd:YAG lasers. The difference between the two lasers is the beam size and operating wavelength. The first laser, at Quantronix Corporation, uses a 50 micrometer diameter beam that must be scanned across a wafer to anneal the entire surface. The beam has a repetition rate of 5 kHz, and each 50 micrometer spot must overlap the preceding spot by approximately 50 percent to compensate for the nonuniformities of the beam. With the existing X-Y translation equipment at Quantronix, a 10 x 10 cm area can be annealed in 36 minutes. This laser can be used in either the 1.064- or 0.532-micrometer wavelength mode, but all annealing was performed at 0.532-micrometer wavelength.

The second laser, at Battelle Columbus, is also a Nd:YAG type, but has a beam size greater than 5 cm in diameter. An entire 5.08 cm diameter wafer is annealed in a single pulse (30 nanoseconds) with a fluence of 3 J/cm^2; this laser was operated in the 1.06-micrometer mode. Figure 2-5 shows a resistivity map of a wafer annealed with this laser. Resistivity maps are routinely used in determining the uniformity of ion-implant annealing when sheet resistivities are measured using a Veeco four-point probe.

A pulsed electron beam anneal (PEBA) resistivity map is shown in Figure 2-6. A 3-inch diameter silicon wafer was implanted with arsenic (implant uniformity is ± 1 percent) and pulse annealed with a 3-inch diameter electron beam in 0.1 microsecond. The resistivity map was obtained by repeated four-point probe measurements. Two-inch diameter wafers processed under this contract have slightly better uniformity, since only the center 2 inches of the beam are utilized. Electron beam processing was the only anneal to be done under vacuum; the vacuum chamber was pumped to 1×10^{-5} torr with a trapped oil diffusion pump.

All pulse annealing was optimized to give sheet resistances of the n^+ region of less than 50 ohms/square. This assured almost complete activation of the implanted phosphorus.

SPIRE 05-29/79 PHOSPHOROUS

WAFER NO. 2030-3 1.2 PERCENT

AVERAGE RESISTANCE 48.5 OHMS/SQUARE

STD. DEV. = +/- 2.56 RANGE =+/- 5.13 OHMS/SQUARE

IMPLANT CONDITIONS-

TILT-10 ENERGY= 10KEV FLUENCE=2.50E15 /CM2

IMPLANT SPEC- ANNEAL SPEC- LASER

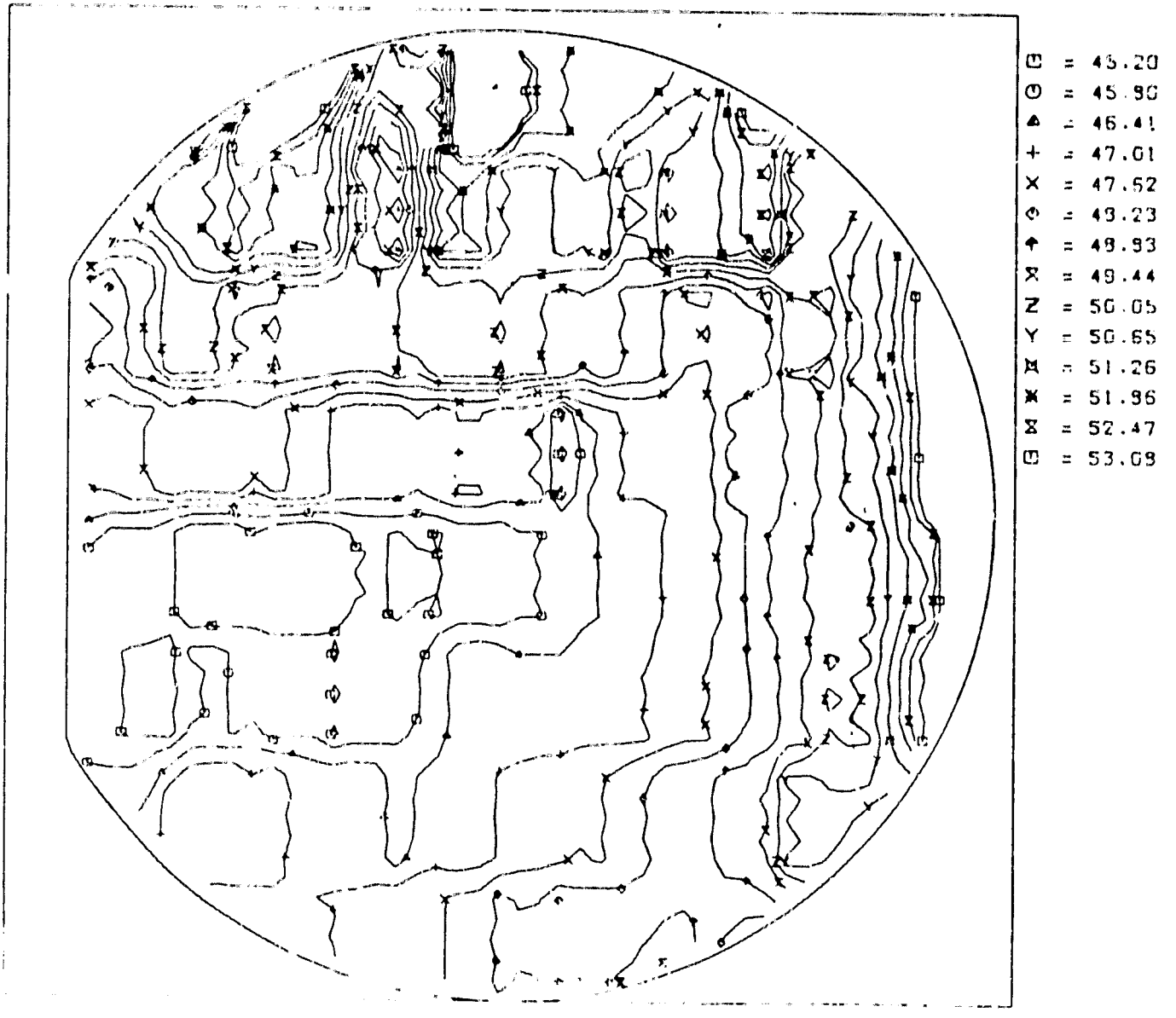

FIGURE 2-5. SHEET RESISTANCE CONTOUR MAP FOR ION IMPLANTED/ LASER ANNEALED (SINGLE-PULSE) JUNCTION

SPIRE 06/22/79 ARSENIC RS

WAFER NO. 2055-6

AVERAGE RESHEET)=34.5 OHMS/SQUARE

STD. DEV. = +/-3.73 RANGE =+/- 7.45 OHMS/SQUARE

IMPLANT CONDITIONS-

TILT= 7 ENERGY= 25KEV

ANNEAL SPEC- PEBA 280

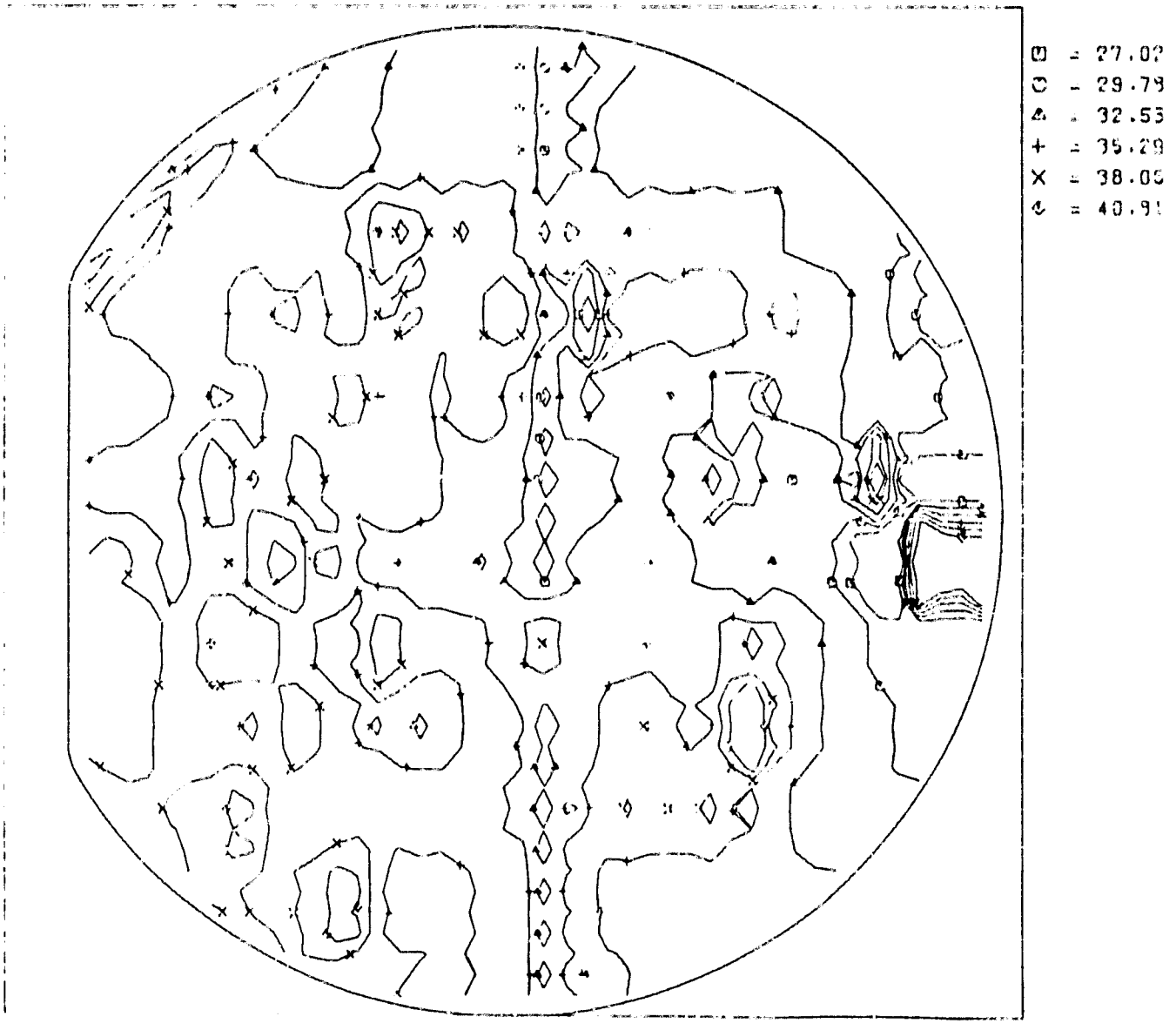

FIGURE 2-7. RESISTIVITY MAP FOR A PEBA ANNEALED WAFER

2.2.4 Diffused Junction Solar Cells

All phosphorus diffused cells were fabricated at Applied Solar Energy Corporation (formerly OCLI) under subcontract to Spire. These cells were made with the same silicon and metallization geometry as the ion-implanted cells made at Spire.

2.3 SOLAR CELL PERFORMANCE MEASUREMENTS

All measurements reported were performed under AM0-25°C conditions using a Spectrolab X25-Mk II simulator and a NASA-LeRC secondary standard cell for calibration of intensity. Cell temperature was held to within $\pm 1^{\circ}$C of 25°C by a suitable test block.

Typical AM0 I-V characteristics for implanted and furnace or pulse annealed, as well as diffused junction cells, are shown in Figures 2-7 through 2-11 for 0.1, 1.0 and 10 ohm-cm substrates. Prior to electron irradiation, the curve factors were, in general, poor for 0.1-ohm-cm substrates due to large junction recombination currents. Open-circuit voltage for the 0.1-ohm-cm cells was lower than for previously implanted cells processed by Spire because of surface recombination.[12] For example, 0.64V open-circuit voltages are typical for implanted cells when annealed in an oxidizing atmosphere resulting in a low surface recombination velocity. The process utilized for the 0.1-ohm-cm cells was identical to the conventional nitrogen anneal process, and no voltage enhancement was obtained.

Of all cells processed, the highest efficiency devices were ion implanted and furnace annealed. Cells processed by diffusion had equivalent efficiencies for 10-ohm-cm substrates, but were not as efficient for 0.1- and 1-ohm-cm substrates. Figure 2-12 shows the maximum cell efficiencies for all substrate resistivities and all processes employed. The performance trend for implanted/furnace annealed cells shows increasing efficiency with higher substrate doping; however, this trend would be reversed had a BSF been included in the cell structure. At the 10-ohm-cm level there is little spread between diffused and implanted cells with the exception of the pulsed electron beam annealed cells. This performance limitation is attributed to the use of a nonoptimized electron beam, which heated a much deeper region than the lasers (see Section 2.3.2).

Junction depths were determined by grooving and staining with results as shown in Figure 2-13. Since furnace annealing produces a sharp phosphorus dopant profile, the junction depth did not change with resistivity. The other junction formation processes produce a more gradual phosphorus profile, which results in a variation of the junction

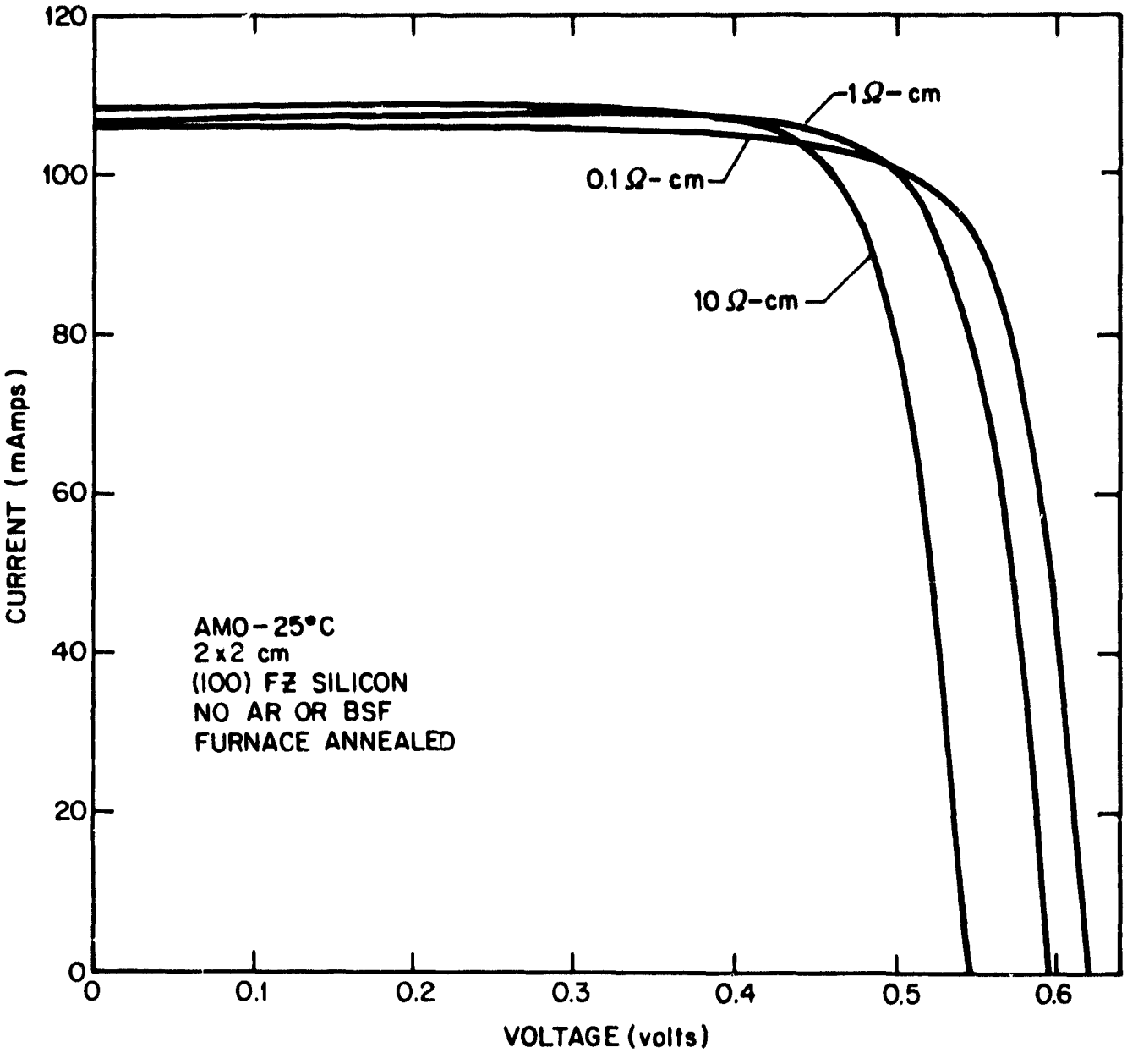

FIGURE 2-7. I-V CHARACTERISTICS OF AN n^+p ION IMPLANTED/ FURNACE ANNEALED SOLAR CELL WITH 0.1, 1.0 AND 10 ohm-cm SUBSTRATES

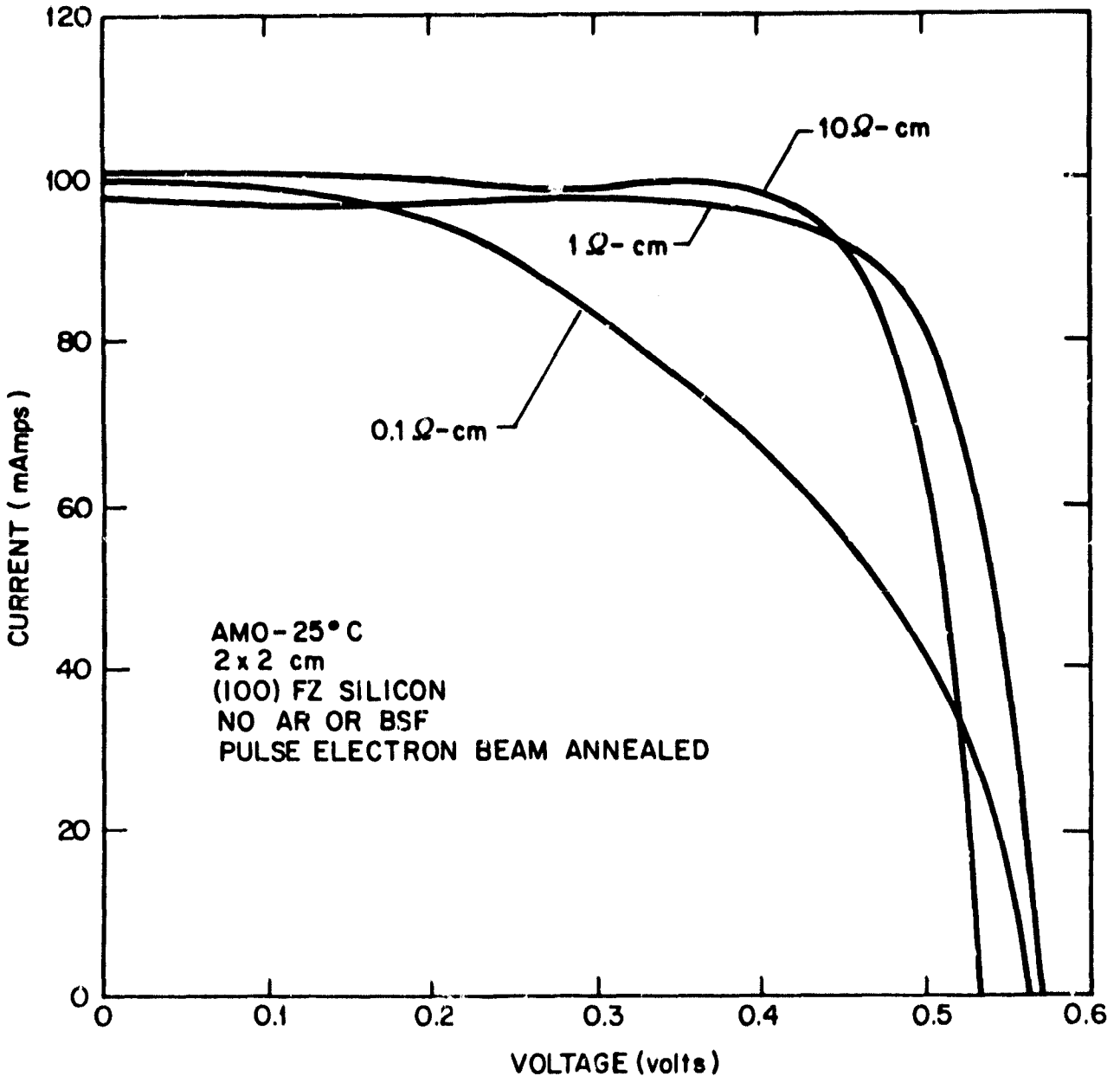

FIGURE 2-8. I-V CHARACTERISTICS OF AN n^+p ION IMPLANTED/ PULSED ELECTRON BEAM ANNEALED SOLAR CELL WITH 0.1, 1.0 AND 10 ohm-cm SUBSTRATES

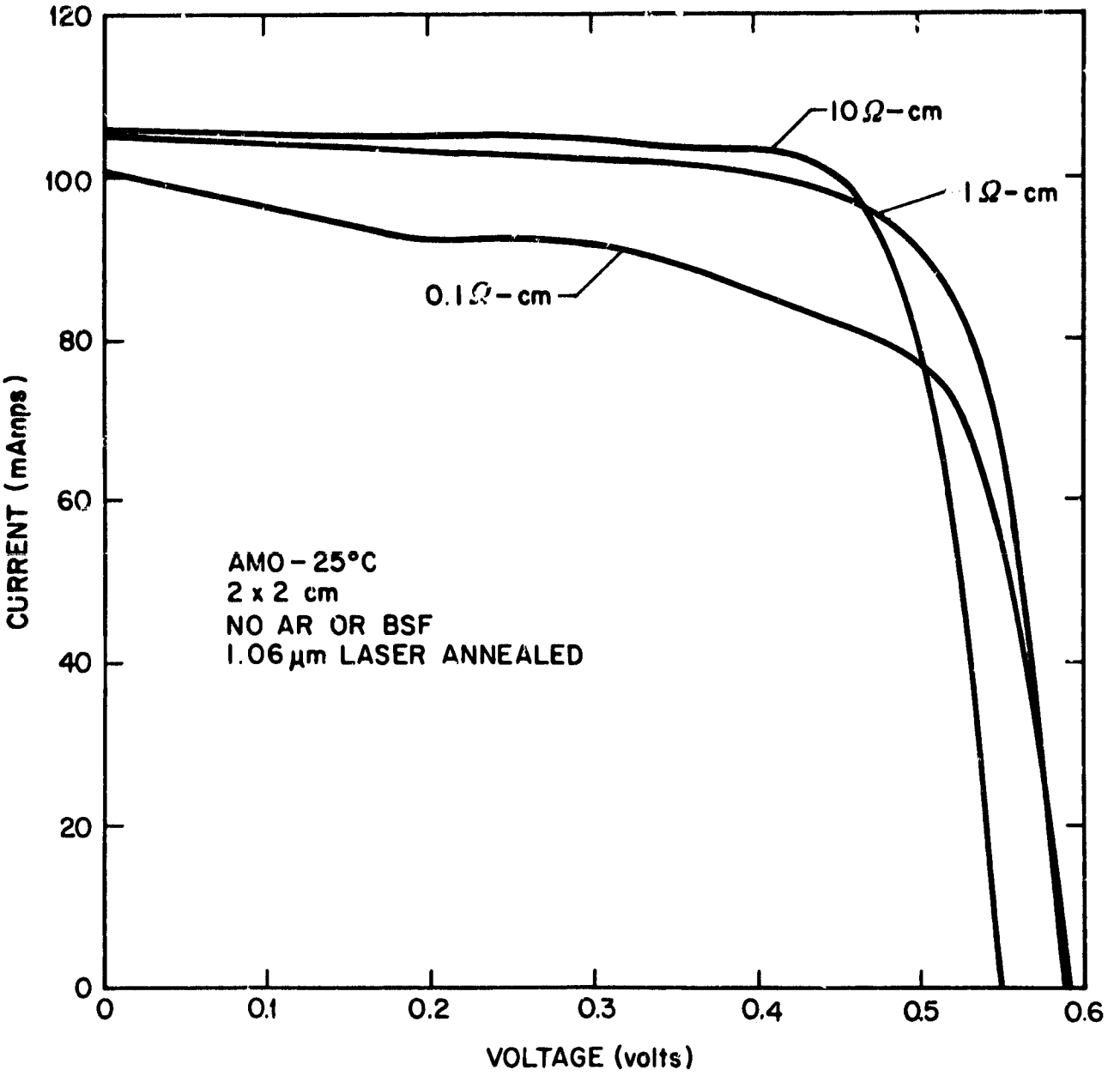

FIGURE 2-9. I-V CHARACTERISTICS OF AN n^+p ION IMPLANTED/ 1.06 MICRON LASER ANNEALED SOLAR CELL WITH 0.1, 1.0 AND 10 ohm-cm SUBSTRATES

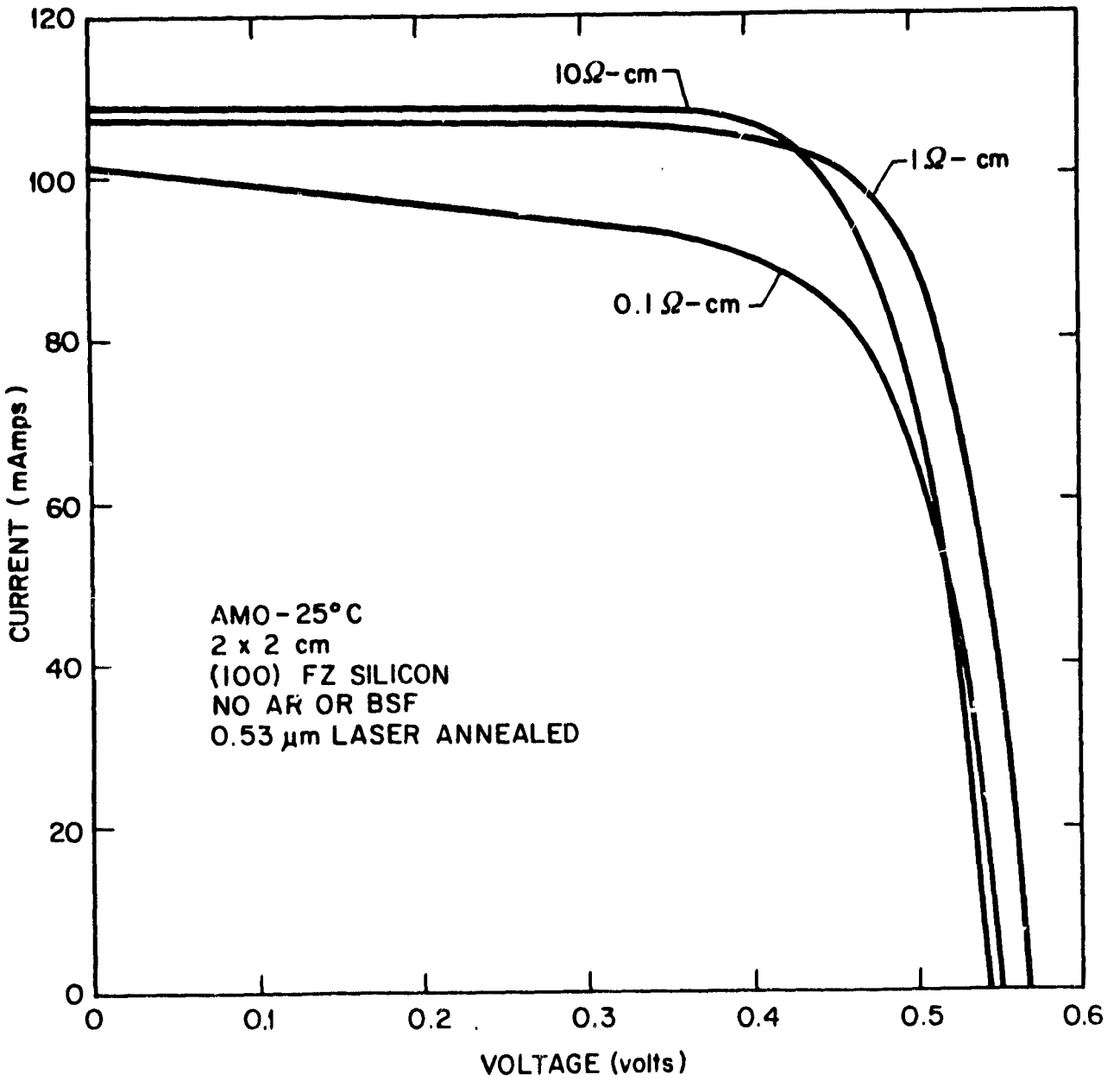

FIGURE 2-10. I-V CHARACTERISTICS OF AN n^+p ION IMPLANTED/ 0.53 MICRON LASER ANNEALED SOLAR CELL WITH 0.1, 1.0 AND 10 ohm-cm SUBSTRATES

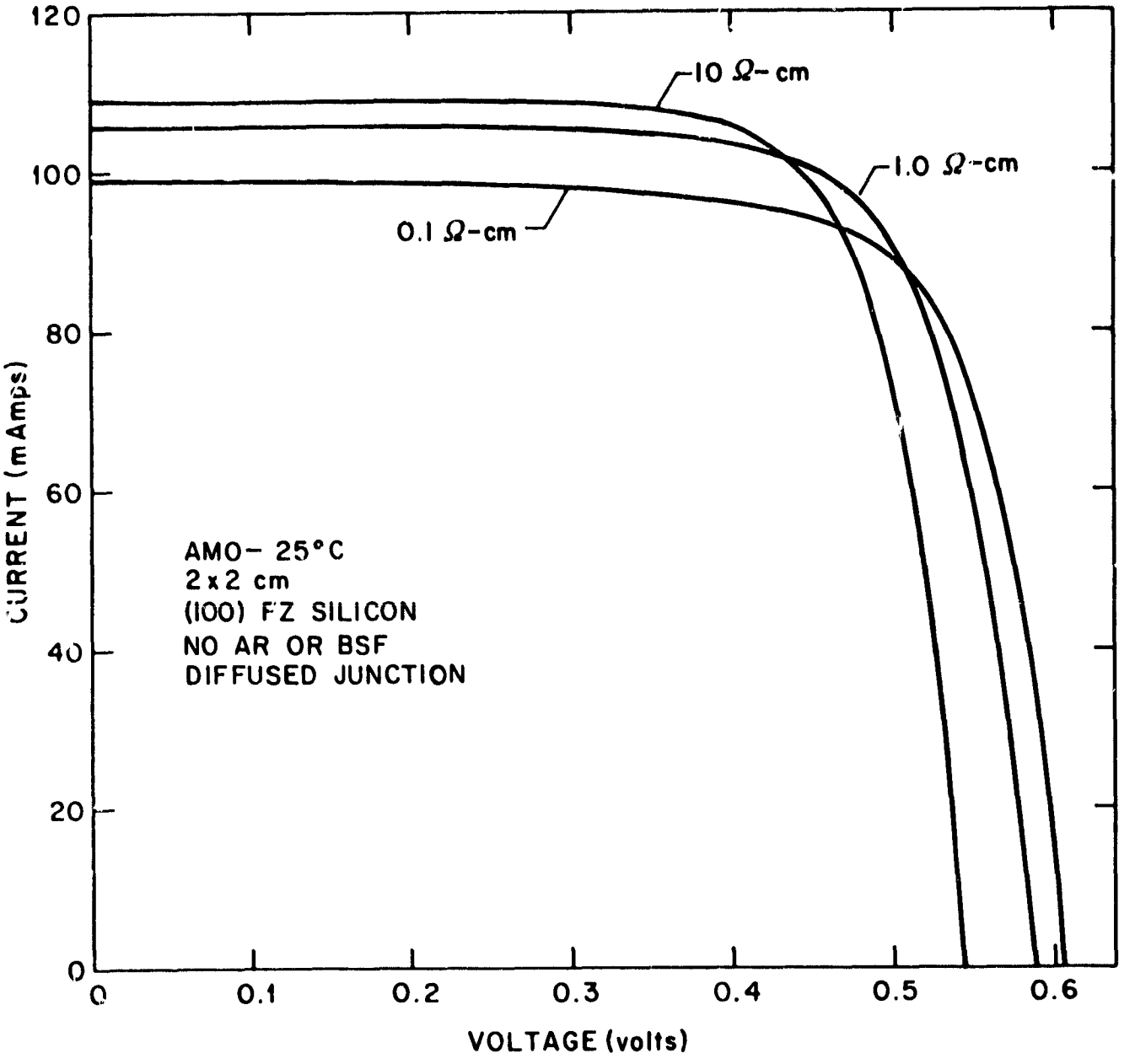

FIGURE 2-11. I-V CHARACTERISTICS OF AN n^+p DIFFUSED JUNCTION SOLAR CELL WITH 0.1, 1.0 AND 10 ohm-cm SUBSTRATES

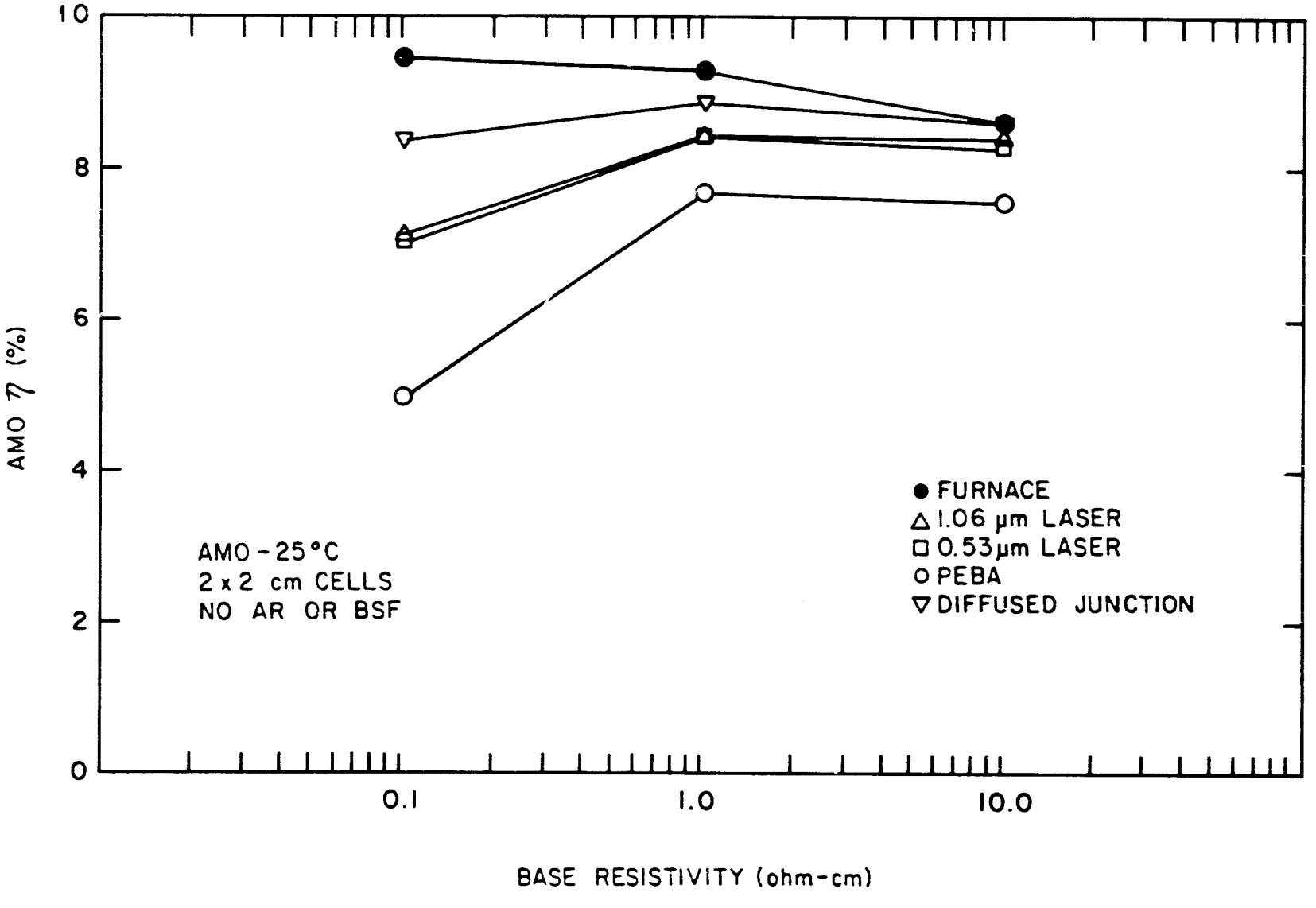

FIGURE 2-12. MAXIMUM AMO CELL EFFICIENCIES ATTAINED FOR EACH ANNEAL TYPE AND SILICON BASE RESISTIVITY

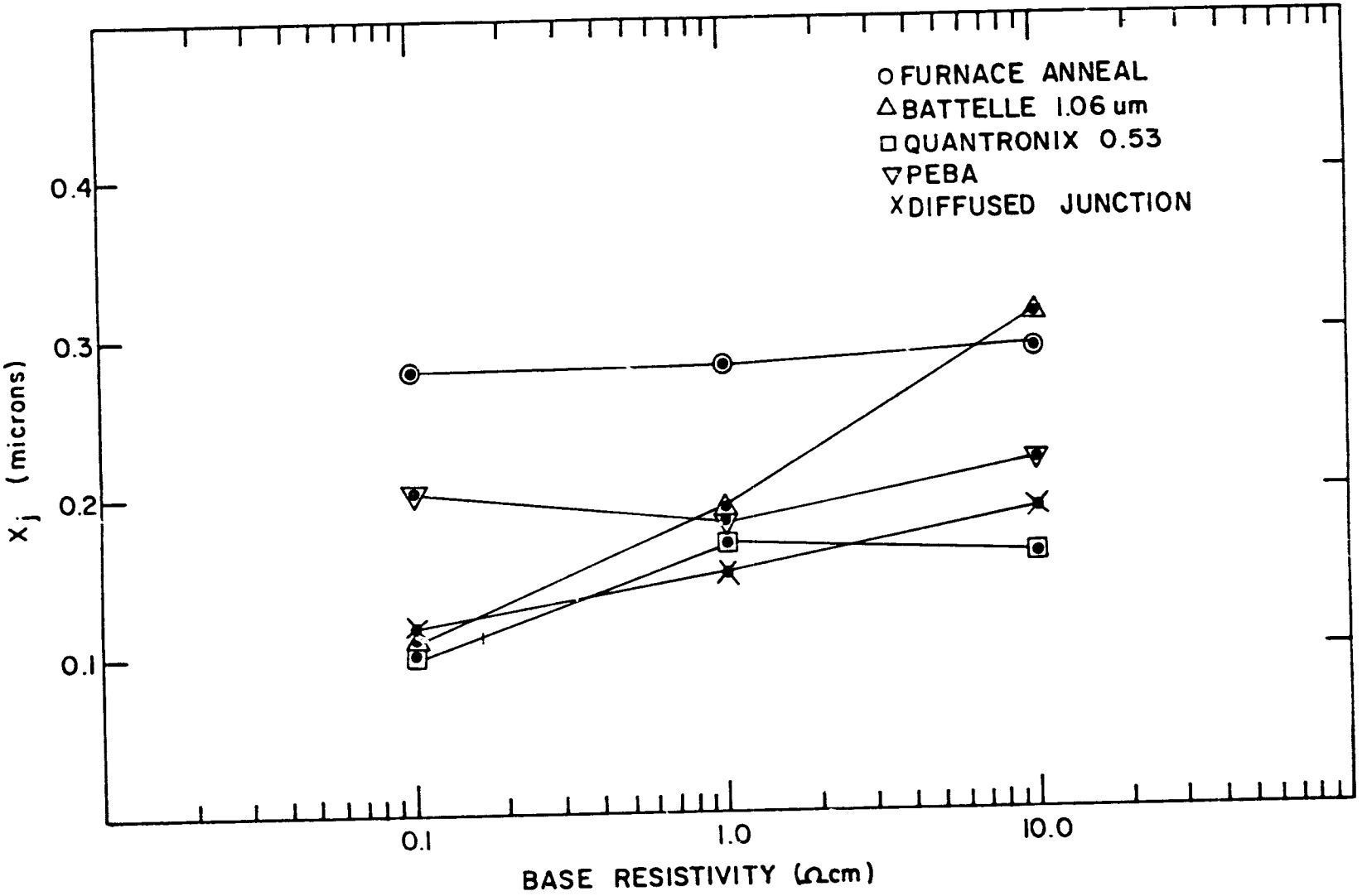

FIGURE 2-13. MEASURED JUNCTION DEPTHS FOR EACH ANNEAL TYPE AND SILICON BASE RESISTIVITY

depth with substrate doping level. Characteristic junction depths are important for the interpretation of postirradiation cell performance, as discussed in Section 2.3.2. Additional preirradiation cell performance data are given in Appendix 1 of this report. These figures show average and maximum-minimum performance data.

2.3.1 Carbon and Oxygen Detection

A sensitive diagnostic method for surface induced carbon and oxygen contaminants was desired, so that knock-on carbon — from adsorbed hydrocarbons — and knock-on oxygen — from thin native oxides — could be determined within the junction and depletion regions of the completed solar cells.

Because the ASTM specifications describing infrared absorption in silicon do not apply for silicon slices less than 2 - 10 millimeters thick, small concentrations of carbon and oxygen near the surface of a wafer cannot be measured by the infrared absorption technique. The infrared absorption technique is not applicable to detecting small amounts of carbon and oxygen that are introduced into 300 micrometer thick wafers during processing. SIMS is the only analytical service available that can detect and measure small concentrations (1 ppm) of carbon and oxygen near the surface of single crystal silicon. Both carbon and oxygen profiles can be determined by the SIMS method.

The detection limit prior to changes in the SIMS vacuum chamber for carbon and oxygen was 10^{17} atoms cm^{-3}, but modifications were made to increase detection limits with a goal of 10^{15} atoms cm^{-3} of sensitivity.

Figure 2-14 shows the SIMS impurity profiles of an unprocessed silicon wafer before vacuum system improvements were made. The large amounts of carbon and oxygen apparent on the surface are due to the nascent oxide and residual organics. Background impurity levels, 10^{18} carbon cm^{-3} and 3×10^{18} oxygen cm^{-3}, are from the SIMS vacuum chamber, not the silicon crystal. The large SiH peak at the surface is from adsorbed water vapor.

This sample was chemically cleaned in sulfuric acid/hydrogen peroxide and buffered HF prior to storage in a plastic container for shipment to Charles Evans and Associates for SIMS analysis. The surface contamination is from exposure to laboratory air following the cleaning process.

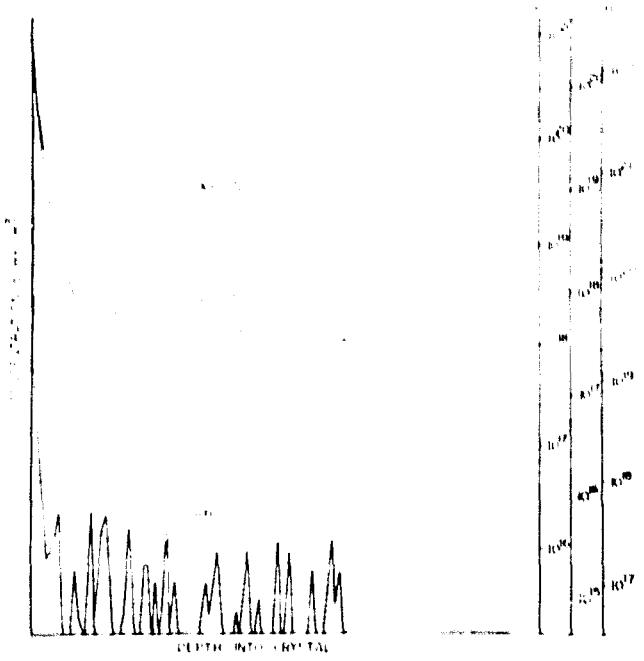

FIGURE 2-14. SIMS PROFILES OF AN UNPROCESSED, SILICON CONTROL WAFER BEFORE MODIFICATION OF THE SIMS VACUUM SYSTEM

Impurity profiles of two additional wafers, both phosphorus implanted (when the diffusion pump was on the implanter end station) to a dose of 2.5×10^{15} ions cm^{-2} at 10 keV, were also measured by the SIMS technique. One was annealed in nitrogen, the other in dry oxygen at 850°C for 15 minutes to introduce oxygen intentionally. Following the anneal step, both wafers received a sulfuric/peroxide clean followed by an HF dip to remove any oxide. A third unimplanted wafer was used as a SIMS control sample.

The carbon, oxygen and phosphorus profiles for each of the three wafers are shown in Figures 2-15 and 2-16. The unimplanted wafer (Figure 2-16) has large peaks of carbon and oxygen near the surface. These peaks are probably caused by organic compounds adsorbed on the wafer surface from the ambient, not the SIMS vacuum chamber. When the surface is exposed to the primary ion beam (15 keV $^{133}Cs^{+}$) used for sputtering, some of the carbon and oxygen adsorbed on the surface is mixed into the first 500A of silicon by a "knock-on" process that is similar to that which takes place during phosphorus ion implantation. The carbon and oxygen peaks knocked into the silicon lattice by SIMS have obscured measurement of carbon and oxygen induced by the phosphorus implantation.

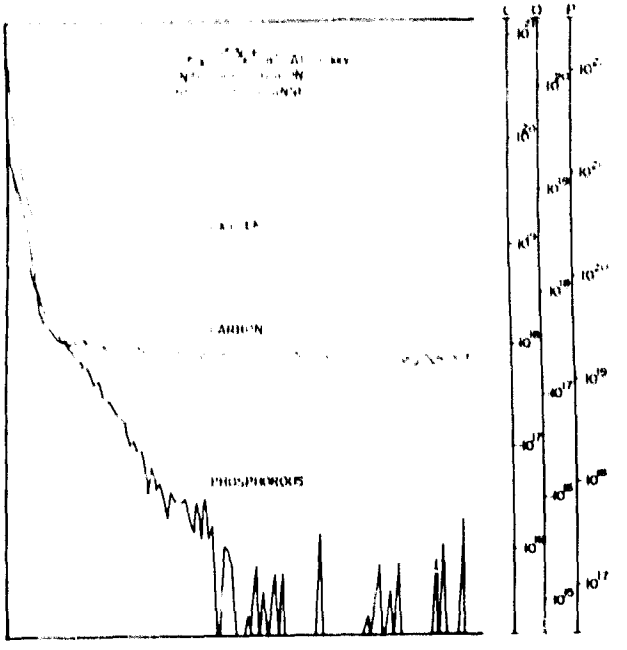

FIGURE 2-15. SIMS IMPURITY PROFILES OF PHOSPHORUS IMPLANTED SILICON ANNEALED IN OXYGEN

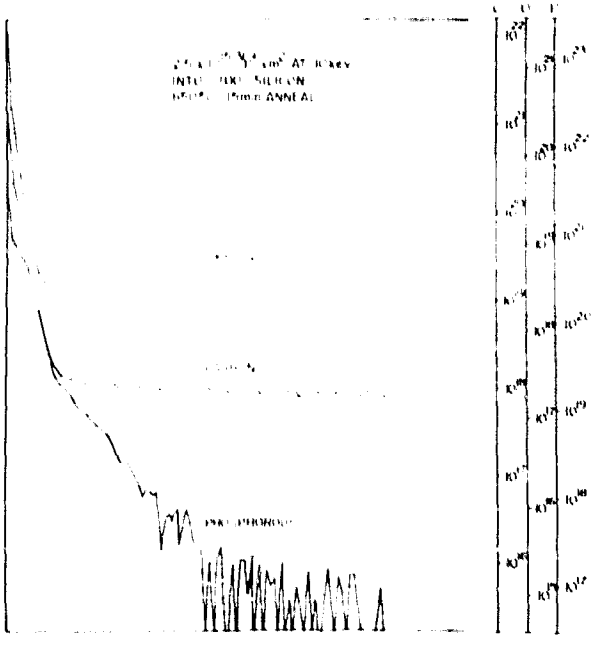

FIGURE 2-16. SIMS IMPURITY PROFILES OF PHOSPHORUS IMPLANTED SILICON ANNEALED IN NITROGEN

The same samples were analyzed again by SIMS after modifications were made to the vacuum chamber of the analyzing instrument to reduce residual hydrocarbon levels. The samples were HF and UV/ozone cleaned prior to their insertion into the SIMS vacuum chamber. The results of these analyses are shown in Figures 2-17 through 2-20. The apparent thickness of the native oxide layer and adsorbed hydrocarbons is reduced compared to Figures 2-15 and 2-16. No carbon or oxygen was detected in the junction region down to the maximum depth analyzed (approximately 1500A). The background levels of carbon and oxygen (between 0.5 and 1.0×10^{16} cm^{-3}) were greatly improved over the last analysis, but were still a factor of 2 to 10 higher than measured bulk concentrations (Section 2.1.2).

2.3.2 Junction Profiles

Boron and phosphorus impurity profiles in cells representative of those delivered to NASA were measured by the SIMS technique. Figures 2-21 through 2-23 show the distribution of boron (the substrate dopant) at the front surface of the cells. Most of the cells have some boron accumulated at the front surface, probably gettered as a result of the high concentrations of phosphorus present. The pulsed electron beam annealed (PEBA) samples have larger amounts of boron accumulated at the surface, perhaps due to the longer time at melt temperature the front surface is exposed to during electron pulsing and deeper phosphorus profile. There is a deep (0.2 micrometer) accumulation of boron in the 0.1 ohm-cm PEBA annealed samples that may contribute to their poor junction electrical characteristics. Phosphorus profiles of the same cells are shown in Figures 2-24 through 2-26. Of special interest are the phosphorus profiles of the PEBA samples, where a wide peak of phosphorus is evident at the surface. This peak would explain the wide boron peaks for the same samples, since boron is gettered by high concentrations of phosphorus. It is also significant that the accumulated boron concentration is within 10^{17} to 10^{18} cm^{-3} for all junction processes and all starting material resistivities.

2.3.3 Radiation Testing at Spire

Three cells of each process type and silicon resistivity were tested for radiation resistance. The cells were subjected to 1 MeV electrons up to a total dose of 1×10^{16} e^{-} cm^{-2}. All irradiations were performed at the USAF Hanscom Dynamitron Laboratory in Bedford, Massachusetts.

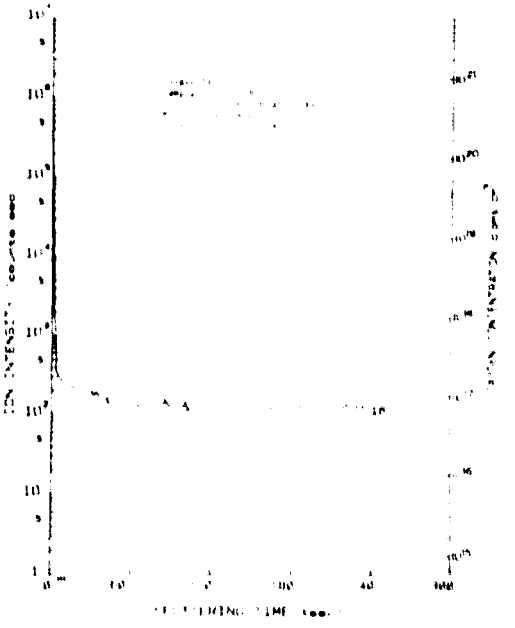

FIGURE 2-17. SIMS OXYGEN PROFILE IN PHOSPHORUS IMPLANTED SILICON, FURNACE ANNEALED IN N_2

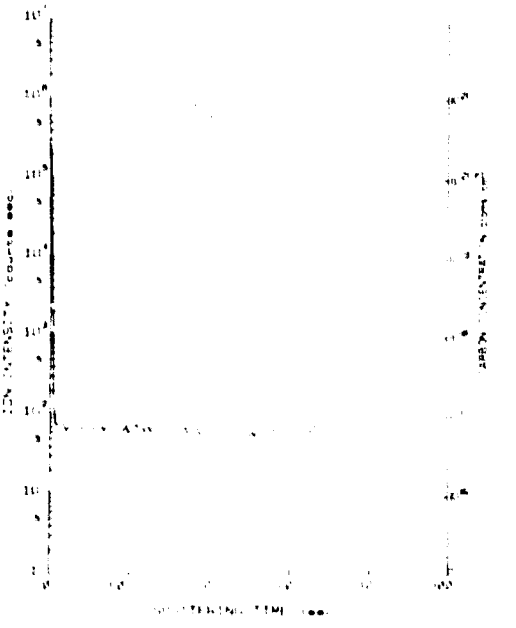

FIGURE 2-18. SIMS CARBON PROFILE IN PHOSPHORUS IMPLANTED SILICON, FURNACE ANNEALED IN N_2

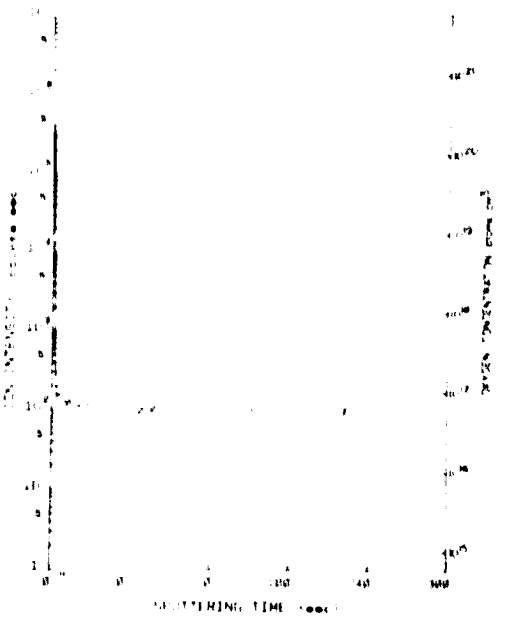

FIGURE 2-19. SIMS OXYGEN PROFILE OF AN UNPROCESSED SILICON CONTROL WAFER

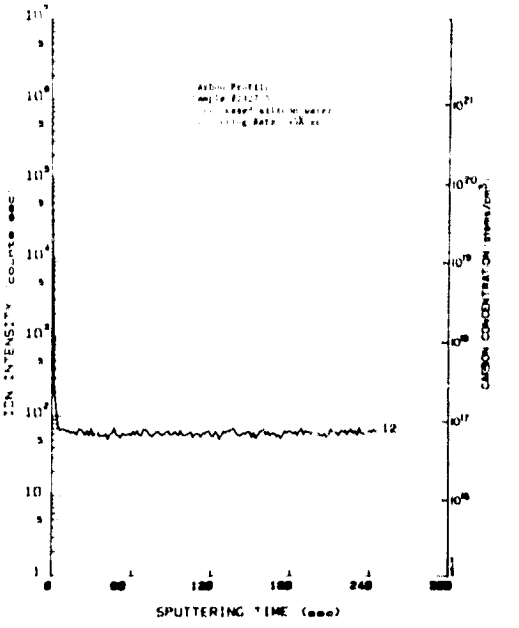

FIGURE 2-20. SIMS CARBON PROFILE OF AN UNPROCESSED SILICON CONTROL WAFER

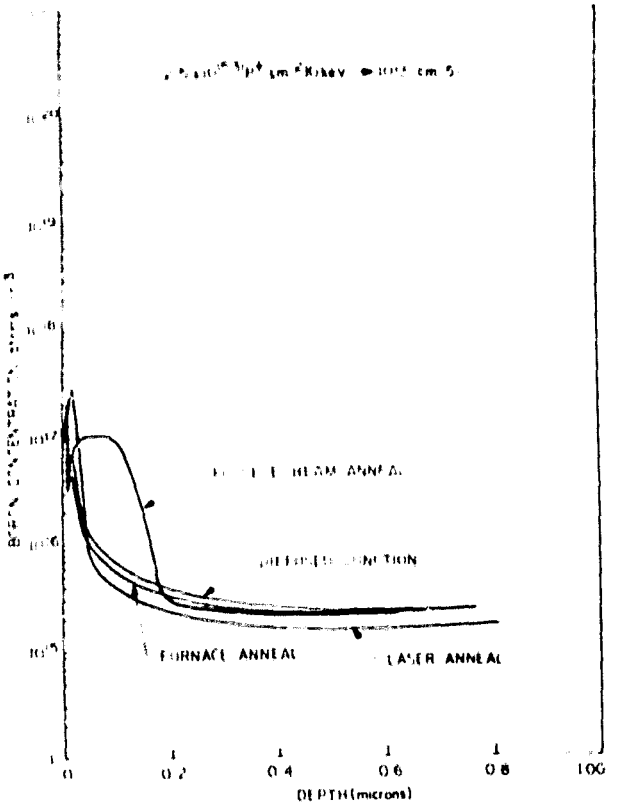

FIGURE 2-21. BORON CONCENTRATION FOR PHOSPHORUS IMPLANTS IN 10.0 ohm-cm SILICON

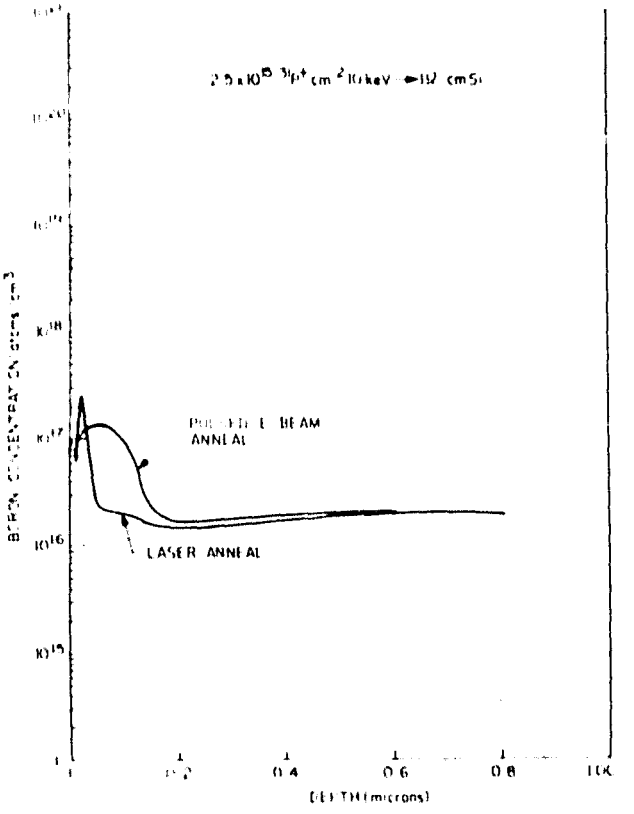

FIGURE 2-22. BORON CONCENTRATION FOR PHOSPHORUS IMPLANTS IN 1.0 ohm-cm SILICON

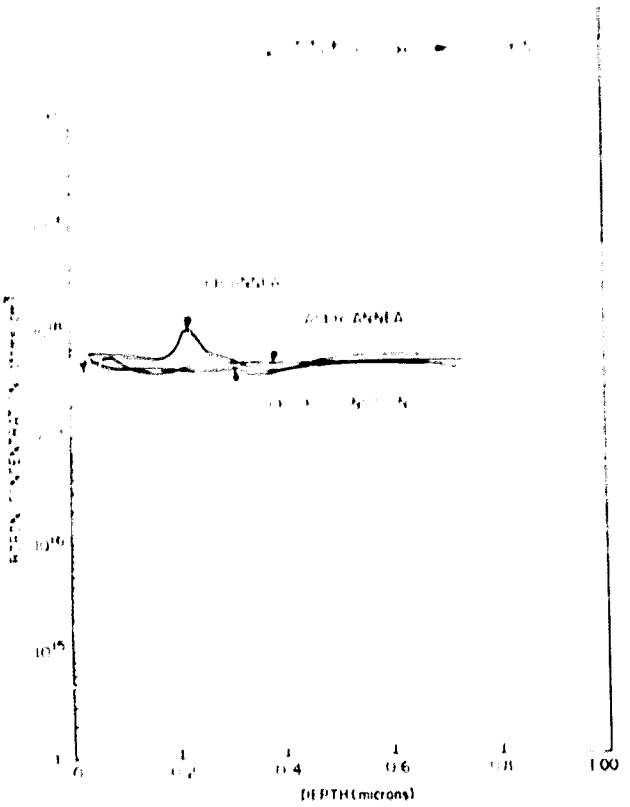

FIGURE 2-23. BORON CONCENTRATION FOR PHOSPHORUS IMPLANTS IN 0.1 ohm-cm SILICON

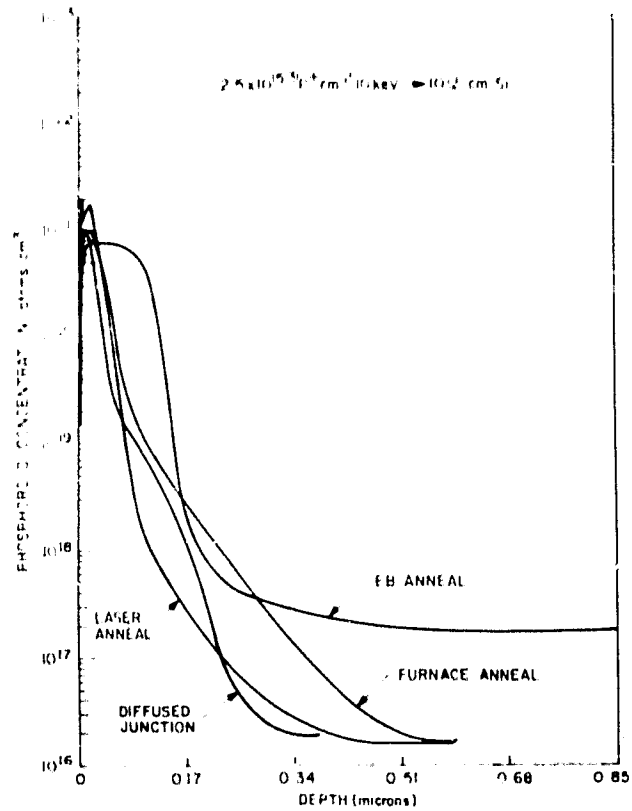

FIGURE 2-24. PHOSPHORUS CONCENTRATIONS FOR PHOSPHORUS IMPLANTS IN 10 ohm-cm SILICON

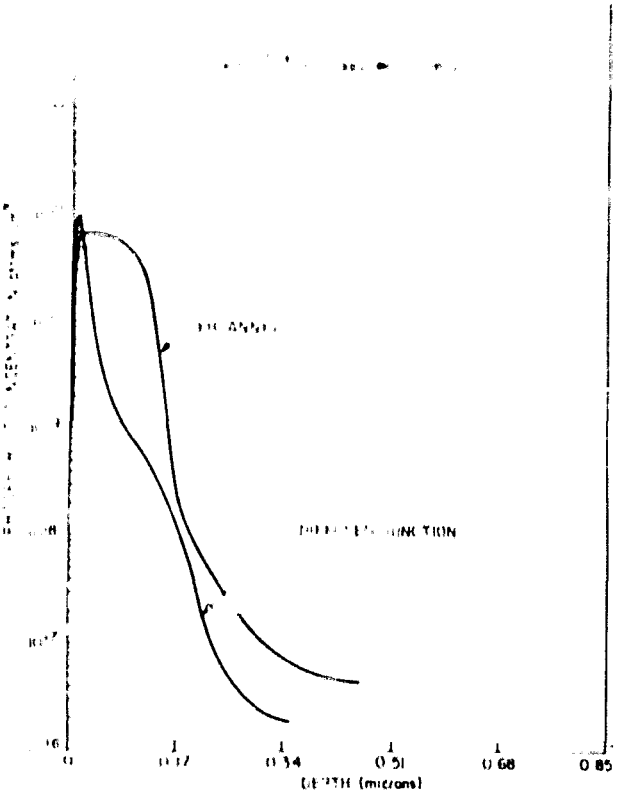

FIGURE 2-25. PHOSPHORUS CONCENTRATIONS FOR PHOSPHORUS IMPLANTS IN 1.0 ohm-cm SILICON

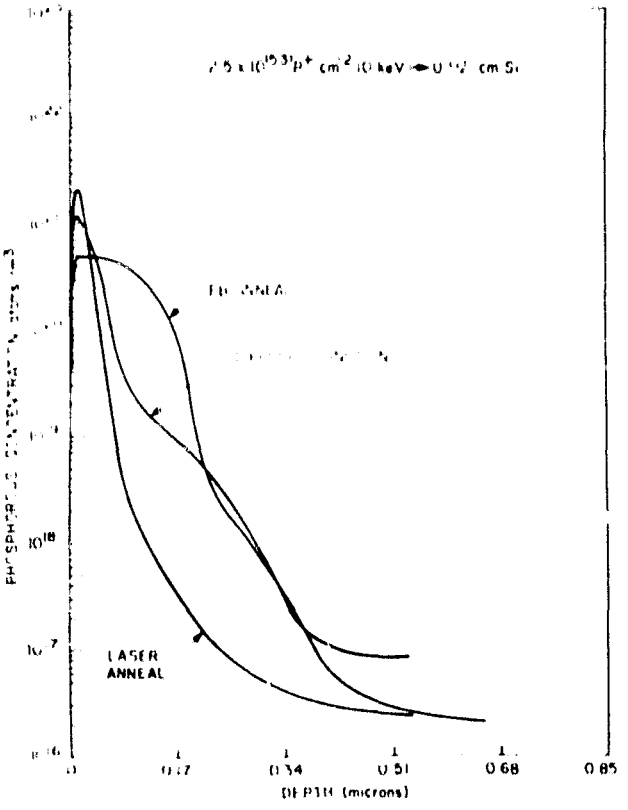

FIGURE 2-26. PHOSPHORUS CONCENTRATIONS FOR PHOSPHORUS IMPLANTS IN 0.1 ohm-cm SILICON

Thirty-eight cells were irradiated simultaneously. The cells were mounted on an aluminum plate 20 inches from the electron window of the dynamitron. The beam profile shown in Figure 2-27 was calculated from the monitor TLD dosimeters placed at the target plane prior to the cell irradiations. The dynamitron's electron energy was adjusted to 1.1 MeV to compensate for energy loss due to the titanium window and 20 inches of air. The electron energy at the target plane was estimated to be 0.95 MeV.

The irradiation schedule is shown in Table 2-3. The incremental and total doses are accurate for the center of the beam at the target plane. The doses for all other cell positions at the target plane were calculated from the beam profile shown in Figure 2-28.

Cell I-V characteristics and minority carrier lifetime measurements were made immediately following each radiation increment. All I-V characteristics were made on a Spectrosun Mark II solar simulator under AM0 (135.3 mW/cm^2), 25°C conditions.

In all cases, radiation degradation increased with decreasing silicon base resistivity. Figures 2-28 through 2-33 show P_{max} versus electron dose for furnace, laser and electron beam annealed cells and diffused junction cells. I_{sc} and V_{oc} data are included in Appendix 2 of this report. No process offered significantly higher radiation tolerance than any other process of our experiment. The P_{max} of cells fashioned from 10 ohm-cm material after 10^{16} $e^- cm^{-2}$ was between 50-60 percent of the initial Po_{max}. For 10 ohm-cm material, the lowest end-of-life power (P_{EOL}) was 50 percent of the beginning-of-life power (P_{BOL}) for cells implanted and furnace annealed before the cryopump was added to the end station of the ion implanter; the highest P_{EOL} (56 percent of P_{BOL}) was for diffused junction cells.

TABLE 2-3. ELECTRON DOSE INCREMENTS AT TARGET CENTER

	Incremental Dose ($e^- cm^{-2}$)	Total Dose ($e^- cm^{-2}$)
1.	3×10^{13}	3×10^{13}
2.	3×10^{14}	3.3×10^{14}
3.	1×10^{15}	1.33×10^{15}
4.	2×10^{15}	3.33×10^{15}
5.	7×10^{15}	1.033×10^{16}

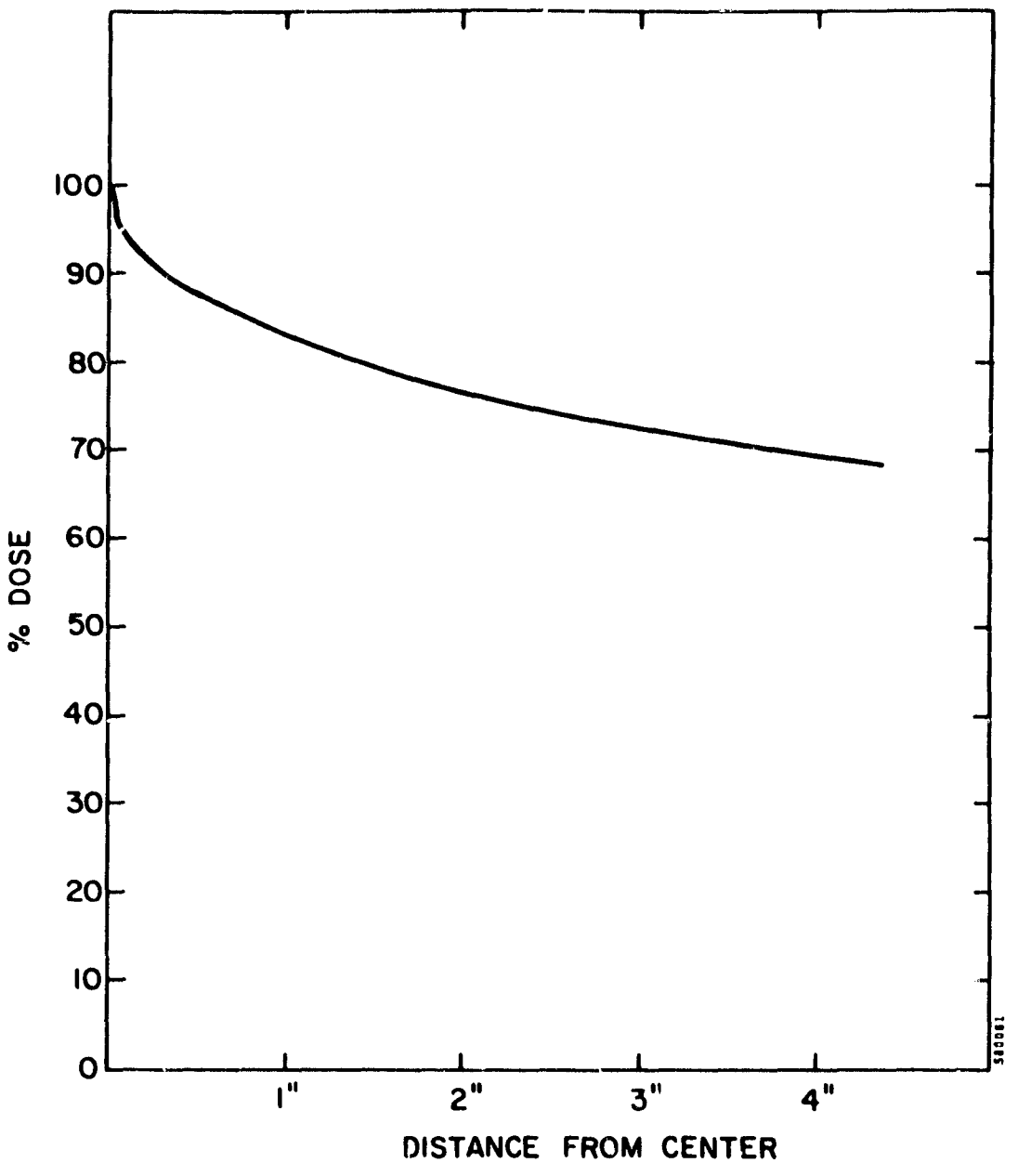

FIGURE 2-27. 1 MeV ELECTRON BEAM PROFILE AT 20 INCHES FROM THE DYNAMITRON'S WINDOW

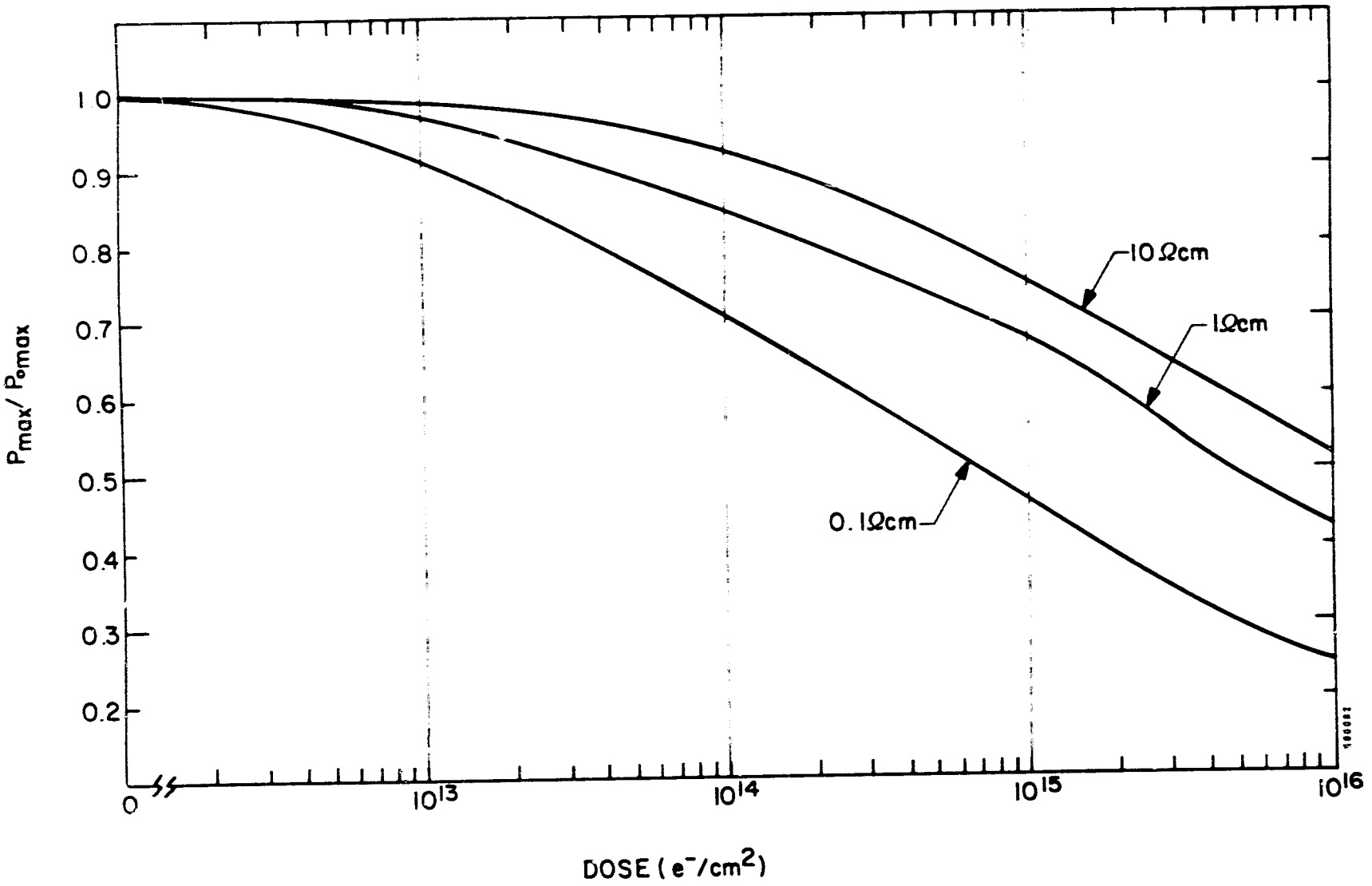

FIGURE 2-28. NORMALIZED P_{max} VERSUS 1 MeV ELECTRON FLUENCE FOR FURNACE ANNEALED SOLAR CELLS

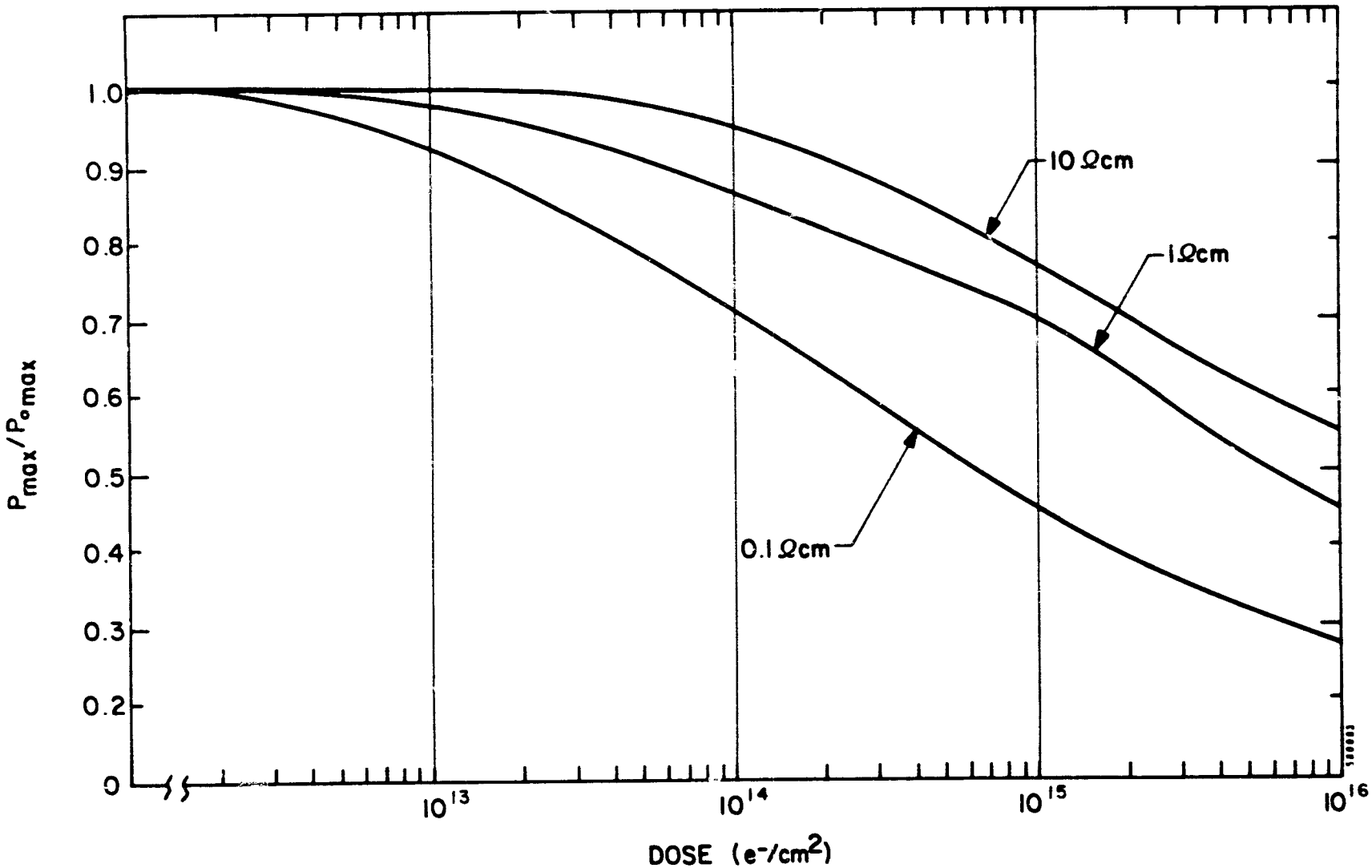

FIGURE 2-29. NORMALIZED P_{max} VERSUS 1 MeV ELECTRON FLUENCE FOR 0.53 MICROMETER LASER ANNEALED SOLAR CELLS

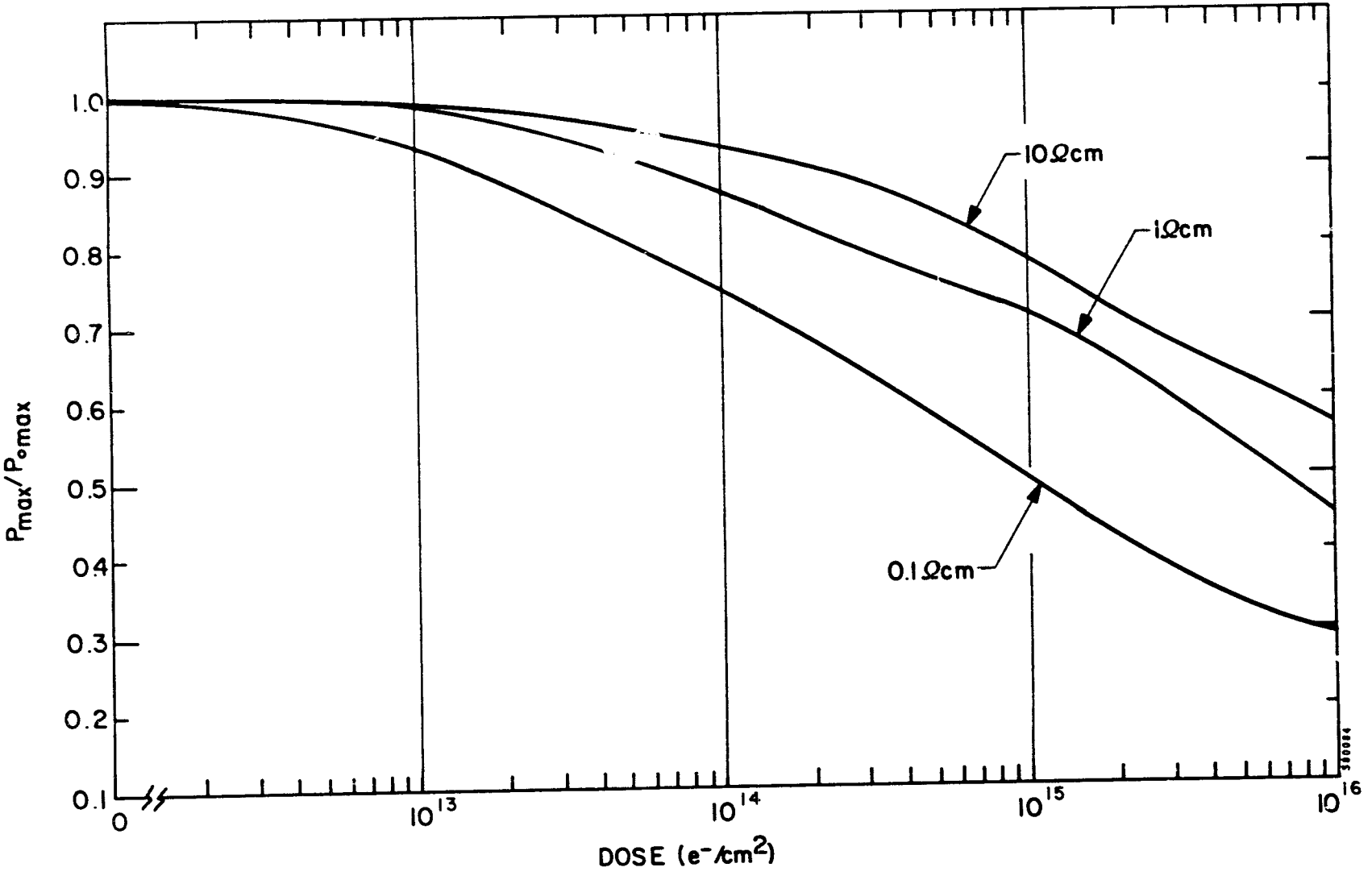

FIGURE 2-30. NORMALIZED P_{max} VERSUS 1 MeV ELECTRON FLUENCE FOR DIFFUSED JUNCTION SOLAR CELLS

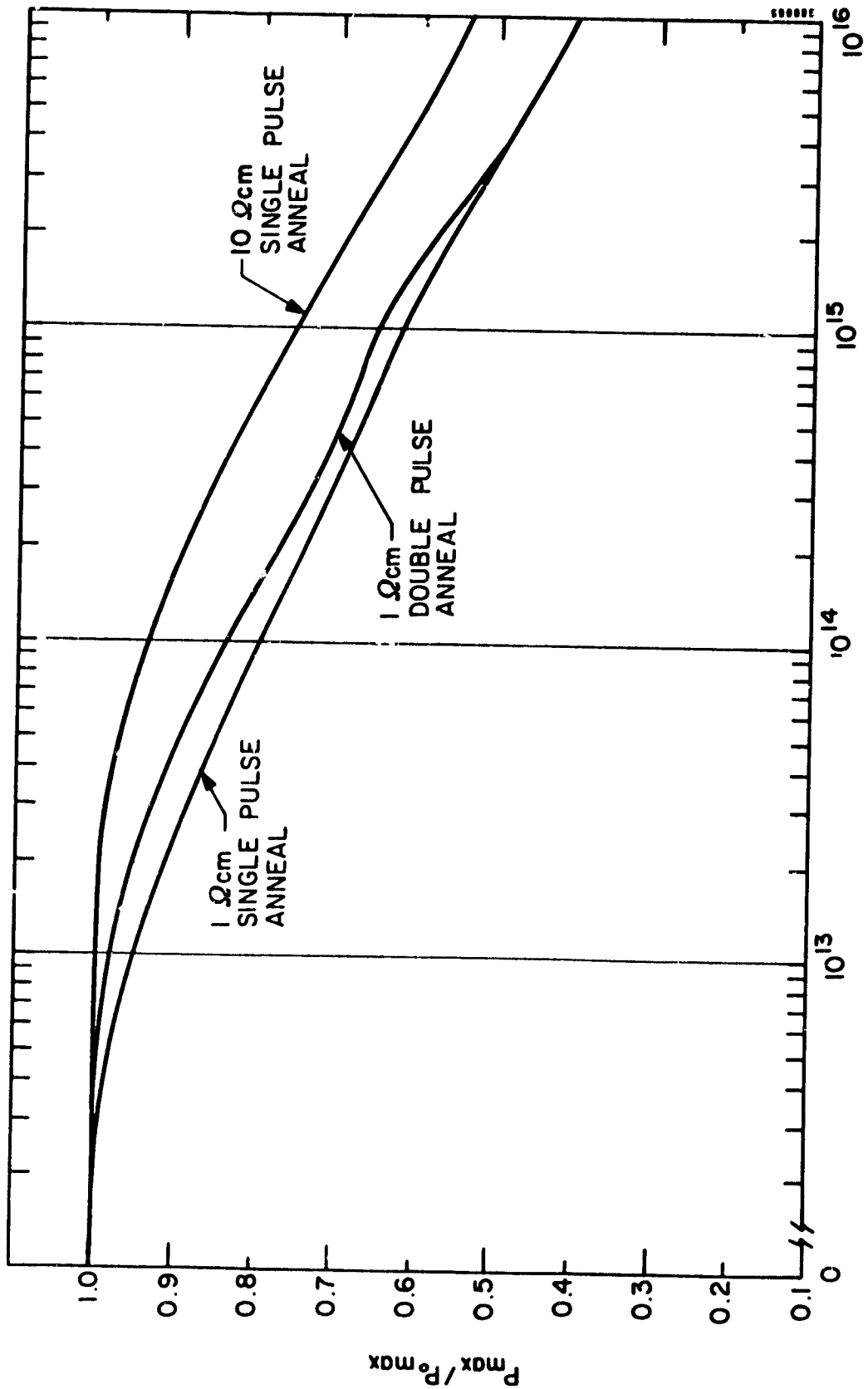

FIGURE 2-31. NORMALIZED P_{max} VERSUS 1 MeV ELECTRON FLUENCE FOR 1.06 MICROMETER LASER ANNEALED SOLAR CELLS

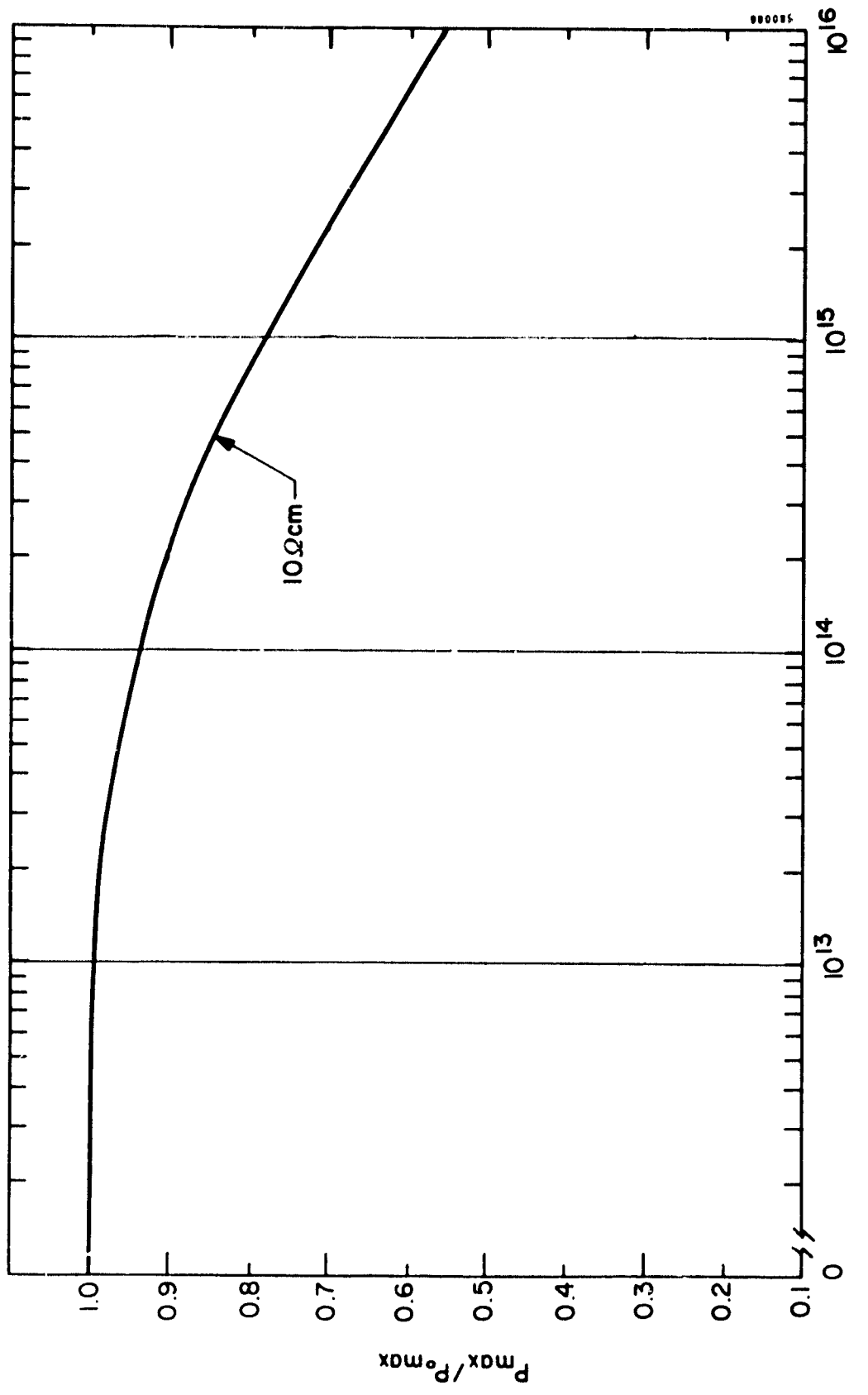

FIGURE 2-32. NORMALIZED P_{max} VERSUS 1 MeV ELECTRON FLUENCE FOR PULSED ELECTRON BEAM ANNEALED SOLAR CELLS

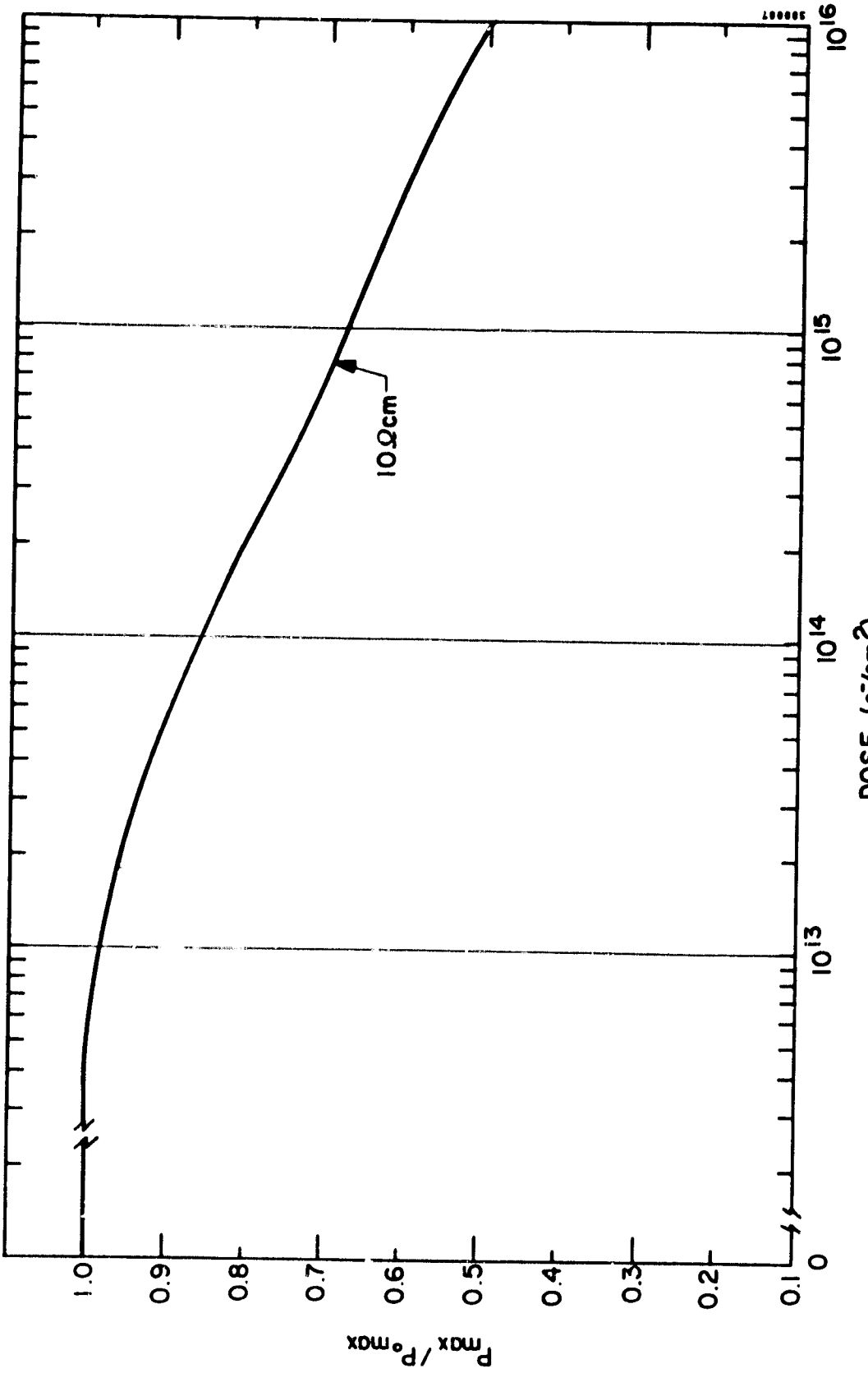

FIGURE 2-33. NORMALIZED P_{max} VERSUS 1 MeV ELECTRON FLUENCE FOR PRECRYOPUMP ION IMPLANTED AND FURNACE ANNEALED SOLAR CELLS

The minority carrier lifetime data exhibited an unusual increase in lifetime after 1×10^{15} e^- cm^{-2}. Since the lifetime should always decrease with increasing electron dose, we concluded that the photoinduced open circuit voltage decay method[13] of measuring minority carrier lifetime is not accurate following large (10^{15} cm^2) 1 MeV electron doses. Generally, the 1 ohm-cm cells maintained a higher lifetime than the 0.1 and 10 ohm-cm cells for all processes.

The minority carrier diffusion lengths were measured by the surface photovoltage technique[14], following the final irradiation to a fluence of 1×10^{16} e^- cm^{-2}, with results as shown below:

FZ Silicon Resistivity (ohm-cm)	Minority Carrier Diffusion Length (micrometers)	
	As-Received	After Irradiation
10	102	14
1	55	9
0.1	70	2

Although the diffusion lengths were not measured after each increment of electron fluence, the surface photovoltage method requires less data analysis and is more reliable than photoinduced open-circuit voltage lifetime data.

No one annealing process exhibited significantly better radiation tolerance -- when tested at Spire -- than any other. The slightly higher EOL ratio of normalized maximum power P/Po for diffused junction cells was balanced by the slightly lower initial cell efficiency. The lower EOL performance of the precryopump ion implanted and furnace annealed cells may be attributed to factors other than increased contamination, as these cells were fashioned under a different contract with different processing. In particular, they had an ion implanted back surface field (BSF), and their performance may have been more sensitive to radiation damage. No conclusions were drawn about carbon and oxygen contamination from the irradiated cell performance data. A boron related recombination center might explain the strong EOL performance variations with silicon base resistivity.

2.3.4 Radiation Testing at NASA-LeRC

Two cells of each process type and silicon resistivity were used for radiation hardness tests at NASA-LeRC. The cells were irradiated with 1 MeV electron fluences up to 1×10^{15} and then tested using the NASA-LeRC facilities under AM0-25°C conditions.

Results of the NASA-LeRC tests are shown in Figures 2-34 through 2-36. They indicate a small advantage (10 percent effect) in radiation hardness for pulsed electron beam annealed cells when compared with implanted and furnace or laser annealed cells. This might be attributed to annealing in vacuum during electron beam processing compared to annealing in air, using lasers, or annealing in nitrogen in a furnace.

The initial cell performance, as shown in Table 2-4, was slightly lower for the NASA-LeRC test cells compared to results shown in Figures 2-7 through 2-12. The best cells were selected for radiation damage studies at Spire, as reported in Section 2.3.3. This data, in Table 2-4, clearly shows that all pulse processing must be optimized in the future, since laser or electron beam annealed cells were not as good as either the implanted furnace annealed or diffused junction cells.

At least one cell from each process and resistivity was not irradiated, but will be prepared for deep level transient capacitance spectroscopy (DLTS)[15] analysis by NASA-LeRC personnel. Analysis of the DLTS data was beyond the scope of this contract. After identification of the dominant, deep level carrier traps in the depletion region, a recommendation can be prepared for future cell processing investigations. The possible directions for further materials development include cold wall Czochralski, implanted detector grade float-zone and gallium doped silicon.

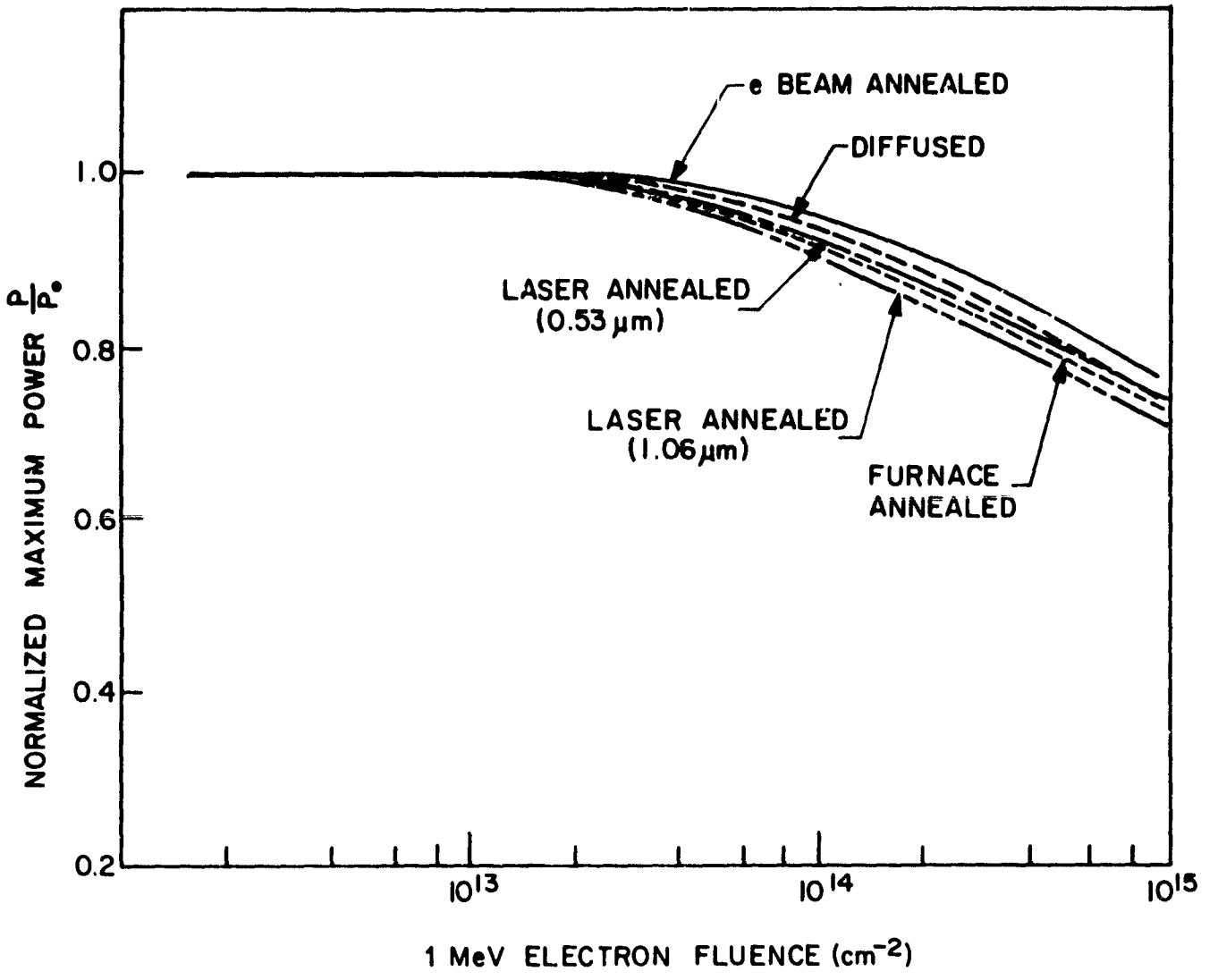

FIGURE 2-34. NORMALIZED P_{max} VERSUS 1 MeV FLUENCE FOR ALL PROCESSES AND 10-ohm-cm FZ SILICON

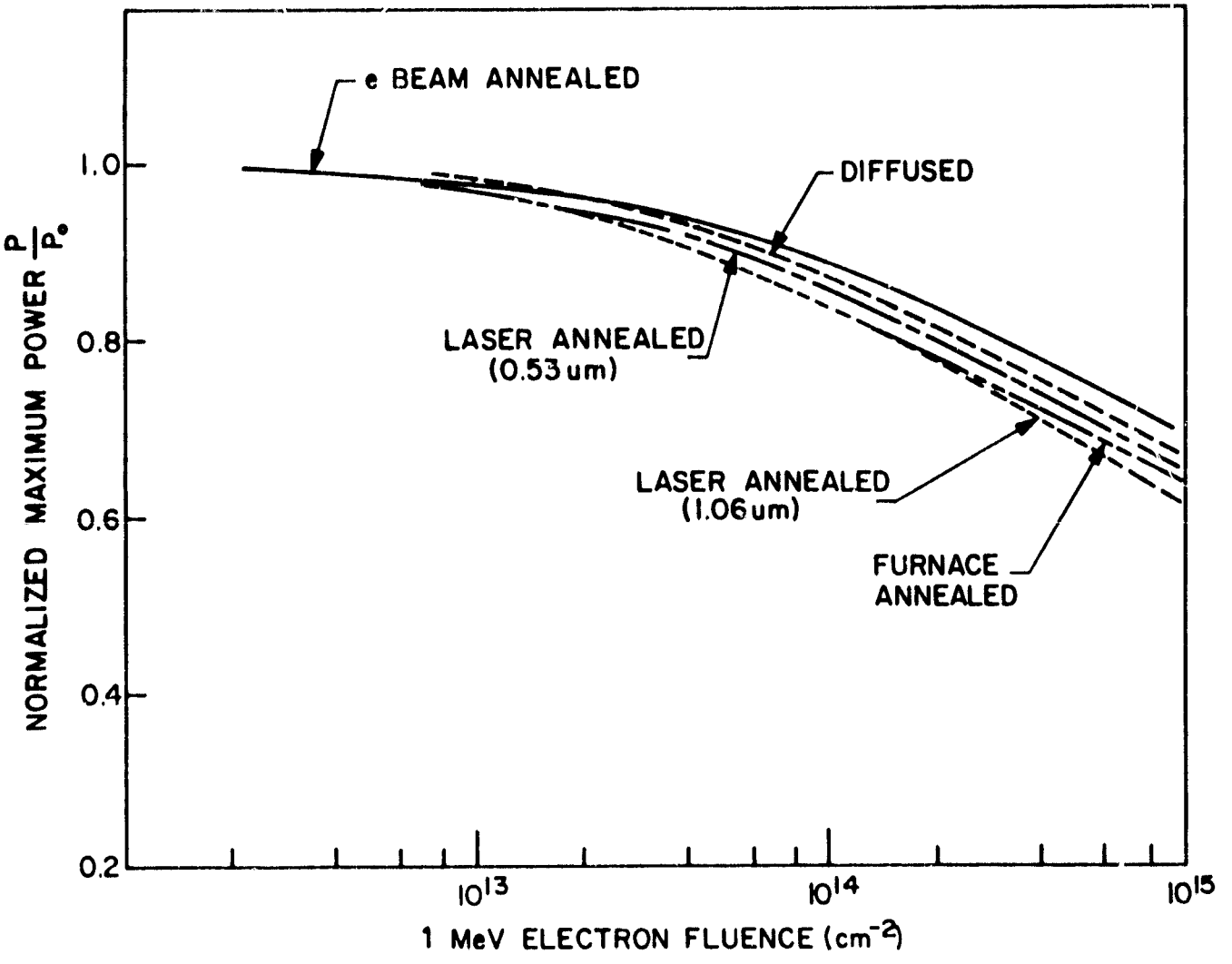

FIGURE 2-35. NORMALIZED P_{max} VERSUS 1 MeV ELECTRON FLUENCE FOR ALL PROCESSES AND 1 ohm-cm FZ SILICON

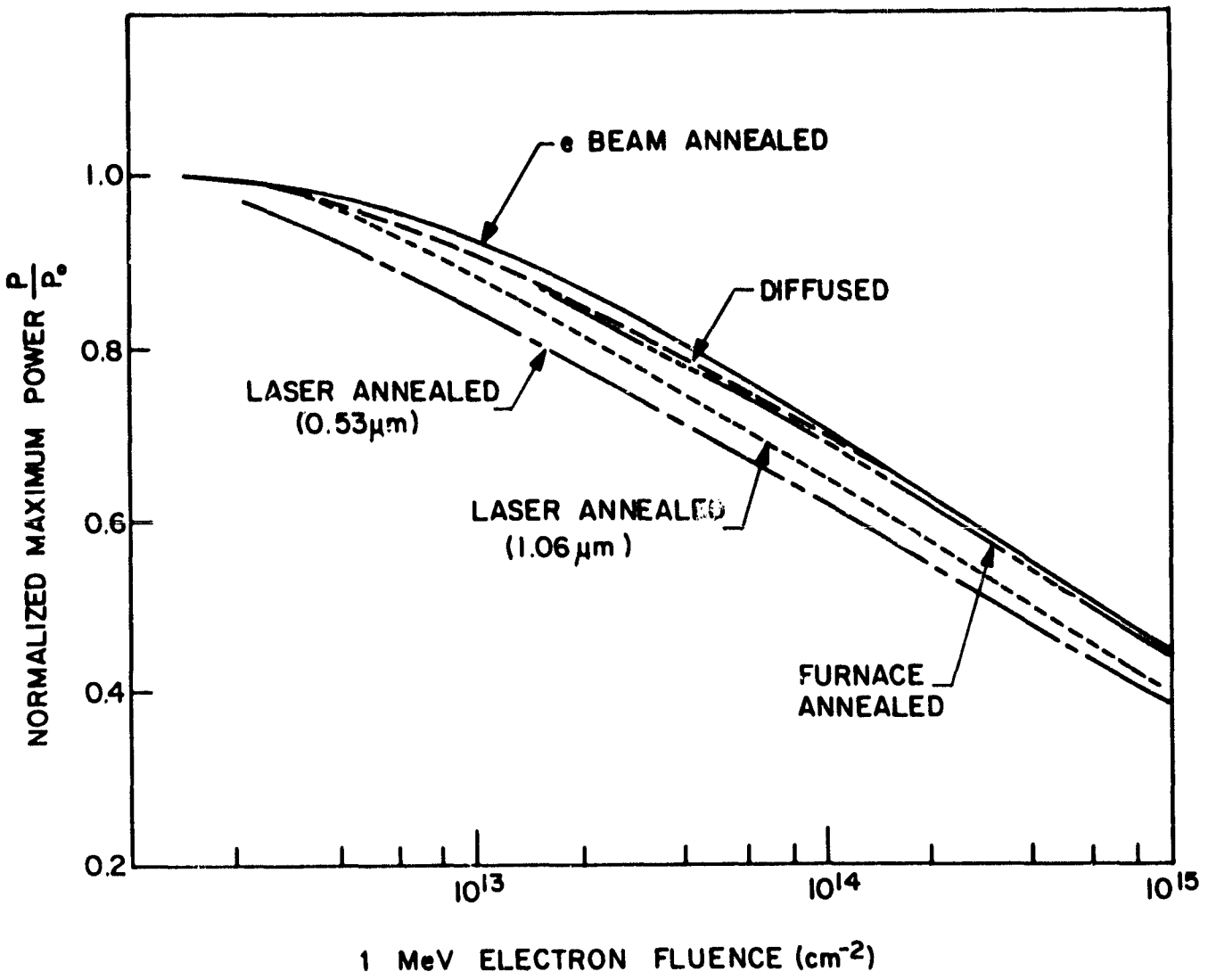

FIGURE 2-36. NORMALIZED P_{max} VERSUS 1 MeV FLUENCE FOR ALL PROCESSES AND 0.1 ohm-cm FZ SILICON

TABLE 2-4. INITIAL (PREIRRADIATION) CELL PERFORMANCE FOR CELLS TESTED AT NASA-LeRC

Process	Resistivity (ohm-cm)	P_{max} (mW)	I_{sc} (mA)	V_{oc} (mV)	F.F. (%)	Diffusion Length (micrometers)
Implanted/	10	44.64	106.88	546	76.6	280
Furnace	10	45.40	107.71	546	77.2	290
Annealed	1	44.93	104.79	584	73.4	250
	1	47.77	105.28	587	77.3	297
	0.1	42.09	98.97	599	71.0	135
	0.1	40.82	98.41	597	60.5	126
Implanted/	10	39.30	100.35	530	73.9	192
Electron Beam	10	39.70	99.96	533	74.7	196
Annealed	1	40.68	97.56	567	73.5	165
	1	35.73	95.17	547	68.7	140
	0.1	24.80	98.21	549	46.0	117
Implanted/	10	43.57	105.33	544	76.0	277
Laser	10	43.57	106.90	544	74.9	267
Annealed at	1	42.67	102.29	576	72.1	195
1.06 micrometer	1	40.74	102.50	578	68.7	154
	0.1	36.43	98.65	578	63.9	114
Implanted	10	41.94	107.06	536	73.1	290
Laser	10	41.86	105.88	535	73.9	257
Annealed at	1	43.50	105.61	561	73.4	284
0.53 micrometer	1	43.34	105.61	559	73.3	284
	0.1	35.24	99.82	546	64.7	110
Diffused	10	43.38	108.70	541	73.8	284
	10	43.21	107.92	539	74.3	250
	1	44.42	105.35	584	72.2	203
	1	41.90	105.70	581	68.2	185
	0.1	41.33	96.31	601	71.4	135
	0.1	40.73	96.45	601	70.3	138

(No AR coating or BSF)

SECTION 3
CONCLUSIONS

This contract has examined the effect of the solar cell junction formation processes on the radiation tolerance of the device. It is the first time that cells prepared by diffusion and ion implantation — annealed by furnace and pulse methods — have been compared for radiation tolerance using the same starting material.

Although an attempt was made to utilize the lowest available carbon and oxygen content float-zone silicon, material with impurity concentrations below 5×10^{15} cm^{-3} cannot be procured on a purchase order basis. Improved low-carbon and low-oxygen material is not yet available as a commercial product with resistivities between 0.1 and 10 ohm-cm, which is the material of interest for solar cell fabrication.

The significant results of the contract can be summarized as follows:

1. High efficiency silicon cells were processed by ion implantation and three types of pulse annealing

   - large-area, single-pulse electron beam annealing
   - large-area, single-pulse 1.06-micrometer laser annealing
   - small-spot, step-and-repeat 0.53-micrometer laser annealing

   The 5-cm diameter laser single-pulse annealed cells showed no performance enhancement when compared to 25-micrometer diameter laser repetitive-pulse annealed cells.

2. The most radiation tolerant process, pulsed electron beam annealing of ion implants, had a 10 percent advantage compared to other techniques. All test results, though, were very similar. This conclusion is valid only for silicon already having 5×10^{15} cm^{-3} oxygen and about 10^{16} cm^{-3} carbon impurities and boron as a p-type dopant.

REFERENCES

1. J.W. Corbett et al., Solar Cell High Efficiency and Radiation Damage, NASA Conference Publication 2097, NASA-Lewis Research Center, Cleveland, OH, p. 185 (June 1979).

2. J. Bernard et al., Proc. Twelfth IEEE Photovoltaic Specialists Conf., IEEE No. 76CH1142-9ED, New York, p. 265 (1976).

3. W. Pschunder and H. Fischer, Proc. Twelfth IEEE Photovoltaic Specialists Conf., IEEE No. 76CH1142-9ED, New York, p. 270 (1976).

4. Private communication, Wacker Siltronic Corp., Santa Clara, CA.

5. D.M. Mattox, Thin Solid Films 53, 81 (1978).

6. R.R. Sowell, R.E. Cuthrell, D.M. Mattox and R.D. Bland, J. Voc. Sci. Technol. 11, 474 (1974).

7. J.R. Vig and J.W. LeBus, IEEE Trans. Parts, Hybrids, Packaging PHP 12, 365 (1976).

8. Am. Soc. Test. Mater. Stand. F21-65 (1976): ASTM STANDARDS, Electronics (1978).

9. M.Y. Tsai, B.G. Streetman et al., "Study of Surface Contamination Produced During High Dose Ion Implantation", J. Electrochem. Soc. 126, 98 (1979).

10. A.S. Grove, Physics & Technology of Semiconductor Devices, John Wiley & Sons, Inc., New York (1967).

11. Many, Goldstein and Grover, Semiconductor Surfaces, North-Holland Publishing Co. (1971).

12. J.A. Minnucci and K.W. Matthei, "Study Program to Improve the Open-Circuit Voltage of Low-Resistivity Single Crystal Silicon Solar Cells", NASA CR-159833, NASA-LeRC, Cleveland, OH (February 7, 1980).

13. J.E. Mahan et al., "Measurement of Minority Carrier Lifetime in Solar Cells from Photo-Induced Open-Circuit Voltage Decay", IEEE Trans. Electron Devices ED-26, No. 5, 733 (1979).

14. Am. Soc. Test. Mater. Stand. F391-78: ASTM STANDARDS, Electronics (1978).

15. L.C. Kimerling, Radiation Effects in Semiconductors, 1976, Inst. Phys. Conf. Series 31, p. 221 (1977).

APPENDIX 1
PREIRRADIATION CELL PERFORMANCE DATA

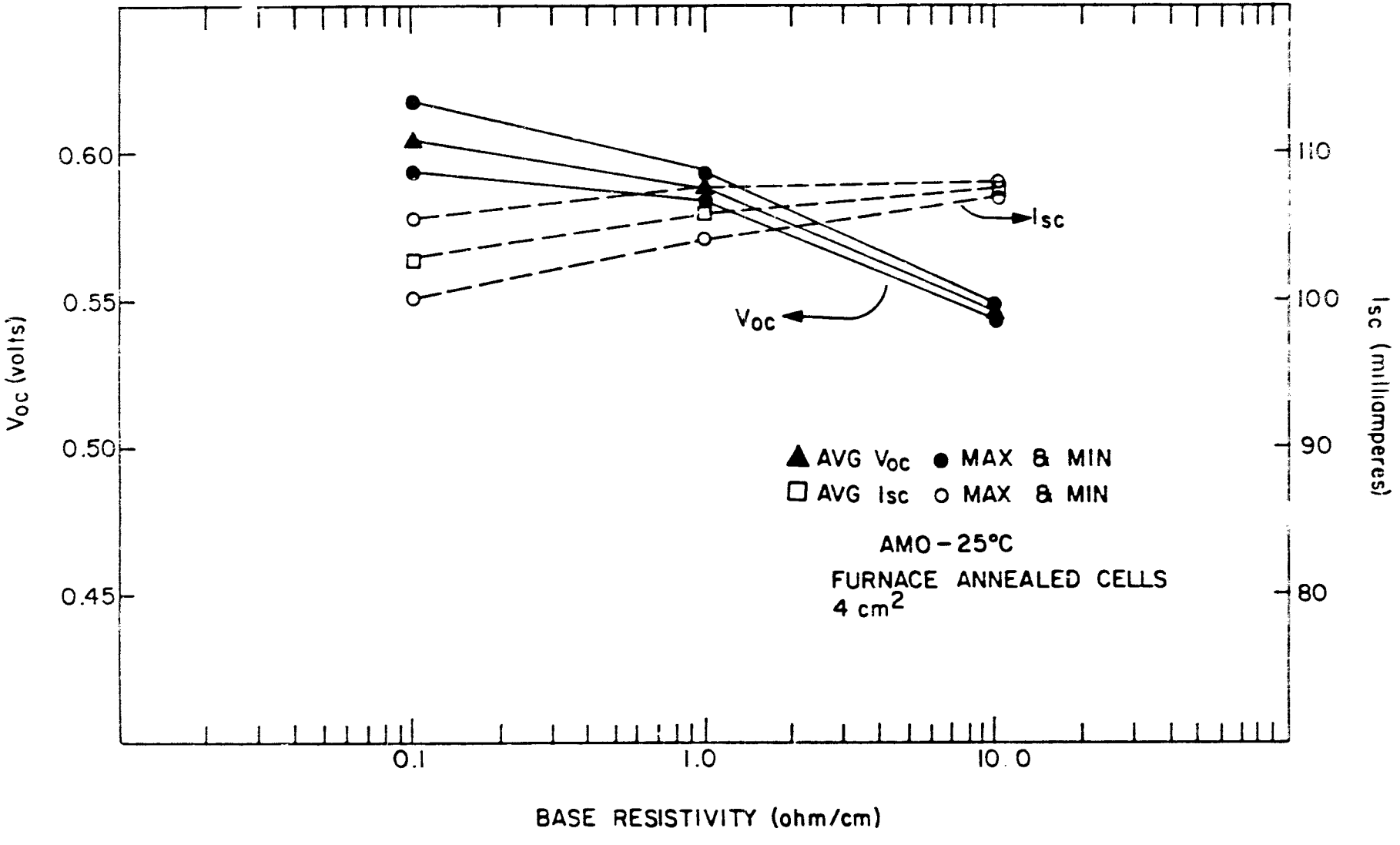

FIGURE A-1. V_{oc} AND I_{sc} DISTRIBUTION FOR FURNACE ANNEALED CELLS OF 0.1, 1.0, AND 10 OHM-CM BASE RESISTIVITIES

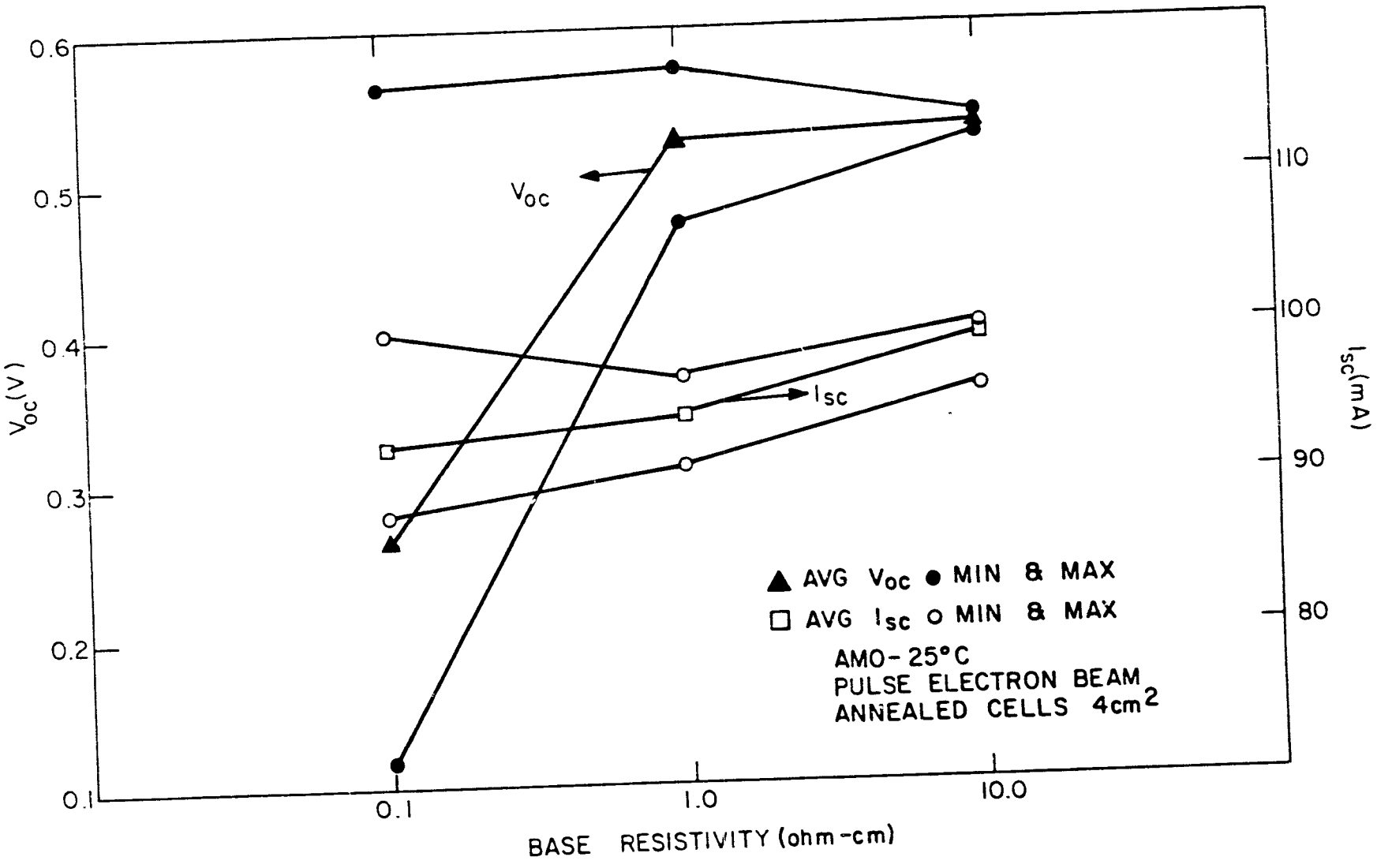

FIGURE A-2. V_{oc} AND I_{sc} DISTRIBUTION FOR PULSED ELECTRON BEAM ANNEALED CELLS

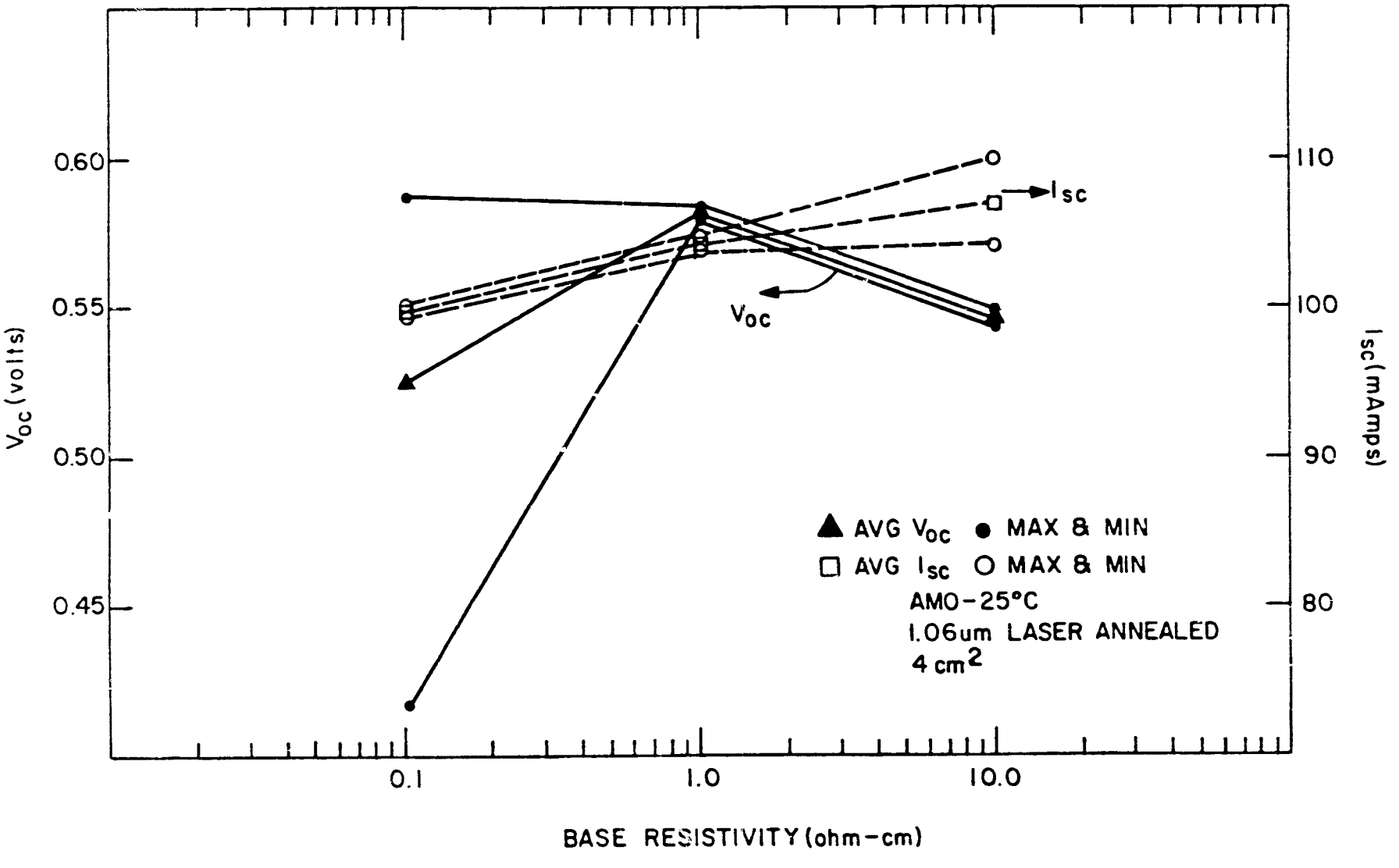

FIGURE A-3. V_{oc} AND I_{sc} DISTRIBUTION FOR 1.06 MICRON LASER ANNEALED CELLS

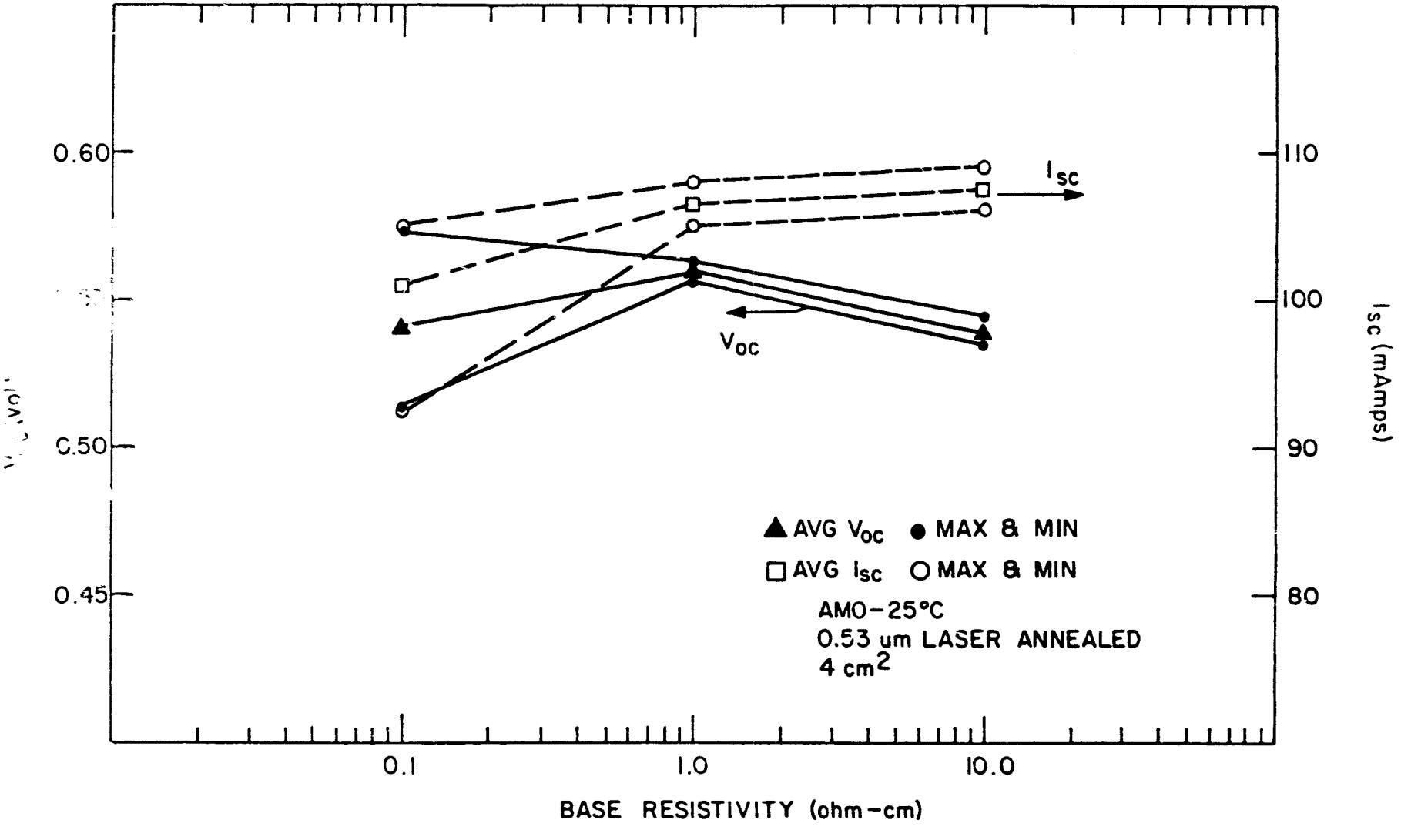

FIGURE A-4. V_{oc} AND I_{sc} DISTRIBUTION FOR 0.53 MICRON LASER ANNEALED CELLS

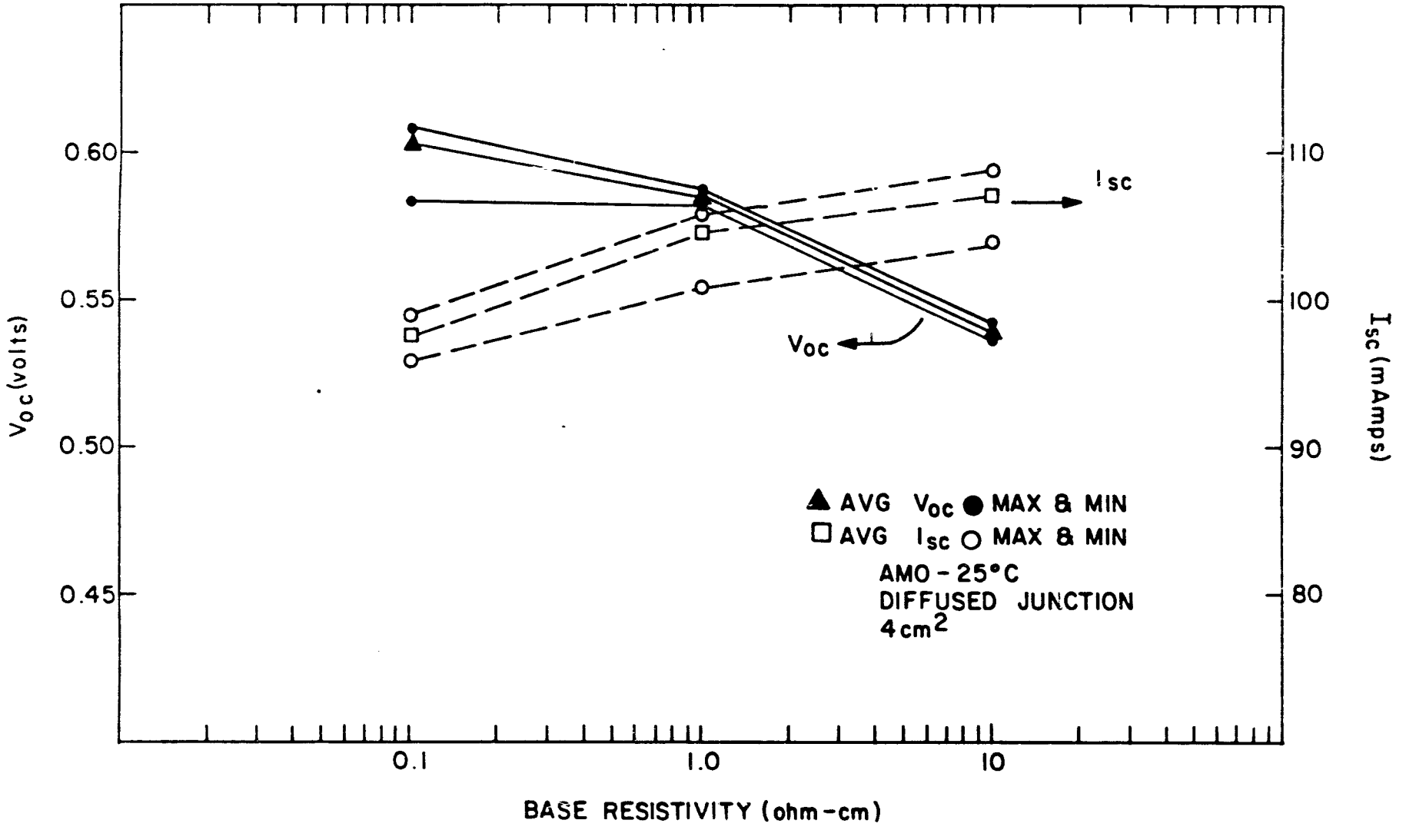

FIGURE A-5. V_{oc} AND I_{sc} DISTRIBUTION FOR DIFFUSED JUNCTION SOLAR CELLS OF 0.1, 1.0, and 10 OHM-CM BASE RESISTIVITIES

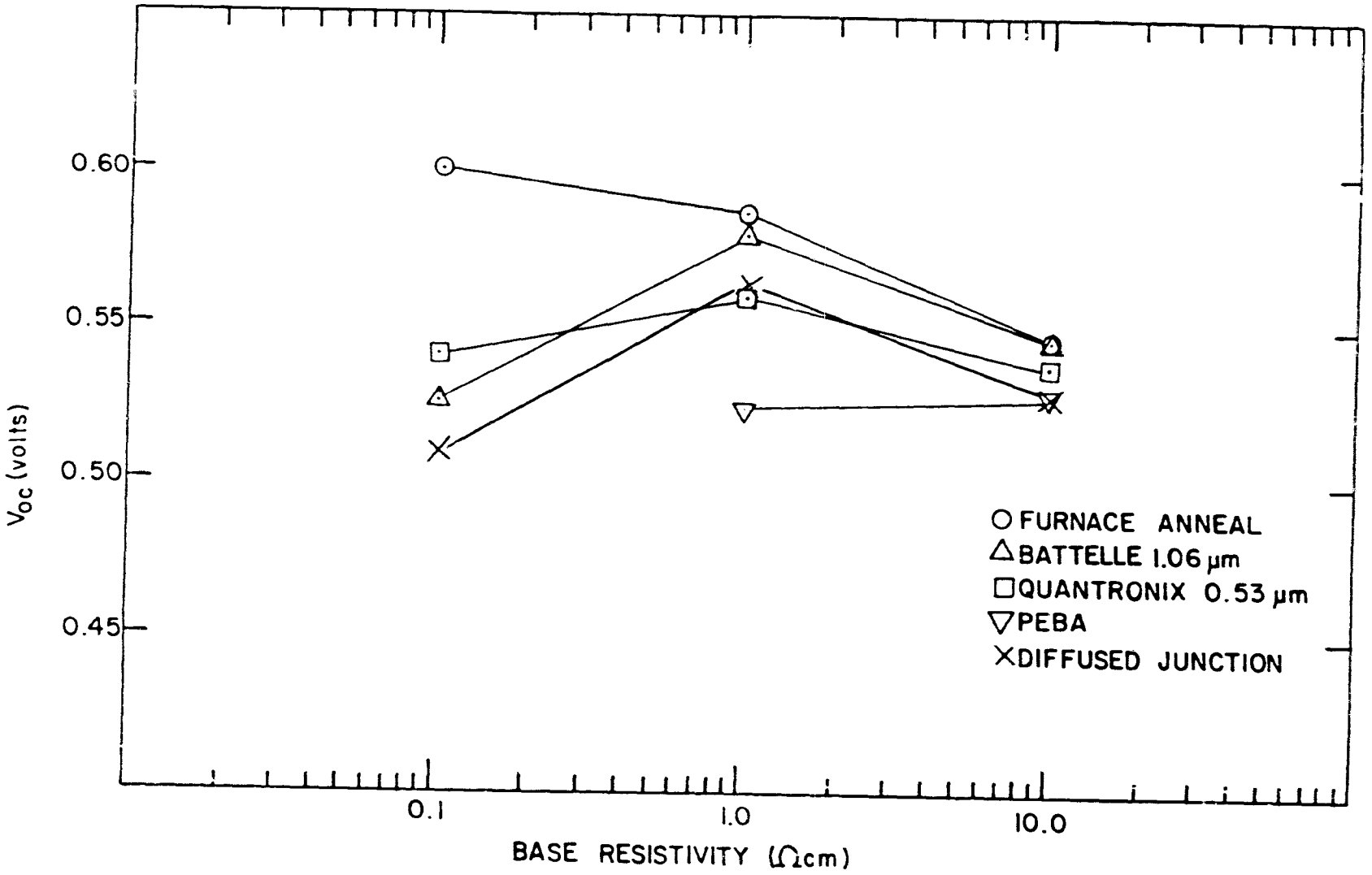

FIGURE A-6. AVERAGE V_{oc} VERSUS BASE RESISTIVITY FOR ALL ANNEALING PROCESSES

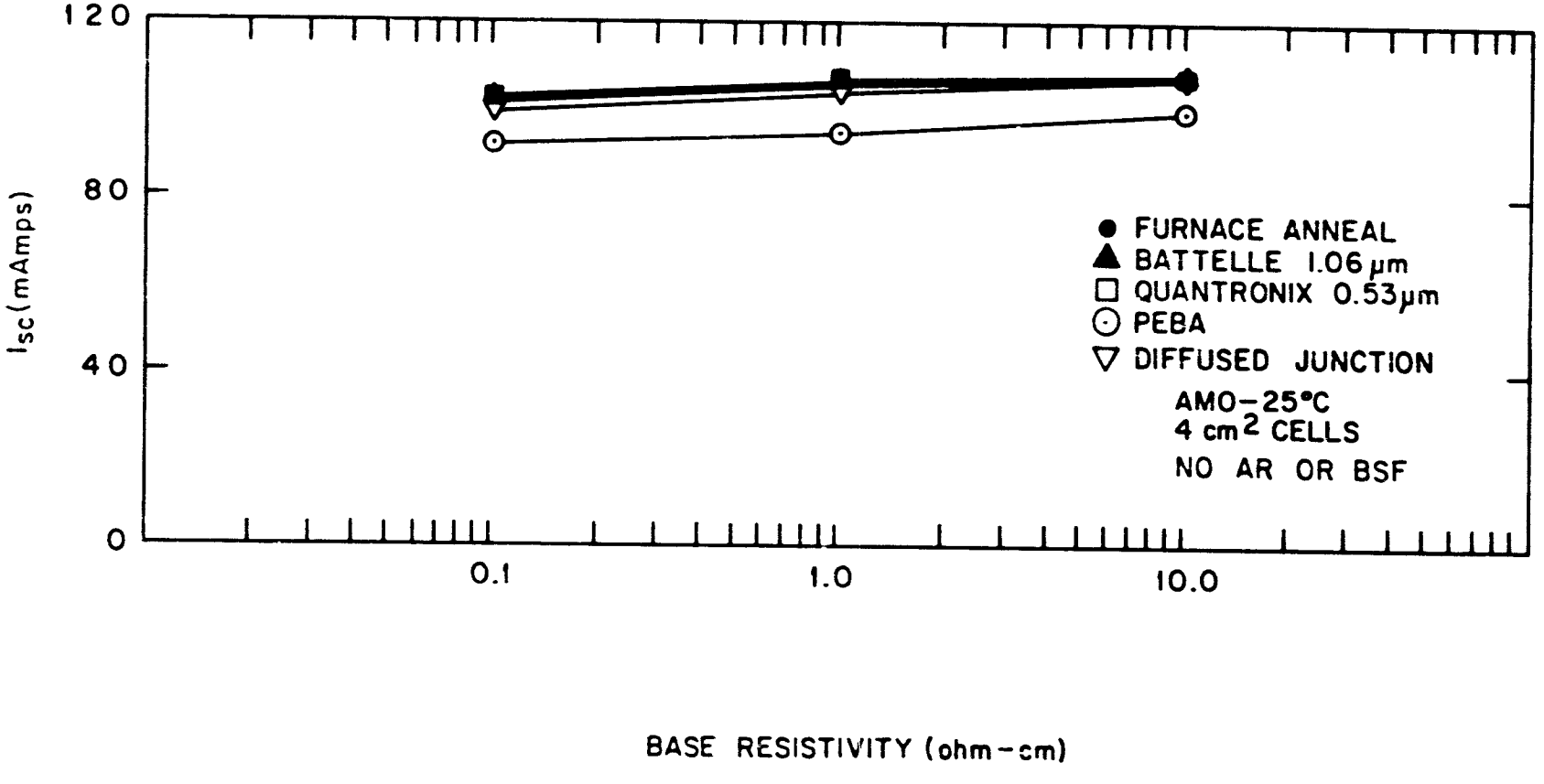

FIGURE A-7. AVERAGE I_{sc} VERSUS BASE RESISTIVITY FOR ALL ANNEALING PROCESSES

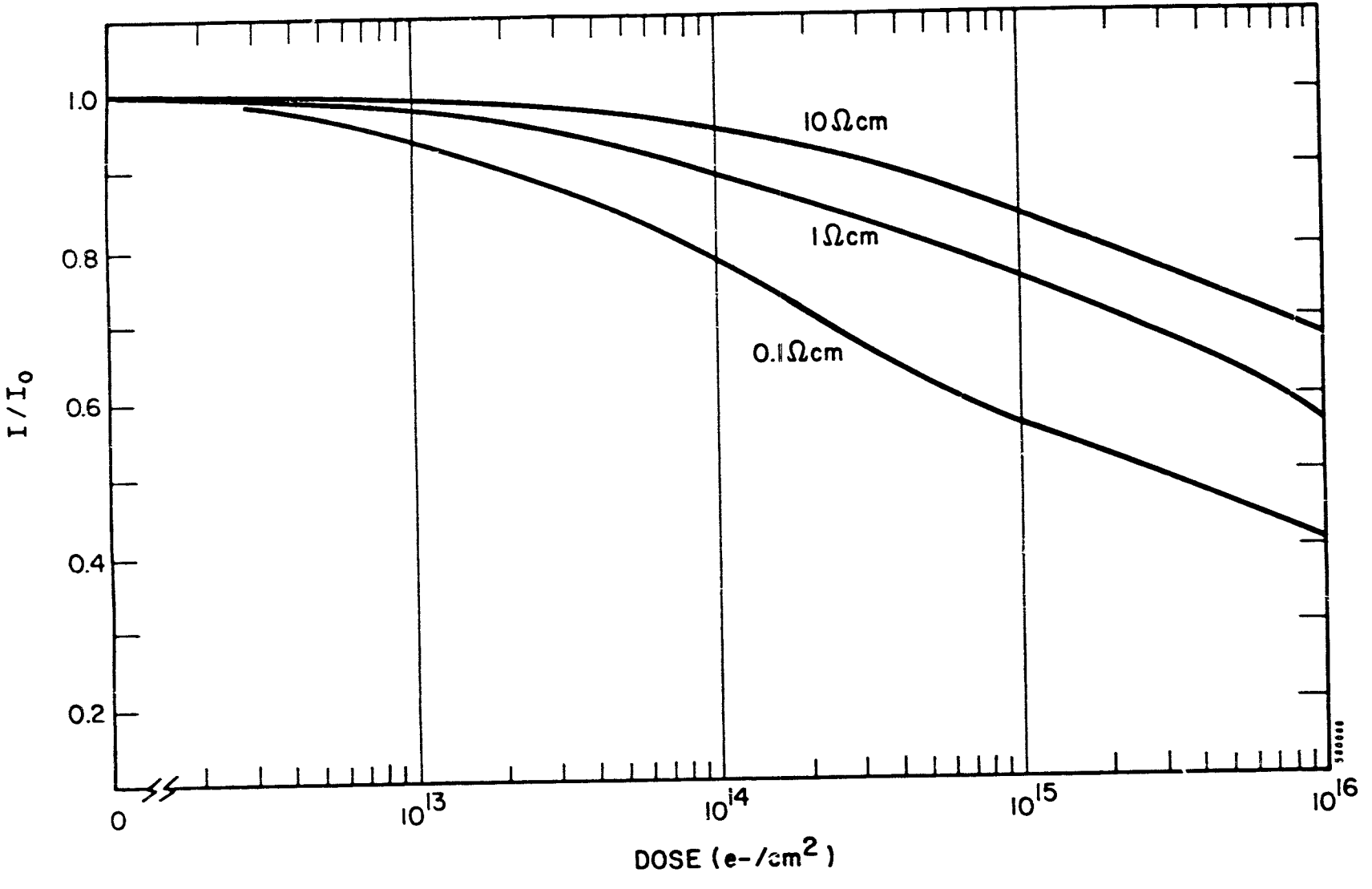

FIGURE A-8. NORMALIZED I_{sc} VERSUS 1 MeV ELECTRON FLUENCE FOR FURNACE ANNEALED SOLAR CELLS

APPENDIX 2
POSTIRRADIATION CELL PERFORMANCE DATA

TABLE A-1. INITIAL (PREIRRADIATION) CELL PERFORMANCE FOR DATA PRESENTED IN APPENDIX 2

Process	Resistivity (ohm-cm)	P_{max} (mW)	I_{sc} (mA)	V_{oc} (mV)
Implanted/ Furnace Annealed	10	46.3	109	547
	1	48.8	108	595
	0.1	47.6	106	620
Implanted/ Electron Beam Annealed	10	39.9	101	535
Implanted/ Laser Annealed at 1.06 microns	10	44.9	112	547
	1	44.3	107	588
	0.1	-	-	-
Implanted/ Laser Annealed at 0.53 micron	10	44.4	109	543
	1	44.6	107	569
	0.1	36.2	105	552
Diffused	10	44.8	111	544
	1	47.3	108	588
	0.1	44.2	97	605
Pre-cryopump Implanted/ Furnace Annealed with AR, BSF	10	69.6	155	

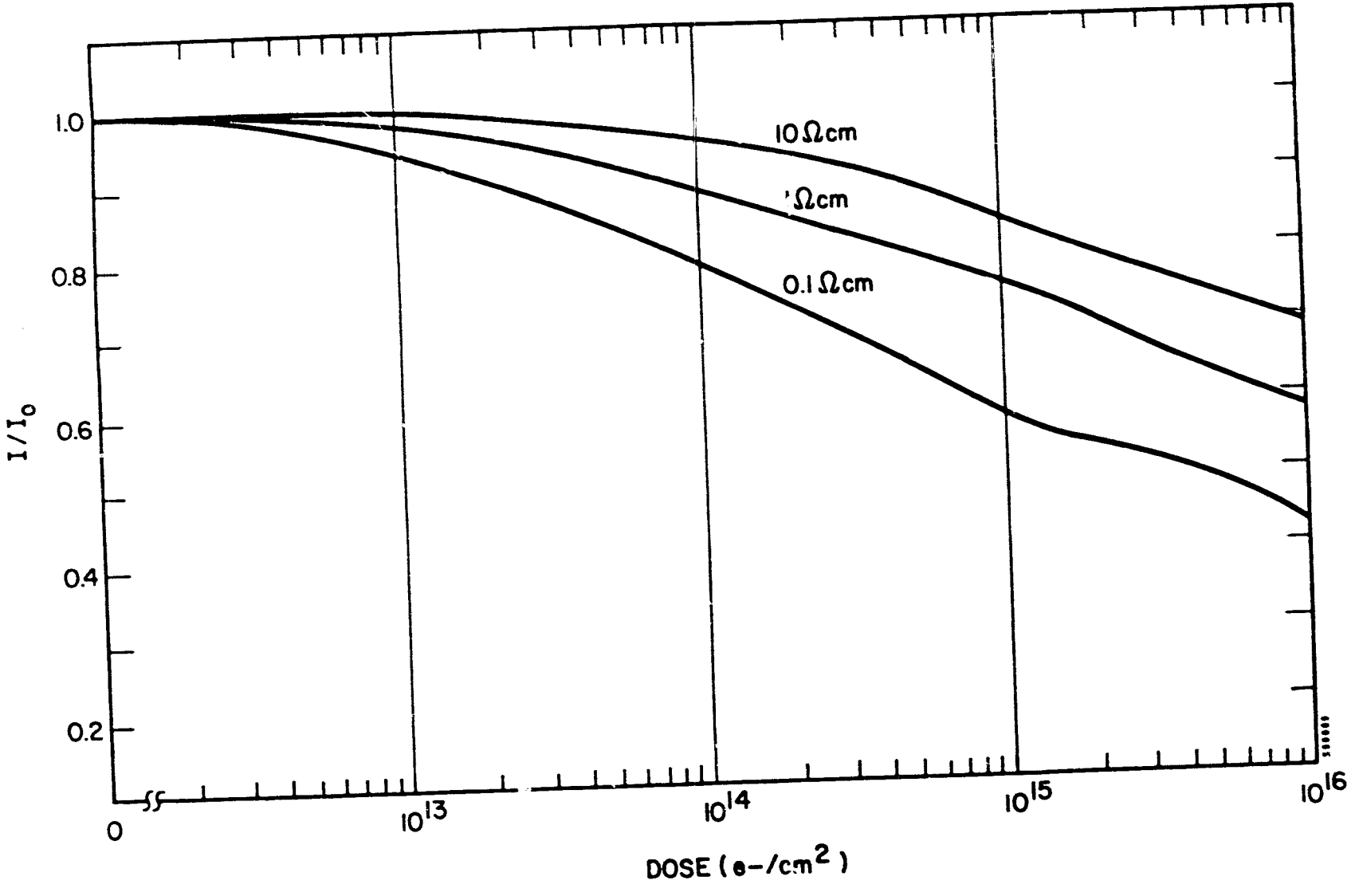

FIGURE A-9. NORMALIZED I_{sc} VERSUS 1 MeV ELECTRON FLUENCE FOR 0.53 μm LASER ANNEALED [illegible] CELLS

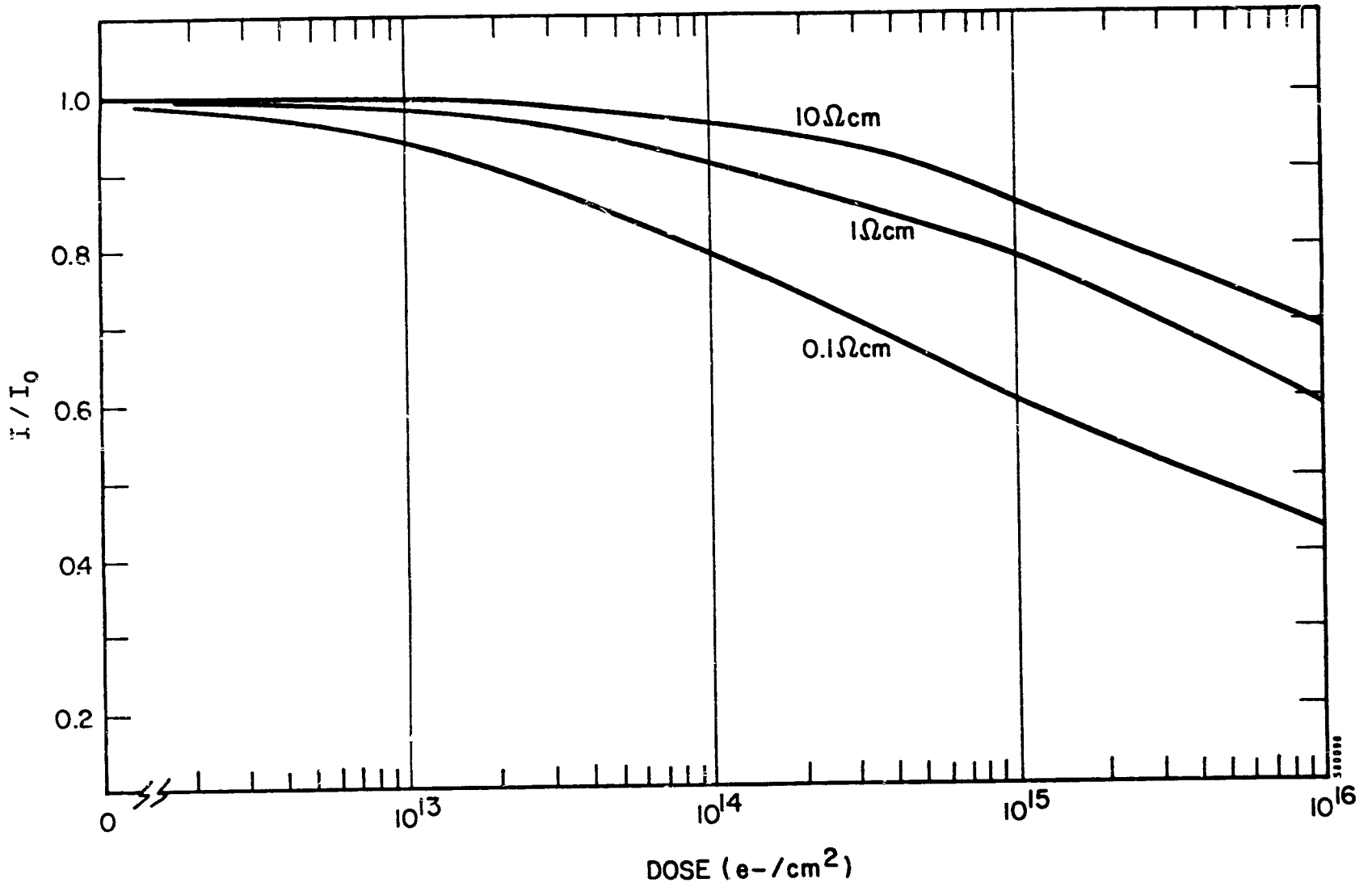

FIGURE A-10. NORMALIZED I_{sc} VERSUS 1 MeV ELECTRON FLUENCE FOR DIFFUSED JUNCTION SOLAR CELLS

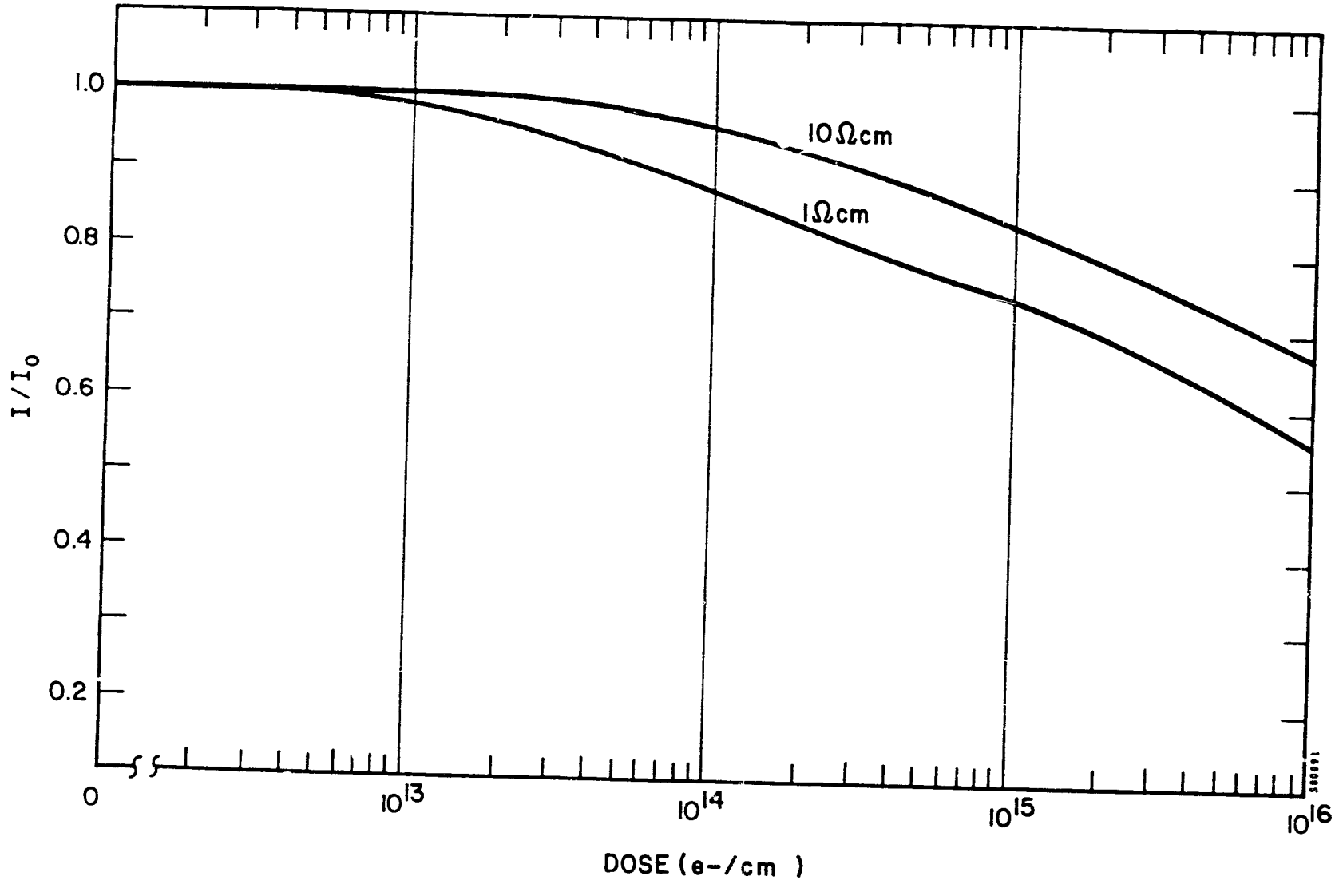

FIGURE A-11. NORMALIZED I_{sc} VERSUS 1 MeV ELECTRON FLUENCE FOR 1.06 μm LASER ANNEALED SOLAR CELLS

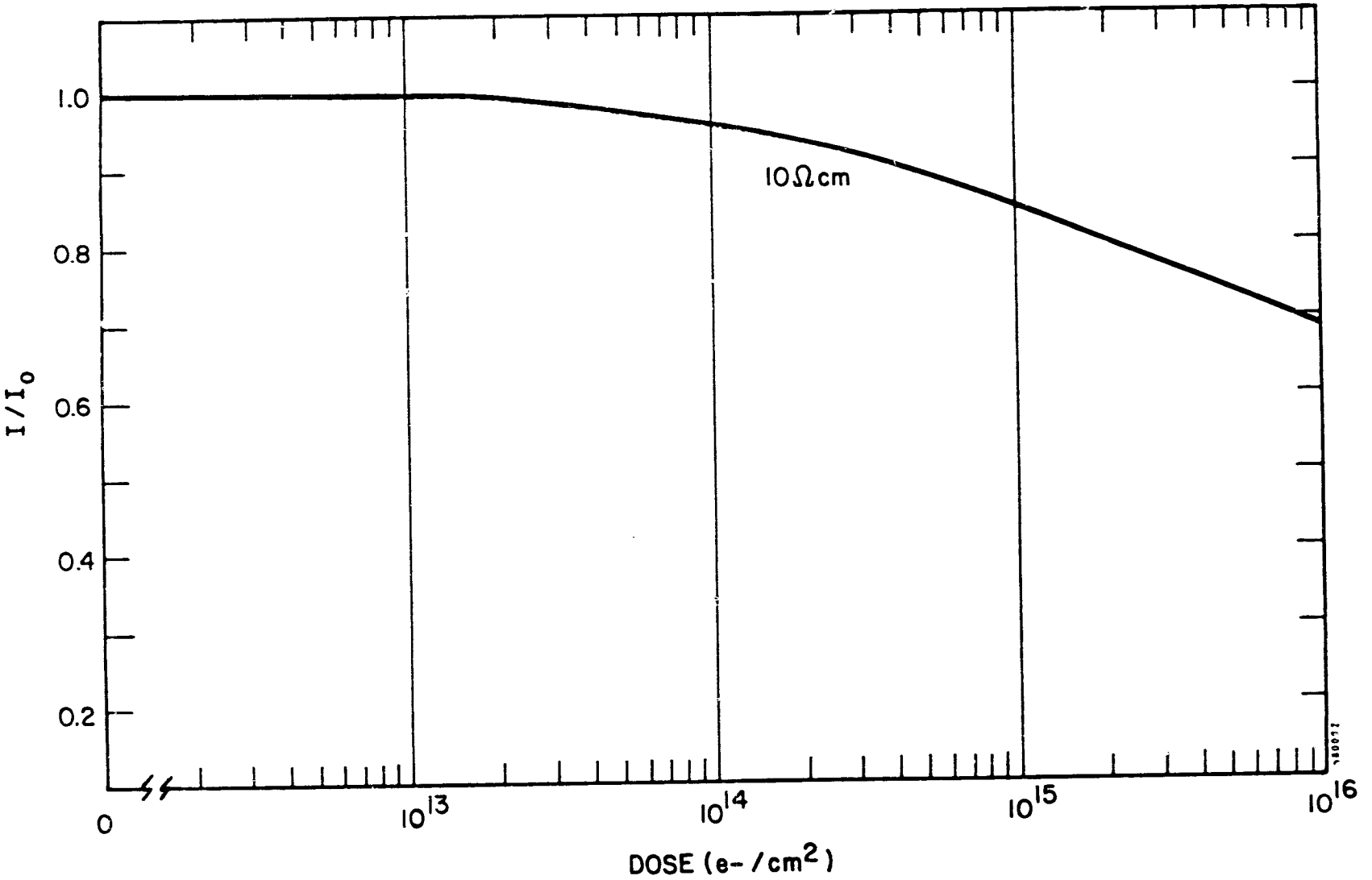

FIGURE A-12. NORMALIZED I_{sc} VERSUS 1 MeV ELECTRON FLUENCE FOR PULSED E-BEAM ANNEALED SOLAR CELLS

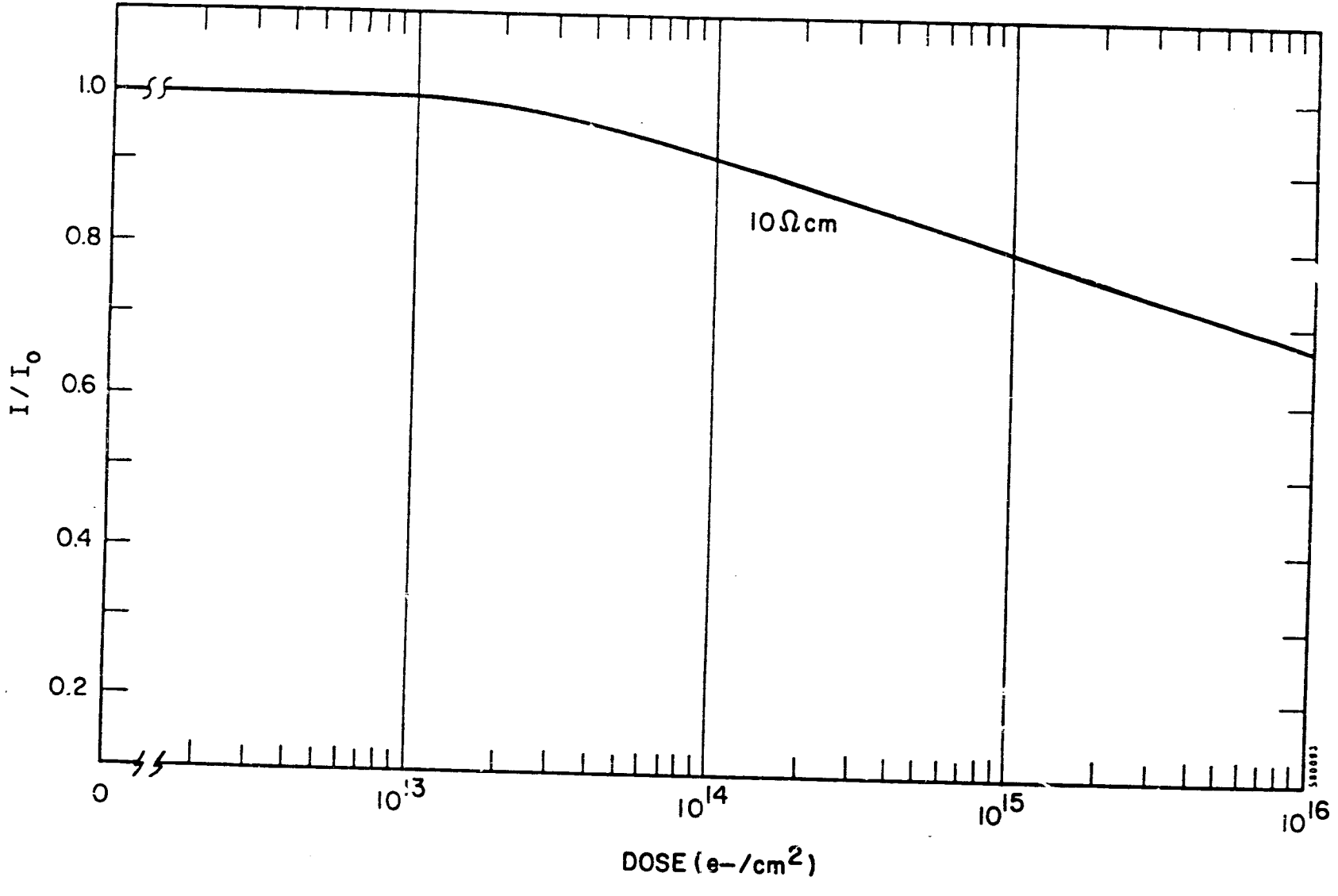

FIGURE A-13. NORMALIZED I_{sc} VERSUS 1 MeV ELECTRON FLUENCE FOR PRE-CRYOPUMP ION IMPLANTED AND FURNACE ANNEALED SOLAR CELLS

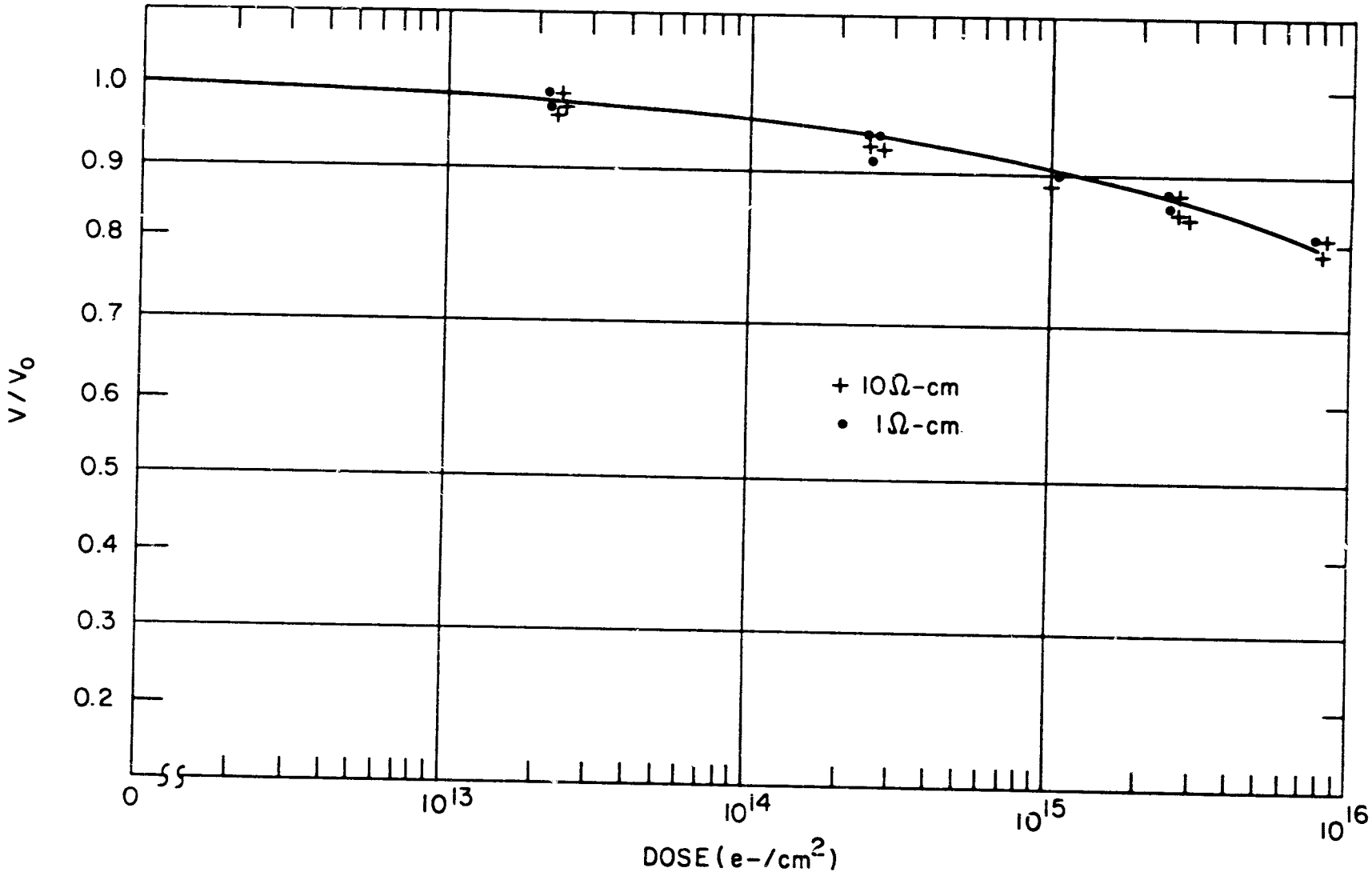

FIGURE A-14. NORMALIZED V_{oc} VERSUS 1 MeV FLUENCE FOR FURNACE ANNEALED CELLS

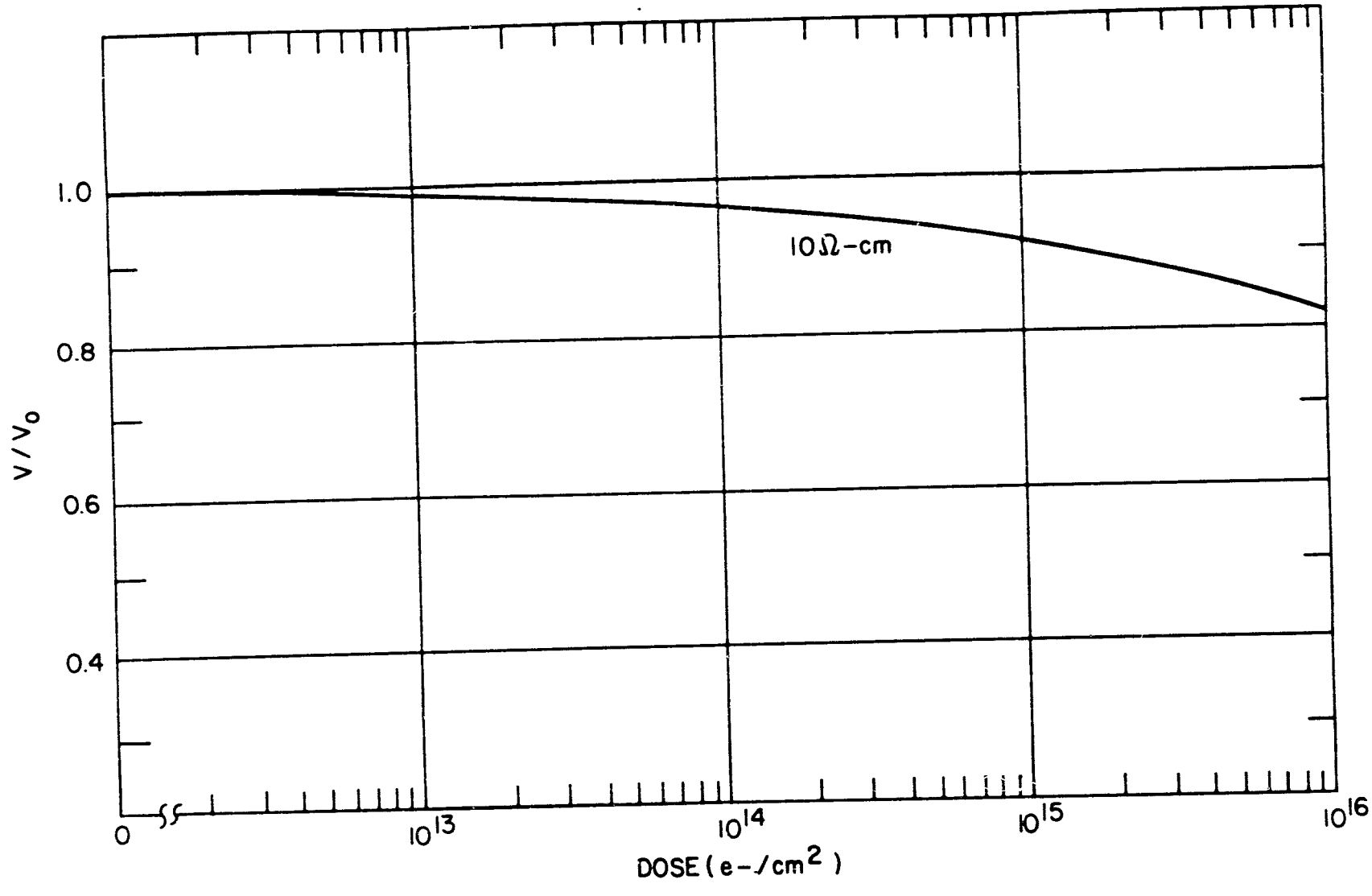

FIGURE A-15. NORMALIZED V_{oc} VERSUS 1 MeV FLUENCE FOR 0.53-MICRON LASER ANNEALED CELLS

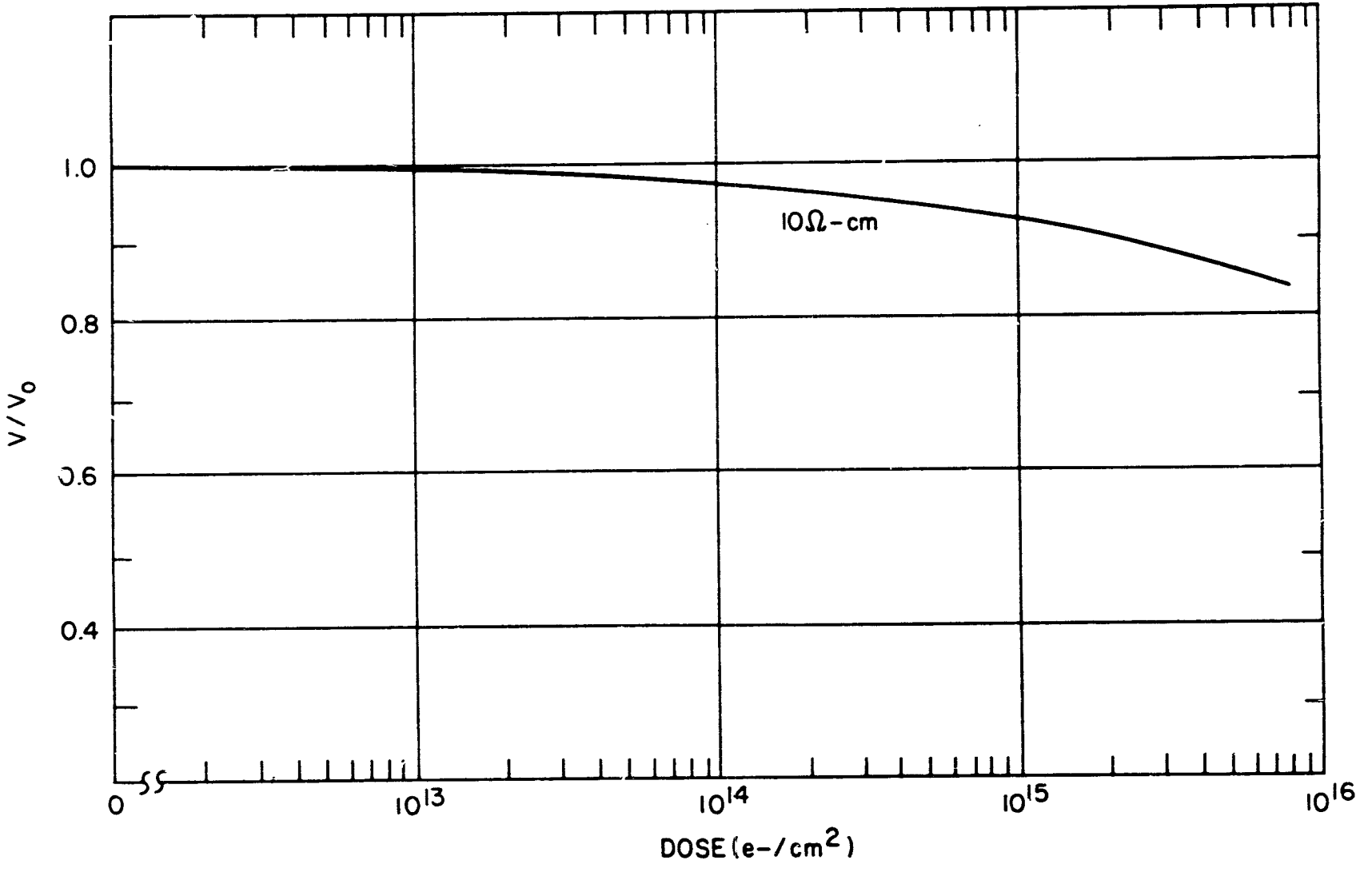

FIGURE A-16. NORMALIZED V_{oc} VERSUS 1 MeV FLUENCE FOR 1.06-MICRON LASER ANNEALED CELLS

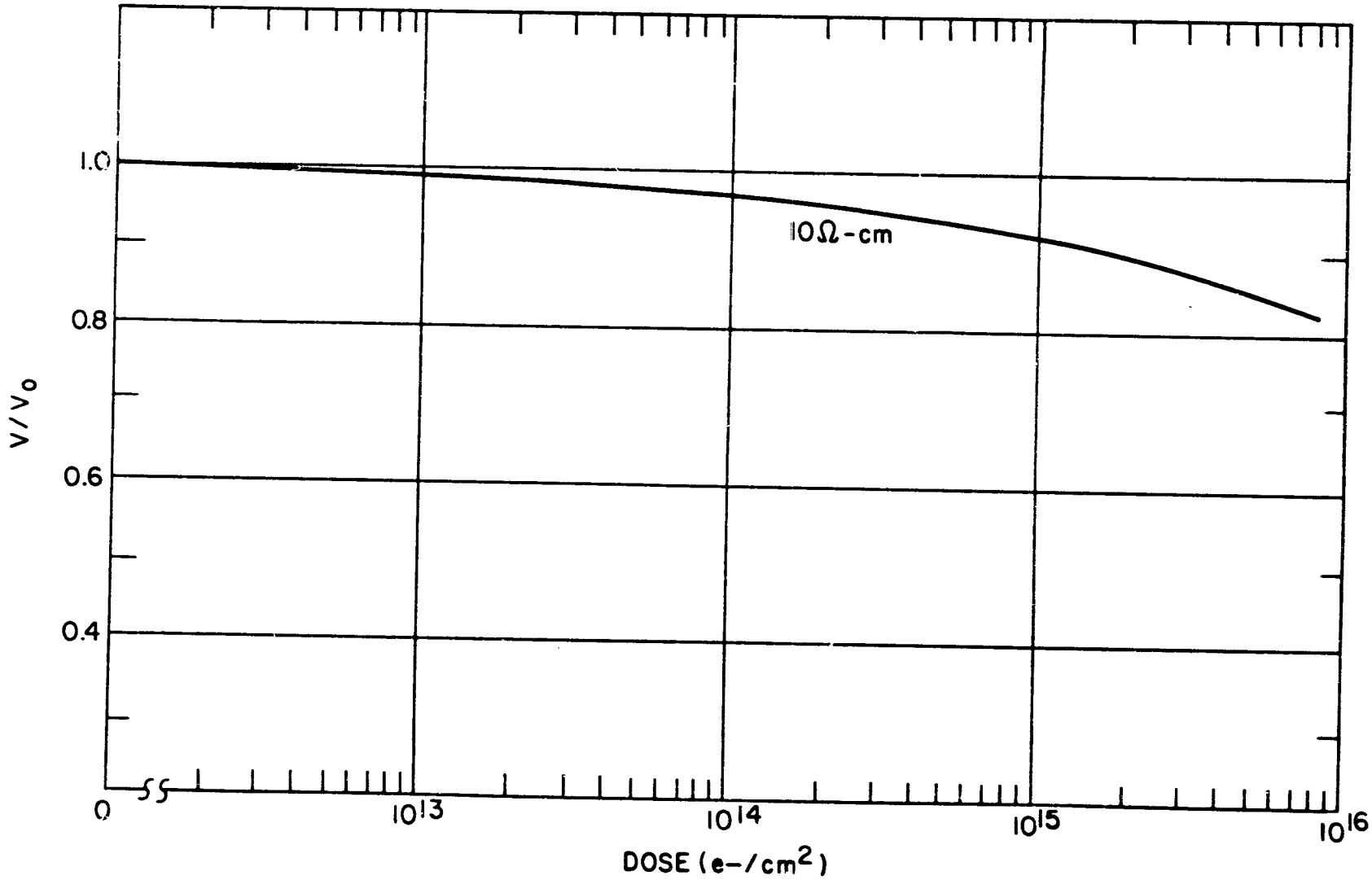

FIGURE A-17. NORMALIZED V_{oc} VERSUS 1 MeV FLUENCE FOR PULSED ELECTRON BEAM ANNEALED CELLS

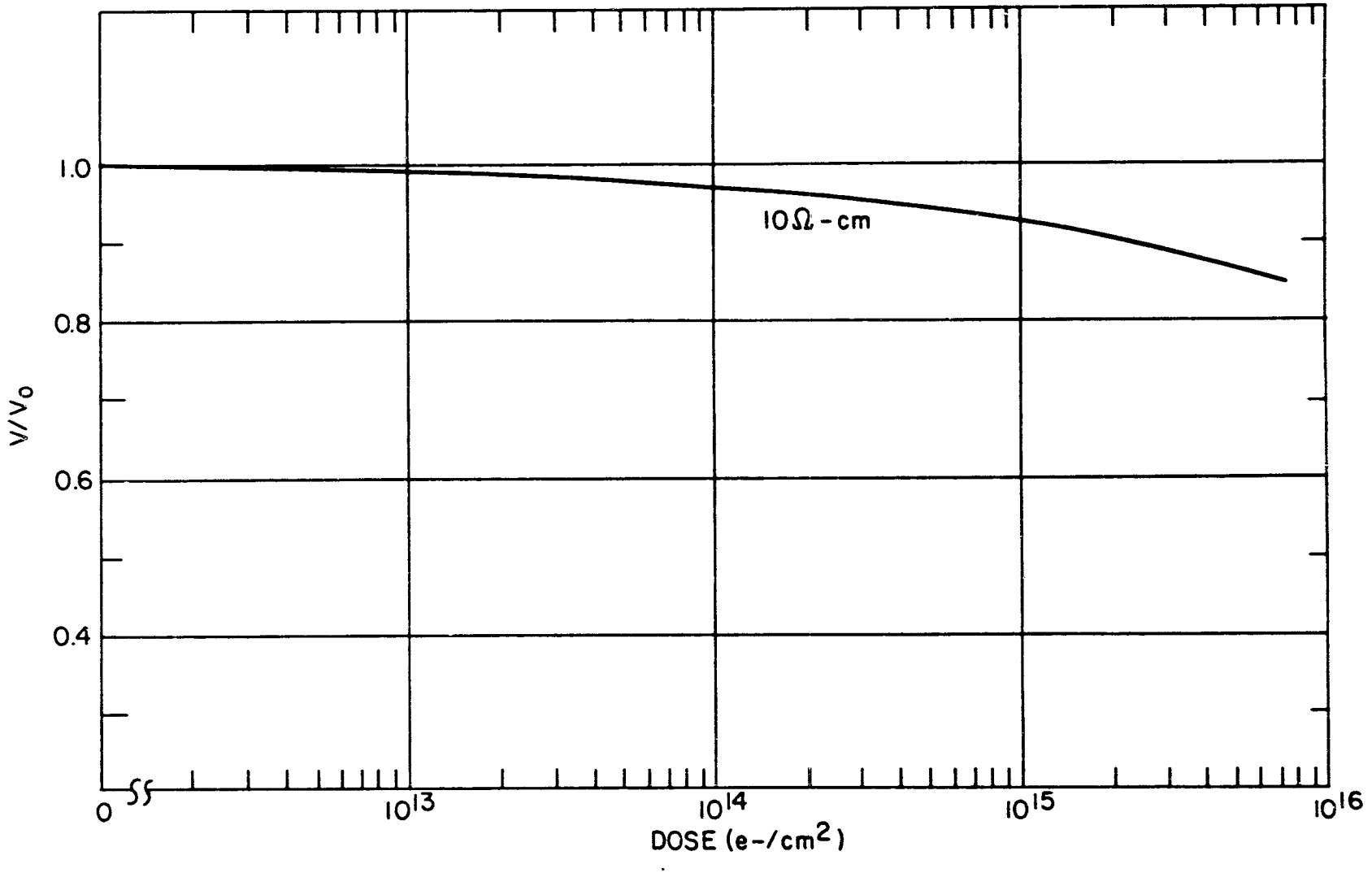

FIGURE A-18. NORMALIZED V_{oc} VERSUS 1 MeV FLUENCE FOR DIFFUSED CELLS